

**ÇUKUROVA UNIVERSITY
INSTITUTE OF NATURAL AND APPLIED SCIENCES**

PhD THESIS

Ahmad Reshad NOORI

**AXISYMMETRIC BENDING AND FLEXURAL VIBRATION
ANALYSIS OF HETEROGENEOUS (FGM) CIRCULAR
PLATES**

DEPARTMENT OF CIVIL ENGINEERING

ADANA-2019

**ÇUKUROVA UNIVERSITY
INSTITUTE OF NATURAL AND APPLIED SCIENCES**

**AXISYMMETRIC BENDING AND FLEXURAL VIBRATION
ANALYSIS OF HETEROGENEOUS (FGM) CIRCULAR PLATES**

Ahmad Reshad NOORI

PhD THESIS

DEPARTMENT OF CIVIL ENGINEERING

We certify that the thesis titled above was reviewed and approved for the award of the degree of the Doctor of Philosophy by the board of jury on 26/04/2019.

.....
Prof. Dr. Beytullah TEMEL
SUPERVISOR

.....
Prof. Dr. Naki TÛTÛNCÛ
MEMBER

.....
Prof. Dr. HÛseyin R. YERLİ
MEMBER

.....
Prof. Dr. Faruk Fırat ÇALIM
MEMBER

.....
Asst. Prof. Dr. Mehmet Fatih ŞAHAN
MEMBER

This PhD Thesis is written at the Department of Civil Engineering of Institute of Natural and Applied Sciences of Çukurova University.

Registration Number:

**Prof. Dr. Mustafa GÖK
Director
Institute of Natural and Applied Sciences**

This thesis was supported by Scientific Researched Project Office of Çukurova University under Contract no: FDK-2017-8254.

Note: The usage of the presented specific declarations, tables, figures, and photographs either in this thesis or in any other reference without citation is subject to "The law of Arts and Intellectual Products" number of 5846 of Turkish Republic.

ABSTRACT

PhD THESIS

AXISYMMETRIC BENDING AND FLEXURAL VIBRATION ANALYSIS OF HETEROGENEOUS (FGM) CIRCULAR PLATES

Ahmad Reshad NOORI

CUKUROVA UNIVERSITY
INSTITUTE OF NATURAL AND APPLIED SCIENCES
DEPARTMENT OF CIVIL ENGINEERING

Supervisor : Prof. Dr. Beytullah TEMEL
Year: 2019, Pages: 162
Jury : Prof. Dr. Beytullah TEMEL
: Prof. Dr. Naki TÜTÜNCÜ
: Prof. Dr. Hüseyin R. YERLİ
: Prof. Dr. Faruk Fırat ÇALIM
: Asst. Prof. Dr. Mehmet Fatih ŞAHAN

In this research, an effective numerical approach is applied to the axisymmetric bending and flexural vibration analysis of two-directional functionally graded (2D-FG) thick circular and annular plates with variable thickness. The material properties are assumed to vary continuously both in thickness and radial directions. The effect of shear deformation is considered in the formulation. The governing equations are converted to a set of ordinary differential equations (ODEs). Obtained canonical equations are solved numerically by the Complementary Functions Method (CFM). For the dynamic analysis, the CFM is combined with the Laplace transform. A powerful inverse algorithm is applied to retransfer the results from the Laplace space to the time domain. The damping model of Kelvin is used in the damped forced vibration analysis. The main purpose is to infuse this method to the bending and dynamic analysis of a wide range of solid circular or annular plates, with linear or non-linear thickness profiles, radially Functionally Graded (FG), FG in the thickness direction or 2D-FG, without any restrictions. The influence of material variation exponents and thickness profiles on the considered problems are investigated. Several examples are presented and results are verified with those obtained by finite element method and available published literature. Excellent agreement is observed.

Key Words: Bending, functionally graded materials, circular plates, annular plates, vibration, complementary functions method, Laplace transforms

ÖZ

DOKTORA TEZİ

**HETEROJEN (FDM) DAİRESEL PLAKLARIN EKSENEL SİMETRİK
EĞİLMESİ VE TİTREŞİM ANALİZİ**

Ahmad Reshad NOORI

**ÇUKUROVA ÜNİVERSİTESİ
FEN BİLİMLERİ ENSTİTÜSÜ
İNŞAAT MÜHENDİSLİĞİ ANABİLİM DALI**

Danışman : Prof. Dr. Beytullah TEMEL
Yıl: 2019, Sayfa: 162
Jüri : Prof. Dr. Beytullah TEMEL
: Prof. Dr. Naki TÜTÜNCÜ
: Prof. Dr. Hüseyin R. YERLİ
: Prof. Dr. Faruk Fırat ÇALIM
: Dr. Öğr. Üyesi Mehmet Fatih ŞAHAN

Bu araştırmada, çift yönlü fonksiyonel derecelenmiş ve değişken kalınlıklı kalın dairesel ve halka plakların, eğilme ve dinamik analizi için etkin bir sayısal yaklaşım uygulanmıştır. Malzeme özelliklerinin hem radyal yönde hem de kalınlık boyunca sürekli olarak değiştiği kabul edilmiştir. Formülasyonda, kayma deformasyonu etkileri göz önünde bulundurulmuştur. Plakların davranışını idare eden denklemler kanonik halde elde edilmiştir. Elde edilen kanonik denklemler Tamamlayıcı Fonksiyonlar Yöntemi (TFY) ile sayısal olarak çözülmüştür. Dinamik analiz için TFY, Laplace dönüşümü ile birlikte kullanılmıştır. Laplace uzayında elde edilen çözümler, etkin bir sayısal ters Laplace tekniği ile zaman uzayına dönüştürülmüştür. Sönümlü zorlanmış titreşim durumunda Kelvin tipi sönüm modeli kullanılmıştır. Bu çalışmanın temel amacı kalınlık boyunca FD, radyel fonksiyonel derecelenmiş (FD) , veya çift yönlü FD, lineer veya nonlineer kalınlık profili olan çeşitli dairesel ve halka plakların eğilme ve dinamik analizlerine TFY'yi uygulamaktır. Malzeme indekslerinin ve kalınlık profillerinin, söz konusu yapıların davranışı üzerindeki etkileri araştırılmıştır. Bu çalışmanın sonuçları literatürde bulunan ve sonlu elemanlar yöntemi kullanılarak hesaplanan sonuçlar ile karşılaştırıp, doğruluğu çeşitli örnekler üzerinde gösterilmiştir.

Anahtar Kelimeler: Eğilme, fonksiyonel derecelendirilmiş malzemeler, dairesel plaklar, halka plaklar, titreşim, Tamamlayıcı Fonksiyonlar Yöntemi, Laplace dönüşümü

GENİŞLETİLMİŞ ÖZET

Çift yönlü fonksiyonel derecelenmiş malzemeden (FDM) yapılmış kalın dairesel ve halka plakların eğilme, serbest titreşim ve zorlanmış titreşim davranışlarının analitik çözümü, yalnızca basit malzeme fonksiyonları ve basit kalınlık profilleri için elde edilebilmektedir. Çift yönlü FDM'ler genellikle, içlerinden birinin veya ikisinin seramik, diğerlerinin ise metal alaşımlı fazları olduğu üç veya dört farklı malzeme fazının düzgün değişimi ile yapılan malzemelerdir. Üretim yöntemlerinde yeni gelişmeler ile birlikte bilgisayar destekli üretim süreçleri kullanılarak çift yönlü FDM'leri üretmek mümkündür.

Analitik çözümlerinin elde edilmesi mümkün olmayan, değişken kalınlıklı FDM dairesel ve halka plakların, eğilme ve titreşim analizleri için, Tamamlayıcı Fonksiyonlar Yöntemi (TFY) gibi etkili ve güçlü sayısal yöntemlere ihtiyaç vardır. Nümerik analizde, TFY ile sınır değer problemi başlangıç değer problemine indirgenmektedir. Bu metodun bilgisayarda programlanması kolay olup, oldukça etkili bir çözüm yöntemidir. Bu çalışmada ele alınan plaklar, eksenel dönel simetrik olarak kabul edilmiştir. Bu çalışmada, plak kalınlığının üstel olarak değiştiği varsayılmıştır. FDM'lerin eksponansiyel ve üstel şekilde değiştiği kabul edilmiştir.

İlk olarak, ele alınan problemin eğilme davranışını idare eden denklemler birinci mertebeden kayma deformasyon teorisine dayanılarak minimum toplam potansiyel enerji prensibi ile elde edilmiş ve bu denklemler adi differansiyel denklem takımına dönüştürülmüştür. Elde edilen kanonik denklemler, TFY ile sayısal olarak çözülmüştür. TFY'ye dayalı başlangıç değer probleminin çözümleri için 5. mertebe Runge-Kutta (RK5) algoritması kullanılmıştır. Öncelikle TFY'nin doğruluğunu ve etkinliğini göstermek için iki adet karşılaştırma çalışması yapılmıştır. İlk karşılaştırmada FDM modelinin eksponansiyel olarak değiştiği kabul edilmiş ve sonuçlar literatürde mevcut sonuçlar ile karşılaştırılmış. Karşılaştırmada plak kalınlığının sabit olduğu kabul edilmiştir. Sonuçların birbiri

ile örtüştüğü görülmüştür. İkinci karşılaştırmada ise malzemenin üstel olarak değiştiği varsayılmıştır. Elde edilen sonuçlar sonlu elemanlar metodunun (ANSYS) sonuçları ile karşılaştırılmıştır. ANSYS'te model oluşturulurken plak kalınlık yönünde 40 ve radyal yönde 200 tabakaya bölünmüştür. Sonlu elemanlar paket programında her tabakaya farklı malzeme özelliği tanımlayarak toplamda 8000 adet malzeme tanımlanmıştır. Bu durumda da sonuçlar karşılaştırılıp, bu tezde sunulan yöntemin doğruluğu ve üstünlüğü gösterilmiştir. Ayrıca malzeme indislerinin, kalınlık profillerinin ve sınır şartlarının dairesel ve halka plak eğilme davranışı üzerindeki etkileri detaylı bir şekilde incelenmiştir.

İkinci problem ise çift yönlü FDM dairesel ve halka plakların serbest titreşim davranışının incelenmesidir. Çeşitli sınır şartlarına sahip kalın dairesel plaklar için serbest titreşim karakteristik değerleri elde edilmiş ve elde edilen sonuçların doğruluğu, literatür sonuçları ile karşılaştırılarak gösterilmiştir. Halka plaklar için literatürde mevcut çalışmalar sınırlı olduğundan dolayı, bu çalışmanın sonuçları ANSYS paket programından elde edilen sonuçlar ile karşılaştırılmış ve doğruluğu teyit edilmiştir. Eğilme durumunda olduğu gibi, serbest titreşim analizinde de ANSYS ile tutarlı sonuçlar elde edebilmek için plak; özellikle kalınlık doğrultusunda birçok katmana bölünmelidir. Plakların serbest titreşim davranışı için de çeşitli parametrik çalışmalar yapılmıştır. Malzeme indislerinin, geometrik sabitlerinin ve çeşitli mesnetlenme durumlarının, yapının doğal titreşim frekansları üzerindeki etkileri detaylı bir şekilde incelenmiştir. Bu tezde sunulan metod ile doğal titreşim frekanslarını elde etmek için mod şekillerinin bulunmasına ihtiyaç duyulmamaktadır.

Üçüncü olarak ele alınan problemde ise söz konusu plakların sönümsüz ve sönümlü zorlanmış titreşimlerin plak davranışlarına etkileri araştırılmıştır. Çift yönlü fonksiyonel derecelenmiş dairesel plakların çeşitli dinamik yükler altında zorlanmış titreşim davranışı Laplace uzayında TFY ile sayısal olarak incelenmiştir. TFY'ye dayalı başlangıç değer probleminin Laplace uzayındaki çözümleri için 5. mertebe Runge-Kutta (RK5) algoritması kullanılmış ve bu amaçla Fortran dilinde

bir bilgisayar programı hazırlanmıştır. Laplace uzayında elde edilen çözümler, etkin bir sayısal ters Laplace dönüşüm tekniği ile zaman uzayına dönüştürülmüştür. Mevcut yöntemin sonuçları, sonlu eleman paket programı olan ANSYS'ın sonuçları ile karşılaştırılmıştır. Yapılan karşılaştırmalar neticesinde önerilen metod ile kaba zaman artım miktarları kullanılarak elde edilen sonuçların, ANSYS programı yardımıyla sık zaman artım miktarları kullanılarak elde edilen değerlerle örtüştüğü görülmüştür. Sönümlü titreşim durumunda Kelvin tipi sönüm modeli kullanılmıştır. Çeşitli malzeme indisleri ve kalınlık profillerinin, FDM dairesel ve halka plakların zorlanmış titreşim davranışlarına etkisini incelemek için detaylı parametrik çalışmalar yapılmıştır. Ayrıca, periyodik yüklerin, ele alınan plakların davranışına etkisi araştırılmıştır. Periyodik yüklerin frekansı yapının doğal titreşim frekanslarına yakın olduğu zaman vuruş olayı meydana gelmektedir.



ACKNOWLEDGEMENTS

Foremost, I would like to express my sincere gratitude to my supervisor Prof. Dr. Beytullah TEMEL for the continuous support of my Ph.D. study and research, for his patience, motivation, and immense knowledge. His guidance helped me in all the time of research and writing of this thesis. I could not have imagined having a better supervisor for my Ph.D. study.

Besides my supervisor, I would like to thank the rest of my thesis committee: Prof. Dr. Naki TTNC, Prof. Dr. Hseyin R. YERL, Prof. Dr. Faruk Frat ALIM, and Asst. Prof. Dr. Mehmet Fatih AHAN for their encouragement and useful comments. Each of the members of the jury committee has provided me extensive personal and professional guidance and taught me a great deal about both scientific research and life in general.

I would like to thank my colleague, Res. Assist. Timuin Alp ASLAN for providing me with a good environment and facilities to complete this thesis. It would be inappropriate if I omit to mention the names of my dear friends: Asst. Prof. Dr. Sefa Yldrm, Fruza KOBOYEVA, and Hasibullah RASOOLI, who have, in their own ways, kept me going on my path to success, assisting me as per their abilities, in whatever manner possible and for ensuring that good times keep flowing.

I would like to thank the Scientific Res. Projects Directorate of ukurova University for supporting the present study and the Scientific and Technical Research Council of Turkey (TBTAK) for supporting my Ph.D. program.

Last but not least, I would like to thank the biggest source of my strength, my family. The blessings of my parents and the love and care of my brother and my sisters have all made a tremendous contribution in helping me reach this stage in my life. I thank them for putting up with me in difficult moments where I felt stumped and for goading me on to follow my dream of getting this degree.

CONTENTS	PAGES
ABSTRACT.....	I
ÖZ	II
GENİŞLETİLMİŞ ÖZET	III
ACKNOWLEDGEMENTS.....	VII
CONTENTS.....	VIII
LIST OF TABLES	X
LIST OF FIGURES	XIV
LIST OF ABBREVIATIONS.....	XX
1. INTRODUCTION	1
2. PREVIOUS STUDIES.....	3
2.1. Axisymmetric Bending of Functionally Graded Circular and Annular Plates.....	3
2.2. Dynamic Analysis of Functionally Graded Circular and Annular Plates	5
3. MATERIAL AND METHOD	11
3.1. Material.....	12
3.1.1. Type A – Exponential Functionally Graded Material.....	12
3.1.2. Type B – Power-Law Functionally Graded Material.....	13
3.2. Axisymmetric Bending of 2D-FG Thick Circular and Annular Plates with Variable Thickness	17
3.2.1. Governing Equations.....	18
3.2.2. Application of the CFM	27
3.3. Dynamic Analysis 2D-FG Thick Circular and Annular Plates with Variable Thickness	31
3.3.1. Governing Equations.....	31
3.3.2. Laplace Transform of the Governing Equations.....	36
3.3.3. Application of the CFM	39
3.3.4. Effect of Damping.....	40

3.3.5. Numerical Inverse Laplace Transform Algorithm.....	41
4. RESULTS AND DISCUSSIONS.....	45
4.1. Axisymmetric Bending of 2D FG Mindlin-Reissner Circular Plates	45
4.1.1. FG through the Thickness Direction.....	45
4.1.2. FG through the Radial Direction.....	48
4.1.3. 2D-FG Circular Plate with Variable Thickness	50
4.2. Axisymmetric bending of 2D-FG Mindlin-Reissner Annular Plates.....	53
4.2.1. 2D-FG Annular Plate with Uniform Thickness	53
4.2.2. 2D-FG Annular Plate with Variable Thickness	59
4.3. Free Vibration Analysis of 2D-FG Circular Plates	67
4.3.1. Verification	67
4.3.2. Free vibration of 2D-FG Circular Plates with Variable Thickness....	69
4.4. Free Vibration Analysis of 2D-FG Annular Plates	74
4.4.1. Verification	74
4.3.2. Free vibration of 2D-FG Annular Plates with Variable Thickness....	82
4.5. Forced Vibration Analysis of 2D-FG Annular Plates.....	89
4.5.1. Verification	89
4.5.2. Forced Vibration of 2D-FG Annular Plates with Variable Thickness.....	108
4.6. Forced Vibration Analysis of 2D-FG Circular Plates	121
4.6.1. Undamped Forced Vibration.....	121
4.6.2. Damped Forced Vibration.....	136
4.6.3. Beat phenomenon.....	142
5. CONCLUSIONS.....	145
REFERENCES	149
CURRICULUM VITAE.....	159
APPENDICES	160

LIST OF TABLES

PAGES

Table 3.1. Material properties 14

Table 4.1. Comparison of the non-dimensional deflection, w , $\nu = 0.288$, $E_r = 0.396$ ($E_r = E_m/E_c$) and $\lambda_r = 0$ 46

Table 4.2. Comparison of the non-dimensional deflection, w , $\nu = 0.288$, $E_r = 0.396$ ($E_r = E_m/E_c$) and $\lambda_r = 0$ 47

Table 4.3. Comparison of the non-dimensional deflection, w , $\nu = 0.288$, $E_r = 0.396$ ($E_r = E_m/E_c$) and $\lambda_r = 0$ 48

Table 4.4. Comparison of the maximum deflection, $w_{max} \times 10^{-7}$ (m), of clamped, simply and roller supported moderately thick RFG circular plates ($\lambda_z=0$) 49

Table 4.5. Maximum deflection $w_{max} \times 10^{-9}$ (m) of clamped moderately thick 2D-FG circular plate. 51

Table 4.6. Maximum deflection $w_{max} \times 10^{-8}$ (m) of simply supported moderately thick 2D-FG circular plate..... 52

Table 4.7. Comparison of the maximum deflection, shear force and bending moment of C – C supported moderately thick 2D-FG annular plate. . 54

Table 4.8. Comparison of the maximum deflection, shear force and bending moment of C – S supported moderately thick 2D-FG annular plate... 55

Table 4.9. Comparison of the maximum deflection, shear force and bending moment of S – C supported moderately thick 2D-FG annular plate..... 56

Table 4.10. Comparison of the maximum deflection, shear force and bending moment of S – S supported moderately thick 2D-FG annular plate. . 57

Table 4.11. Comparison of the maximum deflection, shear force and bending moment of C – F supported moderately thick 2D-FG annular plate..... 58

Table 4.12. Maximum deflection, $w_{max} \times 10^{-9}$, of C – C supported moderately thick 2D-FG annular plate.....	59
Table 4.13. Maximum deflection, $w_{max} \times 10^{-9}$, of C – S supported moderately thick 2D-FG annular plate.....	60
Table 4.14. Maximum deflection, $w_{max} \times 10^{-9}$, of S – C supported moderately thick 2D-FG annular plate.....	61
Table 4.15. Maximum deflection, $w_{max} \times 10^{-9}$, of S – S supported moderately thick 2D-FG annular plate.....	62
Table 4.16. Maximum deflection, $w_{max} \times 10^{-8}$, of C – F supported moderately thick 2D-FG annular plate.....	63
Table 4.17. Comparison of non-dimensional natural frequencies (Ω) of FG circular plate ($\lambda z = 0$)	68
Table 4.18. Comparison of non-dimensional natural frequencies (Ω) of FG circular plate.....	69
Table 4.19. Natural frequencies of 2D-FG circular plate (Clamped).....	71
Table 4.20. Natural frequencies of 2D-FG circular plate (Simply Supported).	72
Table 4.21. Natural frequencies of 2D-FG circular plate (Roller Supported).....	73
Table 4.22. Comparison of non-dimensional natural frequencies (Ω) of FG annular plate.....	75
Table 4.23. Comparison of natural frequencies of 2D-FG annular plate (C – C)..	76
Table 4.24. Comparison of natural frequencies of 2D-FG annular plate (C – S)...	77
Table 4.25. Comparison of natural frequencies of 2D-FG annular plate (S – C)...	78
Table 4.26. Comparison of natural frequencies of 2D-FG annular plate (S – S)..	79
Table 4.27. Comparison of natural frequencies of 2D-FG annular plate (C – F)...	80
Table 4.28. Comparison of natural frequencies of 2D-FG annular plate (F – C)...	81
Table 4.29. Natural frequencies of 2D-FG annular plate (C – C).	83
Table 4.30. Natural frequencies of 2D-FG annular plate (C – S).....	84
Table 4.31. Natural frequencies of 2D-FG annular plate (S – C).....	85

Table 4.32. Natural frequencies of 2D-FG annular plate (S – S).....	86
Table 4.33. Natural frequencies of 2D-FG annular plate (C – F).....	87
Table 4.34. Natural frequencies of 2D-FG annular plate (F – C).....	88





LIST OF FIGURES	PAGES
Figure 3.1. Schematic of an annular plate	12
Figure 3.2. Modulus of elasticity	13
Figure 3.3. Modulus of elasticity	15
Figure 3.4. Volume fraction of SiC	15
Figure 3.5. Volume fraction of Alumina	16
Figure 3.6. Volume fraction of Titanium alloy.....	16
Figure 3.7. Volume fraction of Aluminum alloy	17
Figure 4.1 Deflection of the clamped plate.....	53
Figure 4.2. Rotation of the clamped plate.....	53
Figure 4.3. Vertical deflection of C-C supported annular plate.....	64
Figure 4.4. Rotation of C – C supported annular plate	64
Figure 4.5. Vertical deflection of S – S supported annular plate	65
Figure 4.6. Rotation of S – S supported annular plate	65
Figure 4.7. Vertical deflection for various boundary conditions	66
Figure 4.8. Bending moment for various boundary conditions	66
Figure 4.9. Illustration of thickness profile.....	70
Figure 4.10. (a) Perspective view of the plate (b) Section and dynamic load	91
Figure 4.11. Comparison of the maximum vertical displacement.	92
Figure 4.12. Comparison of the maximum bending moment.	92
Figure 4.13. Comparison of the maximum shear force.	93
Figure 4.14. Comparison of the maximum vertical displacement.	93
Figure 4.15. Comparison of the maximum bending moment.	94
Figure 4.16. Comparison of the maximum shear force.	94
Figure 4.17. Comparison of the maximum vertical displacement.	95
Figure 4.18. Comparison of the maximum bending moment.	95
Figure 4.19. Comparison of the maximum shear force.	96
Figure 4.20. Comparison of the maximum vertical displacement.	96

Figure 4.21. Comparison of the maximum bending moment.	97
Figure 4.22. Comparison of the maximum shear force.....	97
Figure 4.23. Comparison of the maximum vertical displacement.	98
Figure 4.24. Comparison of the maximum bending moment.	98
Figure 4.25. Comparison of the maximum shear force.....	99
Figure 4.26. Comparison of the maximum vertical displacement.	99
Figure 4.27. Comparison of the maximum bending moment.	100
Figure 4.28. Comparison of the maximum shear force.....	100
Figure 4.29. Comparison of the maximum vertical displacement.	101
Figure 4.30. Comparison of the maximum bending moment.	101
Figure 4.31. Comparison of the maximum rotation.....	102
Figure 4.32. Comparison of the maximum shear force.....	102
Figure 4.33. Comparison of the maximum vertical displacement.	103
Figure 4.34. Comparison of the maximum bending moment.	103
Figure 4.35. Comparison of the maximum rotation.....	104
Figure 4.36. Comparison of the maximum shear force.....	104
Figure 4.37. Comparison of the maximum vertical displacement.	105
Figure 4.38. Comparison of the maximum bending moment.	105
Figure 4.39. Comparison of the maximum rotation.....	106
Figure 4.40. Comparison of the maximum shear force.....	106
Figure 4. 41. Illustrations of thickness profiles ($\lambda h = 0.25$; $\lambda h = -0.25$; $\lambda h = 1$).....	108
Figure 4.42. Comparison of the maximum vertical displacement.	109
Figure 4.43. Comparison of the maximum rotation.....	110
Figure 4.44. Comparison of the maximum vertical displacement.	110
Figure 4.45. Comparison of the maximum rotation.....	111
Figure 4.46. Comparison of the maximum vertical displacement.	111
Figure 4.47. Comparison of the maximum rotation.....	112
Figure 4.48. Comparison of the maximum vertical displacement.	113

Figure 4.49. Comparison of the maximum rotation.....	113
Figure 4.50. Comparison of the maximum vertical displacement.	114
Figure 4.51. Comparison of the maximum rotation.....	114
Figure 4.52. Comparison of the maximum vertical displacement.	115
Figure 4.53. Comparison of the maximum rotation.....	115
Figure 4.54. Comparison of the maximum vertical displacement.	116
Figure 4.55. Comparison of the maximum rotation.....	117
Figure 4.56. Comparison of the maximum vertical displacement.	117
Figure 4.57. Comparison of the maximum rotation.....	118
Figure 4.58. Comparison of the maximum vertical displacement.	118
Figure 4.59. Comparison of the maximum rotation.....	119
Figure 4.60. Geometry of the 2D-FG annular plate and dynamic load.....	120
Figure 4.61. Comparison of the maximum vertical displacement.	120
Figure 4.62. Comparison of the vertical displacement ($\lambda r = 0$ and $\lambda z = 0$).	121
Figure 4.63. Comparison of vertical displacement ($\lambda r = 0$ and $\lambda z = 2$).....	122
Figure 4.64. Comparison of vertical displacement ($\lambda r = 0$ and $\lambda z = 4$).....	122
Figure 4.65. Comparison of the vertical displacement ($\lambda r = 1$ and $\lambda z = 0$).	123
Figure 4.66. Comparison of the vertical displacement ($\lambda r = 1$ and $\lambda z = 2$).	123
Figure 4.67. Comparison of the vertical displacement ($\lambda r = 1$ and $\lambda z = 4$).	124
Figure 4.68. Comparison of the vertical displacement ($\lambda r = 2$ and $\lambda z = 0$).	124
Figure 4.69. Comparison of the vertical displacement ($\lambda r = 2$ and $\lambda z = 2$).	125
Figure 4.70. Comparison of the vertical displacement ($\lambda r = 2$ and $\lambda z = 4$).	125
Figure 4.71. Comparison of the vertical displacement ($\lambda z = 0$ and $\lambda h =$ -0.25).....	126
Figure 4.72. Comparison of the vertical displacement ($\lambda z = 2$ and $\lambda h =$ -0.25).....	127
Figure 4.73. Comparison of the vertical displacement ($\lambda z = 4$ and $\lambda h =$ -0.25).....	127

Figure 4.74. Comparison of the vertical displacement ($\lambda z = 0$ and $\lambda h = 1$).	128
Figure 4.75. Comparison of the vertical displacement ($\lambda z = 2$ and $\lambda h = 1$).	128
Figure 4.76. Comparison of the vertical displacement ($\lambda z = 4$ and $\lambda h = 1$).	129
Figure 4.77. Comparison of the vertical displacement ($\lambda z = 0$ and $\lambda h =$ 0.25).	129
Figure 4.78. Comparison of the vertical displacement ($\lambda z = 2$ and $\lambda h =$ 0.25).	130
Figure 4.79. Comparison of the vertical displacement ($\lambda z = 4$ and $\lambda h =$ 0.25).	130
Figure 4.80. Comparison of the vertical displacement ($\lambda r = 0$ and $\lambda h =$ 0.25).	131
Figure 4.81. Comparison of the vertical displacement ($\lambda r = 1$ and $\lambda h =$ 0.25).	132
Figure 4.82. Comparison of the vertical displacement ($\lambda r = 2$ and $\lambda h =$ 0.25).	132
Figure 4.83. Comparison of the vertical displacement ($\lambda r = 0$ and $\lambda h =$ -0.25).	133
Figure 4.84. Comparison of the vertical displacement ($\lambda r = 1$ and $\lambda h =$ -0.25).	133
Figure 4.85. Comparison of the vertical displacement ($\lambda r = 2$ and $\lambda h =$ -0.25).	134
Figure 4.86. Comparison of the vertical displacement ($\lambda r = 0$ and $\lambda h = 1$).	134
Figure 4.87. Comparison of the vertical displacement ($\lambda r = 1$ and $\lambda h = 1$).	135
Figure 4.88. Comparison of the vertical displacement ($\lambda r = 2$ and $\lambda h = 1$).	135
Figure 4.89. Geometry of the clamped circular plate and dynamic load.	137
Figure 4.90. Comparison of the viscoelastic vertical displacement of clamped plate.	137

Figure 4. 91. Comparison of the viscoelastic bending moments of clamped plate.	138
Figure 4.92. Comparison of the viscoelastic shear forces of clamped plate.	138
Figure 4.93. Geometry of the simply supported circular plate and dynamic load.	139
Figure 4.94. Comparison of the viscoelastic displacement of simply supported plate.	139
Figure 4.95. Comparison of the viscoelastic shear forces of simply supported plate.	140
Figure 4. 96. Geometry of the roller supported circular plate and dynamic load.	140
Figure 4.97. Comparison of the viscoelastic displacement of roller supported plate.	141
Figure 4.98. Comparison of the viscoelastic shear forces of roller supported plate.	141
Figure 4.99. Dynamic load function	142
Figure 4.100. Comparison of displacement of clamped circular plate.....	143
Figure 4.101. Square wave dynamic load function.....	144
Figure 4.102. Comparison of displacement of simply supported plate.....	144



LIST OF ABBREVIATIONS

BVPs	: Boundary Value Problems
CFM	: Complementary Functions Method
CLPT	: Classical Plate Theory
DQM	: Differential Quadrature Method
FEM	: Finite Element Method
FFT	: Fast Fourier Transform
FGMs	: Functionally Graded Materials
FSDT	: First-order Shear Deformation Theory
GDQR	: Generalized Differential Quadrature Rule
IVPs	: Initial Value Problems
LPT	: Levinson Plate Theory
ODE	: Ordinary Differential Equation
SSM-DQM	: State Space Method - Differential Quadrature Method
TSDT	: Third-order Shear Deformation Theory
2D	: Two Directional
3D	: Three Dimensional



1. INTRODUCTION

Circular and annular FG plates have been widely used as structural members in many important engineering applications. During their service life, those important structures are often subjected to various static and dynamic loadings. For this reason, axisymmetric bending analysis of the FG circular and annular plates have been very attractive during the last decades.

Recent developments and improvements in the computer-aided manufacturing processes make it possible to fabricate FGMs in two directions. 2D FGMs are made of continuous and smooth gradation of three or four different material phases. Volume fractions of these constituent materials vary smoothly in a predetermined composition profile. Those advanced materials have a wide range of applications in engineering fields. Furthermore, there are just a few studies on the bending and dynamic analysis of 2D-FG circular and annular plates. In this thesis, two types of material variation are considered which their distributions are in exponential and power law form.

Closed-form solution of the static and dynamic response of 2D-FG circular and annular plates are only available for a number of problems with simple boundary conditions and uniform thickness. In order to carry out the axisymmetric bending, free vibration and forced vibration of 2D-FG thick circular and annular plates with variable thickness, efficient and powerful numerical methods such as the CFM are needed. In this study, the obtained canonical equations are solved numerically by the CFM.

The main objective of this research is to suggest a powerful and efficient approach for the axisymmetric bending and dynamic response of radially FG, FG through the thickness and 2D-FG circular and annular plates. In this thesis, the modulus of elasticity and mass density of the plate is considered to vary both in thickness and radial directions. The Poisson's ratio is assumed to be constant. The governing equations of the problem are obtained based on the principle of

minimum total potential energy and Hamilton's principle. The axisymmetric bending, free vibration and forced vibration response of the circular and annular plates for several volume fraction exponents, thickness to radius ratios, boundary conditions, and thickness function are carried out and compared with available literature and the FEM.

Free and forced vibration behaviors of the considered structures are examined in conjunction with FSDT the CFM in the Laplace space. This method is attempted to obtain accurate fundamental frequencies and the transient behavior of the 2D-FG plates. The time-dependent governing equations of the dynamic response of the structure have first been obtained. Then, the canonical equations are transferred to the Laplace space and the CFM has been employed to solve those canonical form for a set of Laplace parameters. Butcher's RK5 method is applied to numerical solutions. To retransform the obtained results to the time-space an accurate inverse Laplace transform method has been used. To verify the proposed scheme, results of fundamental frequencies, displacements, and internal forces are compared with available literature and ANSYS. In this thesis, the effects of shear deformation are taken into account. Furthermore, the Kelvin damping model is used in the viscoelastic material case. Finally, the effects of material gradient index and geometric constants are studied. Tabular results of free vibration and graphical results of the forced vibration are given and conclusions are presented.

2. PREVIOUS STUDIES

2.1. Axisymmetric Bending of Functionally Graded Circular and Annular Plates

Circular and annular FG plates are important structural members in many engineering applications. Axisymmetric bending analysis of the FG circular and annular plates have been very attractive during the last decades.

Alipour (2016) presented an analytical approach for the bending and stress analysis of FG sandwich circular plates. Mousavi and Tahani (2012) suggested an exact solution method for bending analysis of radially FG sector plates. Axisymmetric bending of FG thick circular plates was studied by Sahraee and Saidi (2009). Saidi et al. (2009) used unconstrained TSDT to examine the axisymmetric bending of FG thick circular plates. They used an analytical method in their paper. Reddy et al. (1999) examined the axisymmetric bending of FG circular and annular plates by FSDT. They also developed the exact relationship between the bending analysis for classical plate theory (CLPT) and FSDT for FG circular plates.

Wang et al. (2011) used linear three dimensional theory to investigate the axisymmetric bending of FG circular magneto-electro-elastic plates subjected to arbitrarily distributed loads in radial direction. They compared their results with FEM. Bayat et al. (2009) presented theoretical formulation for the bending analysis of radially FG rotating disks based on the FSDT. They considered both body and bending loads in the analysis. They showed that the transverse shear resultants in FG disks are greater than in homogenous disks. The bending analysis of FG annular sector plates was studied by Fereidoon et al. (2012) with the aid of Kirchhoff plate theory (CLPT) and the extended Kantorovich method. They presented a semi analytical solution method for flexural response of FG sector plates with arbitrarily boundary conditions and loadings. Bending analysis of FG

thick circular sectorial plates was investigated by Sahraee (2009) using the Levinson plate theory (LPT) based on FSDT. They demonstrated that LPT solution for the deflection of the FG sectorial plates is smaller than those of homogenous ones. Closed form solution of axisymmetric bending of circular and annular isotropic plates with variable thickness was derived by Vivio and Vullo (2010). Li et al. (2008b) studied the problem of FG circular plates subjected to axisymmetric loads by the stress functions method for several cases of boundary conditions and material gradient indices. Bending analysis of thick FG fully clamped sector plates subjected to distributed load was presented by Aghdam et al. (2012). They suggested an iterative procedure based on the extended Kantorovich method and FSDT. Li et al. (2008a) developed exact solution of axisymmetric bending of uniformly loaded FGM annular plates. They obtained explicit forms of the deflection functions. They showed the effects of material inhomogeneity on the elastic deformations and stresses. Sayar (1970) studied the static analysis of homogeneous shell and plates.

Ma and Wang (2004) employed the TSDT to examine the axisymmetric bending and buckling of FG circular plates. They discussed the relationship between the bending and buckling of FG plates and the effect of material gradient indices and shear deformation on the axisymmetric bending problem. Rad (2012a) used three-dimensional elasticity theory to study the static response of FG annular and circular plates under axisymmetric transverse loads resting on an elastic foundation. They demonstrated that neutral surface of FG plates depends on the variation of the elasticity modulus and it is not at the mid-surface. Rad et al. (2010) used a semi-analytical approach of state space method - differential quadrature method (SSM-DQM) to carry out the axisymmetric bending of FG circular and annular plates resting on Winkler-Pasternak elastic foundation. They considered several boundary conditions. The direct displacement method was applied by Wang et al. (2016b) to examine the axisymmetric bending of FG plates subjected to arbitrary loads. They introduced a semi-analytical method to derive the

solution for bending problem of FG plates with arbitrary variation of materials in the thickness direction.

Nie and Zhong (2007a) investigated the axisymmetric bending of bi-directional FG circular plates. They applied the SSM-DQM to the three-dimensional elasticity theory based governing equations. They showed that bi-directional FG plates demonstrate a better performance than one-directional FG and isotropic plates. Rad and Alibeigloo (2013) used DQM to study the influence of two parameter elastic foundation on the axisymmetric bending of two-directional FG circular and annular plates. They demonstrated that the displacement and stresses have a non-linear variation through the thickness of the plate. Based on three-dimensional elasticity theory and semi-analytical approach the bending response of two-directional FG circular plates resting on an elastic foundation was studied by Rad (2012b). Zafarmand and Kadkhodayan (2015) examined the static and dynamic behavior of two-dimensional FG thick sector based on Hamilton's principle with the aid of Rayleigh – Ritz method.

2.2. Dynamic Analysis of Functionally Graded Circular and Annular Plates

Circular and annular plates are important structural members in the architectural and industrial designing. Functionally graded materials (FGMs) have a continuous variation of mechanical properties in one or more directions. Those advanced materials have a wide range of applications in engineering fields. Therefore, the free vibration and transient behavior of FG circular and annular plates have been examined and investigated by many researchers.

The free vibration response of thick annular plates was investigated by Irie et al. (1982) based on the Mindlin plate theory. They obtained natural frequencies of uniform thick annular plates for several boundary conditions. The vibration analysis of Mindlin plates was carried out by Liew et al. (1998). Liu and Lee (2000) used finite elements to examine 3D vibration response of thick annular and circular plates. The natural frequencies of solid circular plates were investigated by

Wu et al. (2002) with the aid of the generalized differential quadrature rule (GDQR). They examined the impact of stepped thickness and boundary conditions on the free vibration response of circular plates. The free vibration and transient response of a thin circular FG plate were examined by Allahverdizadeh et al. (2008). In their study, they studied the effects of variation of Poisson's ratio and volume fraction index on the dynamic analysis of circular FG plates. Wirowski (2009) examined the free vibration of FG thin circular plates.

Efrain and Eisenberger (2007) obtained the exact free vibration characteristics of isotropic and FG annular plates of variable thickness. They used the exact element method and the dynamic stiffness method. Influences of material gradient indexes, taper parameters and boundary conditions on the free vibration characteristics of FG circular plates of variable thickness were investigated by Gupta et al. (2007). Nie and Zhong (2007b) achieved the three dimensional dynamic analysis of FG circular plate with the aid of the state space method and the one-dimensional differential quadrature method. They used to same method to investigate the dynamic analysis of FG annular sectorial plates Nie and Zhong, (2008). Dong (2008) applied the Chebyshev–Ritz method to investigated the three-dimensional free vibration of FG annular plates with different boundary conditions. Free axisymmetric vibration of FG circular plates was examined by Wang et al. (2009) based on three dimensional theory. Lal and Ahlawat (2017) studied the influence of hydrostatic loads on the free axisymmetric vibration of FG thick circular plates based on FSDT.

Ebrahimi and Rastgoo (2008) provided an analytical solution for free vibration of a thin annular FG plate with piezoelectric layers based on the Kirchhoff plate model. Ebrahimi et al. (2008) carried out the natural frequencies of moderately thick circular FG plate integrated with piezoelectric layers based on Mindlin plate theory. Ebrahimi and Rastgo (2008) presented an analytical solution for free vibration response of thin circular FG plates with two full size surface-bonded piezoelectric plates. Mirtalaie and Hajabasi (2011) applied the DQM to

obtain the natural frequencies of FG thin annular sector plates. The influences of boundary conditions and variation of Poisson's ratio on the free vibration response of the considered structures were examined. Hosseini-Hashemi et al. (2010) presented exact natural frequencies of circular and annular FG plates with different kinds of boundary conditions based on FSDT. They introduced potential functions and used the method of separation of variables. Su et al. (2014) suggested a unified solution method for the free vibration analysis of FG annular plates with general boundary conditions.

Malekzadeh et al. (2010) examined the free vibration response of FG annular plates subjected to the thermal environment based on FSDT. Malekzadeh et al. (2011) presented the natural frequencies of FG annular plates in the thermal environment by 3D elasticity theory. They showed that the temperature dependence of materials has a significant effect on the free vibration characteristics of FG plates. The free vibration of the FG annular plates with mixed boundary conditions were investigated by Shi and Dong (2012) in the thermal environment. They studied the influence of mixed boundaries, material gradient index and geometrical characteristics and the free vibration. They used Chebyshev-Ritz method in their study. A unified solution approach was presented by Wang et al. (2016a) to investigate the vibration analysis FG circular and annular plates based on FSDT. Natural frequencies of radially FG circular plates with variable thickness were carried out by Sharma et al. (2017) with the Ritz method.

Tornabene (2009) investigated the dynamic analysis of FG annular plates by considering them as a special case of conical shell formulation. Equations were developed based on the FSDT within the theory of linear elasticity. Alipour et al. (2010) studied the free vibration response of two-directional FG circular plates of variable thickness by differential transform method (DTM) based on FSDT. They carried out that thickness variability may have remarkable effects on the free vibration response. Shariyat and Alipour (2010) used differential transformation method to develop the semi analytical solution for free vibration response of two-

directional functionally graded circular plates with restrained edges, resting on elastic foundations. Nie and Zhong (2010) studied the dynamic analysis of multi-directional FG annular plates with state space-based DQM based on the 3D elastic theory. They carried out that the graded materials in the radial direction can improve the stiffness of the plate. Alipour and Shariyat (2011) presented the free vibration analysis of two-directional FG circular plates resting on elastic foundations with the aid of differential transform technique. They showed that the elastic foundation leads to higher free vibration characteristics. Shariyat and Alipour (2011) investigated the modal stress analysis of two-dimensional FG circular plates resting on elastic foundations. Kermani et al. (2012) examined the 3D free vibration behavior of multi-directional FG circular and annular plates are with the aid of the state space based DQM. They showed that the free vibration characteristics of the plates increase when the plate becomes thicker. Vibration analysis of axisymmetric circular plates made up of two-directional FGMs was carried out by Kumar and Lal (2013). They observed that the natural frequencies of clamped plates are greater than those of simply supported plates. Lal and Ahlawat (2015) investigated the radially symmetric vibration parameters of two-directional FG circular plates subjected to in-plane hydrostatic forces using the DQM. They indicated that the natural frequencies increase as the plate becomes stiffer in the radial direction, but when the plate becomes denser in the radial direction the natural frequencies decrease. Ahlawat and Lal (2016) examined the axisymmetric vibration of multi-directional FG circular plate resting on an elastic foundation by using generalized DQM.

Tajeddini et al. (2011) examined three-dimensional free vibrations of FG thick circular plates of variable thickness resting on elastic foundation. They investigated the effects of material gradient and the stiffness of foundation on the natural frequencies. Yas and Tahounch (2012) presented the free vibration characteristics of FG annular plates on the elastic foundation. They used DQM based on the 3D theory of elasticity in their work. Jodaei et al. (2012) studied the

3D free vibration response of FG annular plates based on state-space based DQM and artificial neural network. Free vibration characteristics of FG circular plates with variable thickness was investigated by Shamekhi (2013) using Meshless method. The influence of the thickness variation on the natural frequencies was presented in their work. The exact vibration parameters of thick FG circular and annular plates with stepped thickness were presented by Hosseini-Hashemi et al. (2013). Natural frequencies of elastically supported FG circular plates were carried out by Żur (2018) with the help of the quasi- Green's function. They studied the effects of volume fraction index and boundary conditions on the free vibration response of FG circular plates.

Literature review shows that there are several studies dealing with the axisymmetric bending analysis of one dimensional FG circular and annular plates. Recent developments and improvements in the computer-aided manufacturing processes make it possible to fabricate FGMs in two directions. 2D-FGMs are made of continues and smooth gradation of three or four different material phases. Volume fractions of these constituent materials vary smoothly in a predetermined composition profile. Furthermore, there are just a few studies on the bending analysis of 2D-FG circular and annular plates with uniform thickness. Hence, for the first time, the axisymmetric bending response of 2D-FG thick circular and annular plates with variable thickness based on the FSDT is presented.

When the literature is reviewed, it can be clearly seen that there are many papers deal with dynamic analysis of FG and 2D-FG circular and annular plates of uniform thickness. But there are only a few works on the vibration analysis of 2D-FG circular and annular plates of variable thickness. Therefore, in this work, free and forced vibration behaviors of 2D-FG thick circular and annular plates with variable thickness are examined in conjunction with FSDT and the Complementary Function Method (CFM) in the Laplace space. This method is attempted to obtain accurate fundamental frequencies and the transient behavior of the considered structure. The time-dependent governing equations of the structure have first been

obtained. Then, the canonical equations are transferred to the Laplace space and the CFM has been employed to solve those canonical form for a set of Laplace parameters. Butcher's RK5 method is applied to numerical solutions. To retransform the obtained results to the time-space an accurate inverse Laplace transform method has been used.



3. MATERIAL AND METHOD

Variation of material properties, governing equations of the problem on hand, and the solution procedure are given in this section.

Closed-form solution of the static and dynamic behavior of 2D-FG circular and annular plates are only available for a number of problems with simple boundary conditions and simple thickness functions. In order to carry out the axisymmetric bending, free vibration and transient response of 2D-FG thick circular and annular plates with variable thickness, efficient and powerful numerical methods such as the CFM are needed. In numerical analysis, the CFM is an approach for solving a boundary value problem by reducing it to the solution of an initial value problem.

In this thesis, the governing equations are carried out based on the FSDT. Obtained canonical equations of the static and free vibration behavior of the considered structures are solved numerically by the CFM. The forced vibration behavior of the considered structures is examined by the CFM in the Laplace space. The time-dependent governing equations have first been obtained. Then, the canonical equations are transferred to the Laplace space and the CFM has been employed to solve those canonical form for a set of Laplace parameters. Butcher's RK5 method (see Chapra and Canale (2010)) is applied in numerical solutions. To retransform the obtained results to the time space an accurate inverse Laplace transform method has been used. The damping model of Kelvin is used in the damped forced vibration analysis.

The CFM is successfully applied previously in structural mechanics problems by Temel et al. (2004), Temel (2004), Çalım (2009), Tutuncu and Temel (2009), Çalım (2012), Temel et al. (2014), Yildirim and Tutuncu (2018a), Yildirim and Tutuncu (2018b), Noori et al. (2018a), Aslan et al. (2018), Noori et al. (2018b), Temel and Noori (2019) and Yildirim and Tutuncu (2019).

3.1. Material

Consider a 2D functionally graded Mindlin-Reissner axisymmetric annular or circular plate of variable thickness $h(r)$, inner radius r_i , and outer radius r_o as given in Figure (3.1). In this thesis, two types of material variation are considered.

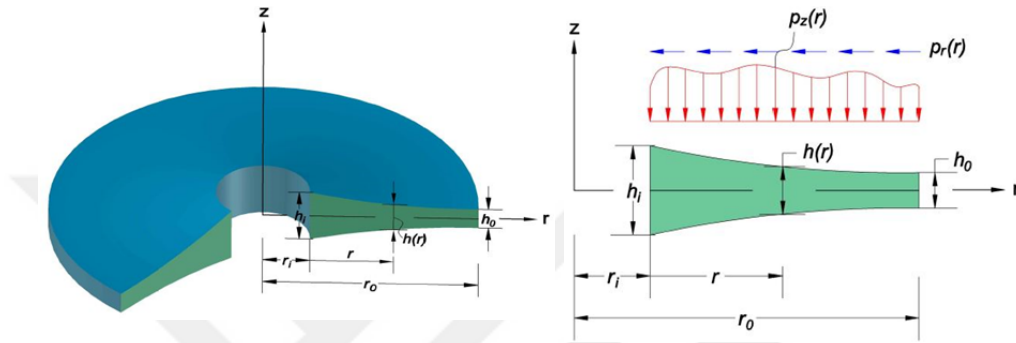


Figure 3. 1. Schematic of an annular plate

3.1.1. Type A – Exponential Functionally Graded Material

The Young's modulus and mass density of the plate vary continuously in both thickness and radial directions, while the Poisson's ratio is assumed to be constant.

$$E(r, z) = E_0 * e^{\lambda_z \left(\frac{z}{h(r)} + \frac{1}{2} \right) + \lambda_r \left(\frac{r+r_i}{r_o} \right)} \quad (3.1)$$

$$\rho(r, z) = \rho_0 * e^{\lambda_z \left(\frac{z}{h(r)} + \frac{1}{2} \right) + \lambda_r \left(\frac{r+r_i}{r_o} \right)} \quad (3.2)$$

Here, λ_r and λ_z are material gradient indices through the radial and thickness directions which take nonnegative values. z is distance from mid-surface of the plate along z axis. The r -coordinate is taken in radial direction outward from the inner radius of the plate. In these equations, $E_0 = 380$ GPa and $\rho_0 = 3800$ kg/m³ are the values of the Young's modulus and mass density at the bottom of the

inner side of the plate ($z = -\frac{h}{2}$, $r = 0$). ($\lambda_r = 0$ and $\lambda_z = 0$) correspond to an isotropic homogeneous material, ($\lambda_z = 0$) corresponds to a radially FG material and ($\lambda_r = 0$) correspond to FG material through the thickness. The gradation of the modulus of elasticity for circular plate ($r_o = 5$; $r_i = 0$; $\lambda_r = 1$; $h = 1$ and $\lambda_z = 1$) is presented in Figure (3.2).

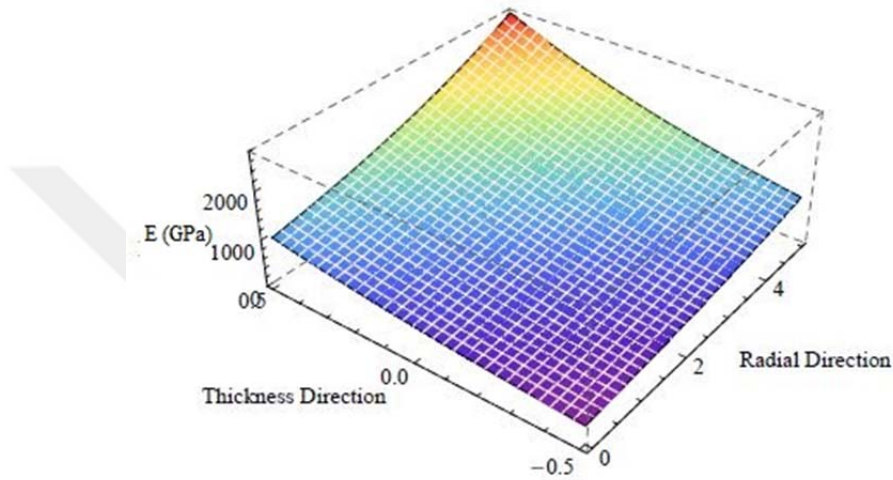


Figure 3. 2. Modulus of elasticity

3.1.2. Type B – Power-Law Functionally Graded Material

The axisymmetric plate is assumed to be made by a smooth variation of two ceramic and two metal alloy phases. The material properties of the plate are supposed to vary along both thickness and radial directions. The volume fractions of the materials are expressed as follows:

$$V_{m1}(r, z) = \left[1 - \left(\frac{r}{r_o - r_i} \right)^{\lambda_r} \right] \left(\frac{h(r) - 2z}{2h(r)} \right)^{\lambda_z} \quad (3.3)$$

$$V_{m2}(r, z) = \left(\frac{r}{r_o - r_i} \right)^{\lambda_r} \left(\frac{h(r) - 2z}{2h(r)} \right)^{\lambda_z} \quad (3.4)$$

$$V_{c1}(r, z) = \left[1 - \left(\frac{r}{r_o - r_i} \right)^{\lambda_r} \right] \left[1 - \left(\frac{h(r) - 2z}{2h(r)} \right)^{\lambda_z} \right] \quad (3.5)$$

$$V_{c2}(r, z) = \left(\frac{r}{r_o - r_i} \right)^{\lambda_r} \left[1 - \left(\frac{h(r) - 2z}{2h(r)} \right)^{\lambda_z} \right] \quad (3.6)$$

where m_1, m_2, c_1 and c_2 shows the first and second metal, and ceramic. λ_r and λ_z are volume fraction exponents through the radial and thickness directions which take nonnegative values. z is distance from mid-surface of the plate along z axis. The r -coordinate is taken in radial direction outward from the inner radii of the plate. The modulus of elasticity and mass density of the two-dimensional FG circular plate is derived by:

$$E(r, z) = E_{m1}V_{m1} + E_{m2}V_{m2} + E_{c1}V_{c1} + E_{c2}V_{c2} \quad (3.7)$$

$$\rho(r, z) = \rho_{m1}V_{m1} + \rho_{m2}V_{m2} + \rho_{c1}V_{c1} + \rho_{c2}V_{c2} \quad (3.8)$$

The gradation of the modulus of elasticity and volume fractions for an annular plate ($r_o = 5$; $r_i = 1$; $\lambda_r = 3$; $h = 1$ and $\lambda_z = 2$) is presented in Figures (3.3 – 3.7).

Table 3.1 Material properties

Component	Material	E (GPa)	ρ (kg/m ³)
m_1	Titanium alloy	115	4515
m_2	Aluminum alloy	70	2715
c_1	Silicon carbide (SiC)	440	3210
c_2	Alumina	380	3800

It is apparent from Eq. (3.7) and Figures (3.2 – 3.6) that the bottom corner at the inner radius ($z = -h_i/2$, $r = 0$) is purely titanium alloy, the upper corner at the inner radius ($z = +h_i/2$, $r = 0$) is purely silicon carbide, the bottom corner at the outer radius ($z = -h_o/2$, $r = r_o - r_i$) is purely aluminum alloy and the upper corner at the outer radius ($z = +h_o/2$, $r = r_o - r_i$) is purely alumina. The basic material properties of the plate are presented in Table 1. The Poisson's ratio is assumed to be constant ($\nu = 0.3$).

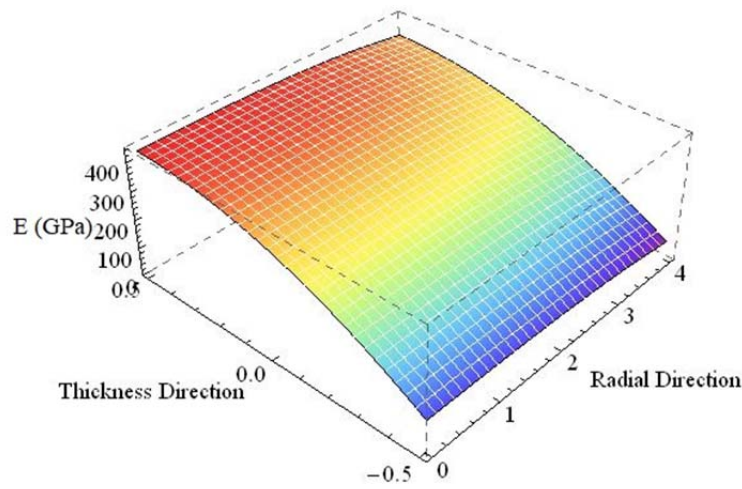


Figure 3. 3. Modulus of elasticity

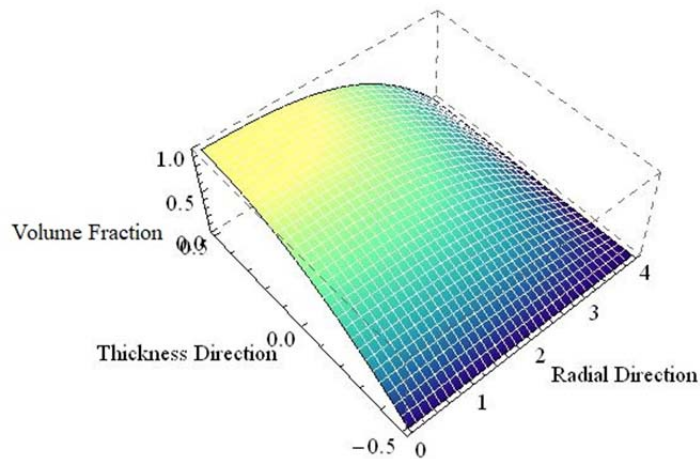


Figure 3. 4. Volume fraction of SiC

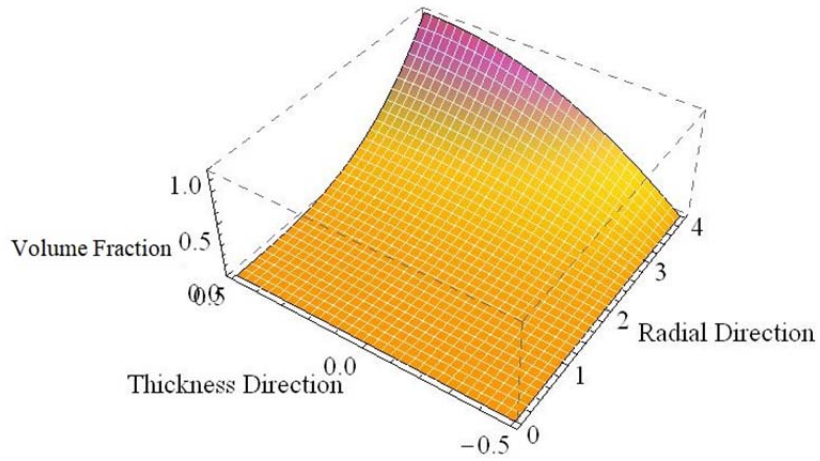


Figure 3. 5. Volume fraction of Alumina

($\lambda_r = 0$ and $\lambda_z = 0$) correspond to an isotropic homogeneous material, ($\lambda_z = 0$) corresponds to a radially FG material and ($\lambda_r = 0$) correspond to FG material through the thickness.

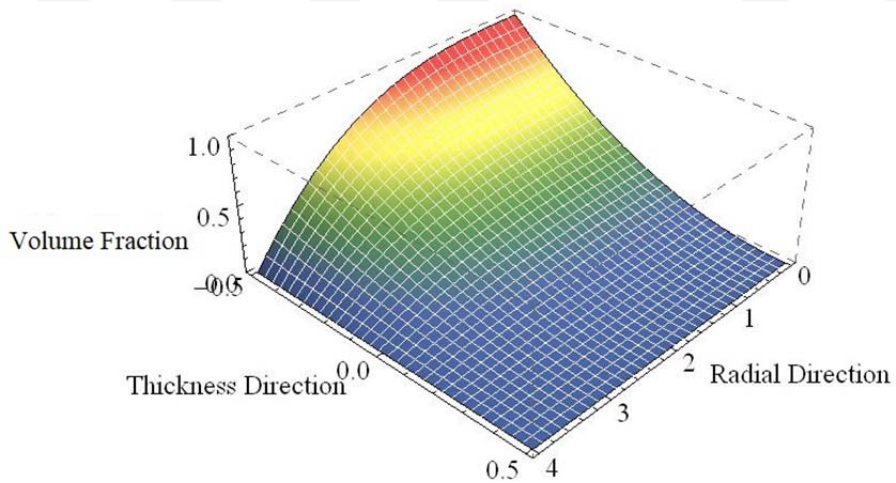


Figure 3. 6. Volume fraction of Titanium alloy

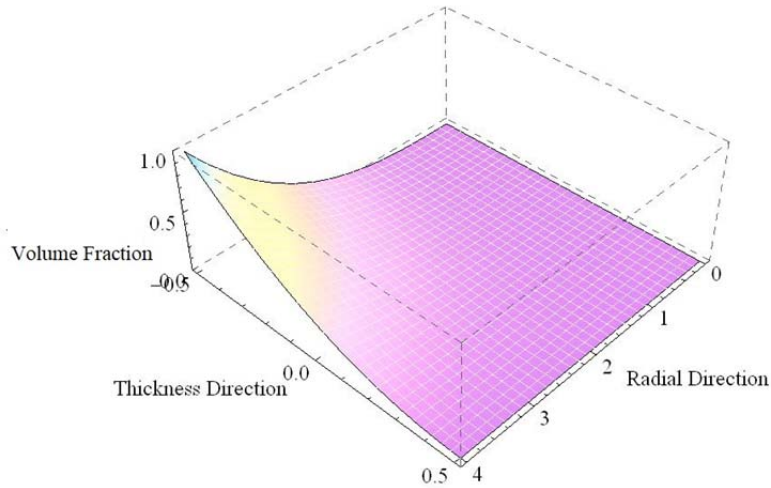


Figure 3. 7. Volume fraction of Aluminum alloy

3.2. Axisymmetric Bending of 2D-FG Thick Circular and Annular Plates with Variable Thickness

In the present thesis, an effective and accurate numerical approach is applied to the axisymmetric bending of 2D-FG Mindlin-Reissner circular and annular plates with variable thickness. The material properties are assumed to vary continuously both in thickness and radial directions. Governing equations are carried out by the principle of minimum total potential energy based on the FSDT. Next, the governing equations are converted to a set of ordinary differential equations (ODEs). Obtained canonical equations are solved numerically by the CFM. The fifth-order Runge–Kutta (RK5) algorithm has been employed in the numerical solution process. The novelty of this study is the infusion of this method to the axisymmetric bending of a wide range of solid or annular plates, with linear or non-linear thickness function, radially FG, FG in the thickness direction or 2D-FG, without any restrictions. The suggested model allows the presence of continuous as well as discrete functions.

3.2.1. Governing Equations

The plate is considered to have a variable thickness. Variation of the plate thickness is described by the following function.

$$h(r) = h_i(1 - n\alpha)^{\lambda_h} \quad (3.9)$$

$$n = 1 - \left(\frac{h_i}{h_0}\right)^{\frac{1}{\lambda_h}} \quad (3.10)$$

$$\alpha = \frac{r}{r_0 - r_i} \quad (3.11)$$

where h_i and h_0 are the thickness of the plate at inner and outer radii, and λ_h is geometric constant. Governing equations are obtained based on the FSDT (see Wang et al. (2000)). The displacements field can be presented as follows:

$$U_r = u(r) + z \chi(r); \quad U_z = w(r); \quad -\frac{h(r)}{2} \leq z \leq \frac{h(r)}{2} \quad (3.12)$$

where $u(r)$ is radial displacement, $w(r)$ is the transverse deflection of a point at the midplane ($z = 0$) and $\chi(r)$ is the rotation.

$$\varepsilon_{rr} = \frac{du}{dr} = u' \quad (3.13)$$

$$\varepsilon_{\theta\theta} = \frac{u}{r_i + r} \quad (3.14)$$

$$\chi_{rr} = \frac{d\chi}{dr} = \chi' \quad (3.15)$$

$$\chi_{\theta\theta} = \frac{\chi}{r_i + r} \quad (3.16)$$

$$\gamma_{rz} = \frac{\partial U_r}{\partial z} + \frac{\partial U_z}{\partial r} = \chi + \frac{dw}{dr} = \chi + w' \quad (3.17)$$

where

$$\frac{d(\cdot)}{dr} = (\cdot)' \quad (3.18)$$

The linear relationship between the stresses and strains of a point of the considered plate can be given by Hooke's law as follows:

$$\sigma_{rr} = \frac{E(z, r)}{1 - \nu^2} (\varepsilon_{rr} + \nu \varepsilon_{\theta\theta} + z \chi_{rr} + z \nu \chi_{\theta\theta}) \quad (3.19)$$

$$\sigma_{\theta\theta} = \frac{E(z, r)}{1 - \nu^2} (\varepsilon_{\theta\theta} + \nu \varepsilon_{rr} + z \chi_{\theta\theta} + z \nu \chi_{rr}) \quad (3.20)$$

$$\tau_{rz} = \frac{E(z, r)}{2(1 + \nu)} \gamma_{rz} \quad (3.21)$$

with the aid of those equations the relationship between the internal forces and the strains can be derived as follows:

$$\begin{aligned}
N_{rr} &= \int_{-h(r)/2}^{+h(r)/2} \sigma_{rr} dz \\
&= \int_{-h(r)/2}^{+h(r)/2} \frac{E(z, r)}{1 - \nu^2} (\varepsilon_{rr} + \nu \varepsilon_{\theta\theta} + z \chi_{rr} + z \nu \chi_{\theta\theta}) dz
\end{aligned} \tag{3.22}$$

$$\begin{aligned}
N_{\theta\theta} &= \int_{-h(r)/2}^{+h(r)/2} \sigma_{\theta\theta} dz \\
&= \int_{-h(r)/2}^{+h(r)/2} \frac{E(z, r)}{1 - \nu^2} (\varepsilon_{\theta\theta} + \nu \varepsilon_{rr} + z \chi_{\theta\theta} + z \nu \chi_{rr}) dz
\end{aligned} \tag{3.23}$$

$$\begin{aligned}
M_{rr} &= \int_{-h(r)/2}^{+h(r)/2} \sigma_{rr} z dz \\
&= \int_{-h(r)/2}^{+h(r)/2} \frac{E(z, r)}{1 - \nu^2} (\varepsilon_{rr} + \nu \varepsilon_{\theta\theta} + z \chi_{rr} \\
&\quad + z \nu \chi_{\theta\theta}) z dz
\end{aligned} \tag{3.24}$$

$$\begin{aligned}
M_{\theta\theta} &= \int_{-h(r)/2}^{+h(r)/2} \sigma_{\theta\theta} z dz \\
&= \int_{-h(r)/2}^{+h(r)/2} \frac{E(z, r)}{1 - \nu^2} (\varepsilon_{\theta\theta} + \nu \varepsilon_{rr} + z \chi_{\theta\theta} \\
&\quad + z \nu \chi_{rr}) z dz
\end{aligned} \tag{3.25}$$

$$Q_{rz} = \int_{-h(r)/2}^{+h(r)/2} k_s \tau_{rz} dz = \int_{-h(r)/2}^{+h(r)/2} k_s \frac{E(z,r)}{2(1+\nu)} \gamma_{rz} dz \quad (3.26)$$

where N_{rr} and $N_{\theta\theta}$ are radial and circumferential components of internal forces, M_{rr} and $M_{\theta\theta}$ are radial and circumferential components of internal moments and Q_{rz} is the shear force. The plate constitutive equations are obtained by integrations of Eqs. (3.22-3.26) and presented as follows:

$$N_{rr} = A_{11}u' + A_{12} \frac{u}{r_i + r} + B_{11}\chi' + B_{12} \frac{\chi}{r_i + r} \quad (3.27)$$

$$N_{\theta\theta} = A_{11} \frac{u}{r_i + r} + A_{12}u' + B_{11} \frac{\chi}{r_i + r} + B_{12} \chi' \quad (3.28)$$

$$M_{rr} = B_{11}u' + B_{12} \frac{u}{r_i + r} + D_{11} \chi' + D_{12} \frac{\chi}{r_i + r} \quad (3.29)$$

$$M_{\theta\theta} = B_{11} \frac{u}{r_i + r} + B_{12}u' + D_{11} \frac{\chi}{r_i + r} + D_{12} \chi' \quad (3.30)$$

$$Q_{rz} = A_{55}(\chi + w') \quad (3.31)$$

where

$$A_{11} = \int_{-h(r)/2}^{+h(r)/2} \frac{E(z, r)}{1 - \nu^2} dz \quad (3.32)$$

$$A_{12} = \int_{-h(r)/2}^{+h(r)/2} \frac{\nu E(z, r)}{1 - \nu^2} dz = \nu A_{11} \quad (3.33)$$

$$B_{11} = \int_{-h(r)/2}^{+h(r)/2} \frac{E(z, r)}{1 - \nu^2} z dz \quad (3.34)$$

$$B_{12} = \int_{-h(r)/2}^{+h(r)/2} \frac{\nu E(z, r)}{1 - \nu^2} z dz = \nu B_{11} \quad (3.35)$$

$$D_{11} = \int_{-h(r)/2}^{+h(r)/2} \frac{E(z, r)}{1 - \nu^2} z^2 dz \quad (3.36)$$

$$D_{12} = \int_{-h(r)/2}^{+h(r)/2} \frac{\nu E(z, r)}{1 - \nu^2} z^2 dz = \nu D_{11} \quad (3.37)$$

$$A_{55} = k_s \int_{-h(r)/2}^{+h(r)/2} \frac{E(z, r)}{2(1 + \nu)} dz = k_s \int_{-h(r)/2}^{+h(r)/2} G(z, r) dz \quad (3.38)$$

where k_s is the shear correction factor and $G(z, r)$ is the shear modulus. To carry out the governing equations the principle of minimum total potential energy is applied. The total potential energy of an axisymmetric plate is:

$$\Pi_t = \Pi_i + \Pi_e \quad (3.39)$$

The potential energy of the internal forces is as follows:

$$\Pi_i = \frac{1}{2} \int_0^r \int_0^{2\pi} (N_{rr} \varepsilon_{rr} + N_{\theta\theta} \varepsilon_{\theta\theta} + M_{rr} \chi_{rr} + M_{\theta\theta} \chi_{\theta\theta} + Q_{rz} \gamma_{rz}) dA \quad (3.40)$$

The potential energy of the external forces is given as:

$$\Pi_e = - \int_0^r \int_0^{2\pi} (p_r u + p_z w) dA \quad (3.41)$$

where p_z is arbitrary distributed transverse, p_r is arbitrary distributed shear load and

$$dA = y d\theta dr ; y = r_i + r \quad (3.42)$$

The total potential energy for the considered plate can be defined as:

$$\Pi_t = 2\pi \int_0^r \left[\frac{1}{2} (N_{rr}\varepsilon_{rr} + N_{\theta\theta}\varepsilon_{\theta\theta} + M_{rr}\chi_{rr} + M_{\theta\theta}\chi_{\theta\theta} + Q_{rz}\gamma_{rz}) - (p_r u + p_z w) \right] y dr \quad (3.43)$$

In this case the minimum total potential energy can be given by

$$\delta \Pi_t = 0 \quad (3.44)$$

$$\delta \int_0^r L dr = 0 \quad (3.45)$$

where L is the Lagrangian function function and may be written as:

$$L = \left[\frac{1}{2} (N_{rr}\varepsilon_{rr} + N_{\theta\theta}\varepsilon_{\theta\theta} + M_{rr}\chi_{rr} + M_{\theta\theta}\chi_{\theta\theta} + Q_{rz}\gamma_{rz}) - (p_r u + p_z w) \right] y \quad (3.46)$$

For a set of ODEs, when the related derivatives are written on the left side and all other terms are written on the right side of the equation, those equations are called the canonical equations. Canonical equations of the considered plate are obtained for the first time in this thesis.

The canonically conjugate momentums to the coordinates (u, w, χ) are defined by:

$$P_1 = \frac{\partial L}{\partial u'} = y \left(A_{11} u' + A_{12} \frac{u}{y} + B_{11} \chi' + B_{12} \frac{\chi}{y} \right) \quad (3.47)$$

$$P_2 = \frac{\partial L}{\partial w'} = y A_{55} (\chi + w') \quad (3.48)$$

$$P_3 = \frac{\partial L}{\partial \chi'} = y \left(B_{11} u' + B_{12} \frac{u}{y} + D_{11} \chi' + D_{12} \frac{\chi}{y} \right) \quad (3.49)$$

By considering Eqs. (3.27 – 3.31), these Eqs. (3.47 – 3.49) can be rewritten as:

$$P_1 = y N_{rr} \quad (3.50)$$

$$P_2 = y Q_{rz} \quad (3.51)$$

$$P_3 = y M_{rr} \quad (3.52)$$

The Legendre transformation of the Lagrangian is called Hamiltonian (H) and it can be written for the considered problem as follows:

$$H = y(N_{rr}u' + Q_{rz}w' + M_{rr}\chi') - L \quad (3.53)$$

the canonical equations of Hamilton could be derived as:

$$P_1' = -\frac{\partial H}{\partial u} \quad ; \quad P_2' = -\frac{\partial H}{\partial w} \quad ; \quad P_3' = -\frac{\partial H}{\partial \chi} \quad (3.54)$$

$$P_1' = A_{11} \frac{u}{y} + A_{12}u' + B_{11} \frac{\chi}{y} + B_{12}\chi' - p_r y \quad (3.55)$$

$$P'_2 = -p_z y \quad (3.56)$$

$$P'_3 = B_{11} \frac{u}{y} + B_{12} u' + D_{11} \frac{\chi}{y} + D_{12} \chi' - y M_{rr} + y Q_{rz} \quad (3.57)$$

The derivatives of the canonically conjugate momentums can be given as:

$$P'_1 = y' N_{rr} + y N'_{rr} \quad (3.58)$$

$$P'_2 = y' Q_{rz} + y Q'_{rz} \quad (3.59)$$

$$P'_3 = y' M_{rr} + y M'_{rr} \quad (3.60)$$

Substitution of the Eqs. (3.50 - 3.52) into Eqs. (3.47 - 3.49) and Eqs. (3.58 - 3.60) into Eqs. (3.55 - 3.57) lead to the following governing ordinary differential equations of the considered plate.

$$\frac{du}{dr} = \frac{D_{11} N_{rr} - B_{11} M_{rr}}{A_{11} D_{11} - B_{11}^2} - v \frac{u}{r_i + r} \quad (3.61)$$

$$\frac{dw}{dr} = \frac{Q_{rz}}{A_{55}} - \chi \quad (3.62)$$

$$\frac{d\chi}{dr} = \frac{A_{11} M_{rr} - B_{11} N_{rr}}{A_{11} D_{11} - B_{11}^2} - v \frac{\chi}{r_i + r} \quad (3.63)$$

$$\frac{dN_{rr}}{dr} = \frac{1 - \nu^2}{(r_i + r)^2} (A_{11} u + B_{11} \chi) + \frac{\nu - 1}{r_i + r} N_{rr} - p_r \quad (3.64)$$

$$\frac{dQ_{rz}}{dr} = -\frac{1}{r_i + r} Q_{rz} - p_z \quad (3.65)$$

$$\frac{dM_{rr}}{dr} = Q_{rz} + \frac{1 - \nu^2}{(r_i + r)^2} (B_{11} u + D_{11} \chi) + \frac{\nu - 1}{r_i + r} M_{rr} \quad (3.66)$$

3.2.2. Application of the CFM

To investigate the axisymmetric bending of the considered structure the CFM is applied. The main principle of this technique is that it reduces the two-point boundary value problems (BVPs) down to initial value problems (IVPs) (See Mengi (1993)). It is an effective and accurate strategy when applied to the present class of problem.

The governing Eqs. (3.61 - 3.66) can be rewritten in matrix form in Eq (3.67). In the following equation $[\Psi]$ is the differential transition matrix, $\{\mathbf{Y}\}$ is the state vector and $\{\mathbf{F}\}$ is the load vector for the considered problem.

$$\underbrace{\begin{Bmatrix} u' \\ w' \\ \chi' \\ N'_{rr} \\ Q'_{rz} \\ M'_{rr} \end{Bmatrix}}_{\{\mathbf{Y}'\}} = \underbrace{\begin{bmatrix} \psi_{11} & 0 & 0 & \psi_{14} & 0 & \psi_{16} \\ 0 & 0 & \psi_{23} & 0 & \psi_{25} & 0 \\ 0 & 0 & \psi_{33} & \psi_{34} & 0 & \psi_{36} \\ \psi_{41} & 0 & \psi_{43} & \psi_{44} & 0 & 0 \\ 0 & 0 & 0 & 0 & \psi_{55} & 0 \\ \psi_{61} & 0 & \psi_{63} & 0 & \psi_{65} & \psi_{66} \end{bmatrix}}_{[\Psi]} \underbrace{\begin{Bmatrix} u \\ w \\ \chi \\ N_{rr} \\ Q_{rz} \\ M_{rr} \end{Bmatrix}}_{\{\mathbf{Y}\}} + \underbrace{\begin{Bmatrix} 0 \\ 0 \\ 0 \\ -p_r \\ -p_z \\ 0 \end{Bmatrix}}_{\{\mathbf{F}\}} \quad (3.67)$$

To find the solution we know that we have to determine the boundary conditions. In this thesis, the following boundary conditions are considered.

- **Solid circular plate ($r_i = 0$)**

- (a) Clamped (C):

$$u = 0; \quad \chi = 0; \quad Q_{rz} = 0 \quad \text{at } r = 0 \text{ (Symmetry boundary conditions)} \quad (3.68)$$

$$u = 0; \quad w = 0; \quad \chi = 0 \quad \text{at } r = r_o \quad (3.69)$$

- (b) Simply supported (S):

$$u = 0; \quad \chi = 0; \quad Q_{rz} = 0 \quad \text{at } r = 0 \text{ (Symmetry boundary conditions)} \quad (3.70)$$

$$u = 0; \quad w = 0; \quad M_{rr} = 0 \quad \text{at } r = r_o \quad (3.71)$$

- (c) Roller supported (R):

$$u = 0; \quad \chi = 0; \quad Q_{rz} = 0 \quad \text{at } r = 0 \text{ (Symmetry boundary conditions)} \quad (3.72)$$

$$w = 0; \quad N_{rr} = 0; \quad M_{rr} = 0 \quad \text{at } r = r_o \quad (3.73)$$

- **Annular plate with inner radius r_i , and outer radius r_o**

- (a) Clamped – clamped (C – C):

$$u = 0; \quad w = 0; \quad \chi = 0 \quad \text{at } r = 0 \quad (3.74)$$

$$u = 0; \quad w = 0; \quad \chi = 0 \quad \text{at } r = r_o - r_i \quad (3.75)$$

(b) Simply supported – clamped (S – C):

$$u = 0; \quad w = 0; \quad M_{rr} = 0 \quad \text{at } r = 0 \quad (3.76)$$

$$u = 0; \quad w = 0; \quad \chi = 0 \quad \text{at } r = r_o - r_i \quad (3.77)$$

(c) Clamped – simply supported (C – S):

$$u = 0; \quad w = 0; \quad \chi = 0 \quad \text{at } r = 0 \quad (3.78)$$

$$u = 0; \quad w = 0; \quad M_{rr} = 0 \quad \text{at } r = r_o - r_i \quad (3.79)$$

(d) Simply – simply supported (S – S):

$$u = 0; \quad w = 0; \quad M_{rr} = 0 \quad \text{at } r = 0 \quad (3.80)$$

$$u = 0; \quad w = 0; \quad M_{rr} = 0 \quad \text{at } r = r_o - r_i \quad (3.81)$$

(e) Clamped – free (C – F):

$$u = 0; \quad w = 0; \quad \chi = 0 \quad \text{at } r = 0 \quad (3.82)$$

$$N_{rr} = 0; \quad Q_{rz} = 0; \quad M_{rr} = 0 \quad \text{at } r = r_o - r_i \quad (3.83)$$

The state vector of the considered problem is

$$\begin{Bmatrix} Y_1 \\ Y_2 \\ Y_3 \\ Y_4 \\ Y_5 \\ Y_6 \end{Bmatrix} = \begin{Bmatrix} u \\ w \\ \chi \\ N_{rr} \\ Q_{rz} \\ M_{rr} \end{Bmatrix} \quad (3.84)$$

The canonical equations for the considered structure are

$$Y_1' = \psi_{11}Y_1 + \psi_{14}Y_4 + \psi_{16}Y_6 \quad (3.85)$$

$$Y_2' = \psi_{23}Y_3 + \psi_{25}Y_5 \quad (3.86)$$

$$Y_3' = \psi_{33}Y_3 + \psi_{34}Y_4 + \psi_{36}Y_6 \quad (3.87)$$

$$Y_4' = \psi_{41}Y_1 + \psi_{43}Y_3 + \psi_{44}Y_4 - p_r \quad (3.88)$$

$$Y_5' = \psi_{55}Y_5 - p_z \quad (3.89)$$

$$Y_6' = \psi_{61}Y_1 + \psi_{63}Y_3 + \psi_{65}Y_5 + \psi_{66}Y_6 \quad (3.90)$$

The general solution for the system of Eqs. (3.85 - 3.90) is:

$$\{\mathbf{Y}\} = \sum_{m=1}^6 C_m [\mathbf{U}^{(m)}] + \{\mathbf{V}\} \quad (3.91)$$

where $[\mathbf{U}^{(m)}]$ are linearly independent complementary solutions. For IVPs m^{th} component is equal to 1, whereas all the others are 0. C_m are constants to be obtained via boundary conditions. $\{\mathbf{V}\}$ is the particular solution with all 0 initial conditions. For the numerical solution of the above system of equations the RK5 algorithm is chosen. The solutions can be calculated for any desired number of collocation points through the radial direction.

3.3. Dynamic Analysis 2D-FG Thick Circular and Annular Plates with Variable Thickness

The dynamic analysis of 2D-FG Mindlin-Reissner circular and annular plates of variable thickness is investigated by the CFM, a powerful and efficient approach in the Laplace space. A powerful inverse algorithm is applied to retransfer the results from the Laplace space. The material properties are graded in both thickness and radial directions. The thickness of the plate is considered to be radially varying. The influence of shear deformation is considered in the formulation and the damping model of Kelvin is used in the damped forced vibration analysis.

3.3.1. Governing Equations

The plate is considered to have a variable thickness. Variation of the plate thickness is given in Eq. (3.9).

In the dynamic case the displacements field can be presented as follows (See Reddy (1984)):

$$U_r = u(r, t) + z \chi(r, t); \quad U_z = w(r, t); \quad (3.92)$$

where $u(r, t)$ is radial displacement, $w(r, t)$ is the transverse deflection of a point at the midplane ($z = 0$) and $\chi(r, t)$ is the rotation.

$$\varepsilon_{rr} = \frac{\partial u}{\partial r} = u' \quad (3.93)$$

$$\varepsilon_{\theta\theta} = \frac{u}{r_i + r} \quad (3.94)$$

$$\chi_{rr} = \frac{\partial \chi}{\partial r} = \chi' \quad (3.95)$$

$$\chi_{\theta\theta} = \frac{\chi}{r_i + r} \quad (3.96)$$

$$\gamma_{rz} = \frac{\partial U_r}{\partial z} + \frac{\partial U_z}{\partial r} = \chi + \frac{\partial w}{\partial r} = \chi + w' \quad (3.97)$$

where

$$\frac{\partial(\cdot)}{\partial r} = (\cdot)' \quad (3.98)$$

The linear relationship between the stresses and strains of a point of the considered plate is be given in Eqs. (3.19 – 3.21). The relationship between the

internal forces and the strains can be derived as in Eqs. (3.22 – 3.26). The plate constitutive equations are given by Eqs. (3.27 - 3.31). The total potential energy of an axisymmetric plate is given in Eq. (3.43).

The Langrangian for a system can be defined by:

$$L = T - \Pi_t \quad (3.99)$$

$$\delta \int_{t_1}^{t_2} L dt = 0 \quad (3.100)$$

where T is the kinetic energy and can be obtained as:

$$T = \frac{1}{2} \int_0^{2\pi} \int_0^r \int_{-h(r)/2}^{+h(r)/2} (\rho(r, z)(\dot{U}_r^2 + \dot{U}_z^2)) dz dA \quad (3.101)$$

where

$$(\dot{\cdot}) = \frac{\partial(\cdot)}{\partial t} \quad (3.102)$$

By substituting the value of dA which is given in Eq. (3.42), the kinetic energy can be derived as follows:

$$T = 2\pi \int_0^r \int_{-h(r)/2}^{+h(r)/2} \frac{1}{2} (\rho(r, z)(\dot{U}_r^2 + \dot{U}_z^2)) y dz dr \quad (3.103)$$

The values of \dot{U}_r^2 and \dot{U}_z^2 are described as:

$$\dot{U}_r^2 = (\dot{u} + z \dot{\chi})^2 = \dot{u}^2 + 2\dot{u} z \dot{\chi} + z^2 \dot{\chi}^2 \quad (3.104)$$

$$\dot{U}_z^2 = \dot{w}^2 \quad (3.105)$$

Substituting Eqs. (3.104 – 3.105) into Eq. (3.103) gives the kinetic energy equation as:

$$T = 2\pi \int_0^r \frac{1}{2} (I_{11}(\dot{u}^2 + \dot{w}^2) + 2 I_{12} \dot{u} \dot{\chi} + I_{22} \dot{\chi}^2) y dr \quad (3.106)$$

where

$$I_{11} = \int_{-h(r)/2}^{+h(r)/2} \rho(r, z) dz \quad (3.107)$$

$$I_{12} = \int_{-h(r)/2}^{+h(r)/2} \rho(r, z) z dz \quad (3.108)$$

$$I_{22} = \int_{-h(r)/2}^{+h(r)/2} \rho(r, z) z^2 dz \quad (3.109)$$

The canonically conjugate momentums to the coordinates (u, w, χ) are defined in Eqs. (3.47 – 3.49). The generalized momentum can be derived as:

$$P_1' = \frac{d}{dt} \frac{\partial L}{\partial \dot{u}} - \frac{\partial L}{\partial u} \quad ; \quad P_2' = \frac{d}{dt} \frac{\partial L}{\partial \dot{w}} - \frac{\partial L}{\partial w} \quad ; \quad P_3' = \frac{d}{dt} \frac{\partial L}{\partial \dot{\chi}} - \frac{\partial L}{\partial \chi} \quad (3.110)$$

$$P_1' = A_{11} \frac{u}{y} + A_{12} u' + B_{11} \frac{\chi}{y} + B_{12} \chi' - p_r y + I_{11} \frac{\partial^2 u}{\partial t^2} y + I_{12} \frac{\partial^2 \chi}{\partial t^2} y \quad (3.111)$$

$$P_2' = -p_z y + I_{11} \frac{\partial^2 w}{\partial t^2} y \quad (3.112)$$

$$P_3' = B_{11} \frac{u}{y} + B_{12} u' + D_{11} \frac{\chi}{y} + D_{12} \chi' - y M_{rr} + y Q_{rz} + I_{12} \frac{\partial^2 u}{\partial t^2} y + I_{22} \frac{\partial^2 \chi}{\partial t^2} y \quad (3.113)$$

The derivatives of the canonically conjugate momentums can be given as:

$$P_1' = y' N_{rr} + y N'_{rr} \quad (3.114)$$

$$P_2' = y' Q_{rz} + y Q'_{rz} \quad (3.115)$$

$$P_3' = y' M_{rr} + y M'_{rr} \quad (3.116)$$

Substitution of the Eqs. (3.50 - 3.52) into Eqs. (3.47 - 3.49) and Eqs. (3.114 - 3.116) into Eqs. (3.111 - 3.113) give the following governing ordinary differential

equations of the considered plate. Canonical equations of the considered plate are obtained for the first time in this thesis.

$$\frac{\partial u}{\partial r} = \frac{D_{11}N_{rr} - B_{11}M_{rr}}{A_{11}D_{11} - B_{11}^2} - v \frac{u}{r_i + r} \quad (3.117)$$

$$\frac{\partial w}{\partial r} = \frac{Q_{rz}}{A_{55}} - \chi \quad (3.118)$$

$$\frac{\partial \chi}{\partial r} = \frac{A_{11}M_{rr} - B_{11}N_{rr}}{A_{11}D_{11} - B_{11}^2} - v \frac{\chi}{r_i + r} \quad (3.119)$$

$$\begin{aligned} \frac{\partial N_{rr}}{\partial r} = & \frac{1 - v^2}{(r_i + r)^2} (A_{11} u + B_{11} \chi) + \frac{v - 1}{r_i + r} N_{rr} - p_r + I_{11} \frac{\partial^2 u}{\partial t^2} \\ & + I_{12} \frac{\partial^2 \chi}{\partial t^2} \end{aligned} \quad (3.120)$$

$$\frac{\partial Q_{rz}}{\partial r} = -\frac{1}{r_i + r} Q_{rz} - p_z + I_{11} \frac{\partial^2 w}{\partial t^2} \quad (3.121)$$

$$\begin{aligned} \frac{\partial M_{rr}}{\partial r} = & Q_{rz} + \frac{1 - v^2}{(r_i + r)^2} (B_{11} u + D_{11} \chi) + \frac{v - 1}{r_i + r} M_{rr} + I_{12} \frac{\partial^2 u}{\partial t^2} \\ & + I_{22} \frac{\partial^2 \chi}{\partial t^2} \end{aligned} \quad (3.122)$$

3.3.2. Laplace Transform of the Governing Equations

The Laplace transform ($\mathcal{L}\{f(t)\}$) of a time-dependent function ($f(t)$) for $t > 0$ is:

$$\mathcal{L}\{f(t)\} = \bar{F}(s) = \int_0^{\infty} e^{-st} f(t) dt \quad (3.123)$$

where "s" is the parameter of Laplace transform. The Laplace transform of the first derivative of a time-dependent function is:

$$\mathcal{L}\{f'(t)\} = \int_0^{\infty} e^{-st} f'(t) dt = \lim_{p \rightarrow \infty} \int_0^p e^{-st} f'(t) dt \quad (3.124)$$

By using integration by parts, we have

$$\begin{aligned} \lim_{p \rightarrow \infty} \int_0^p e^{-st} f'(t) dt &= \lim_{p \rightarrow \infty} \left\{ e^{-st} f(t) \Big|_0^p + s \int_0^p e^{-st} f(t) dt \right\} \\ \mathcal{L}\{f'(t)\} &= \lim_{p \rightarrow \infty} \left\{ e^{-sp} f(p) - f(0) + s \int_0^p e^{-st} f(t) dt \right\} \quad (3.125) \\ \mathcal{L}\{f'(t)\} &= s \int_0^p e^{-st} f(t) dt - f(0) = s\bar{F}(s) + f(0) \end{aligned}$$

The Laplace transform of the second derivative of a time-dependent function Spiegel (1965) can be obtained as follows:

$$\mathcal{L}\{f''(t)\} = s^2 \bar{F}(s) + s f(0) + \dot{f}(0) \quad (3.126)$$

The Laplace transformation of the inertias are given as:

$$\mathcal{L} \left[I_{11} \frac{\partial^2 u}{\partial t^2} \right] = I_{11} \left(s^2 \bar{u} + s u(r, 0) + \frac{\partial u(r, 0)}{\partial t} \right) \quad (3.127)$$

$$\mathcal{L} \left[I_{11} \frac{\partial^2 w}{\partial t^2} \right] = I_{11} \left(s^2 \bar{w} + s w(r, 0) + \frac{\partial w(r, 0)}{\partial t} \right) \quad (3.128)$$

$$\mathcal{L} \left[I_{12} \frac{\partial^2 u}{\partial t^2} \right] = I_{12} \left(s^2 \bar{u} + s u(r, 0) + \frac{\partial u(r, 0)}{\partial t} \right) \quad (3.129)$$

$$\mathcal{L} \left[I_{12} \frac{\partial^2 \chi}{\partial t^2} \right] = I_{12} \left(s^2 \bar{\chi} + s \chi(r, 0) + \frac{\partial \chi(r, 0)}{\partial t} \right) \quad (3.130)$$

$$\mathcal{L} \left[I_{22} \frac{\partial^2 \chi}{\partial t^2} \right] = I_{22} \left(s^2 \bar{\chi} + s \chi(r, 0) + \frac{\partial \chi(r, 0)}{\partial t} \right) \quad (3.131)$$

The second and third terms on the right-hand side of the Eqs. (3.127 – 3.131) are the initial conditions given for $t = 0$; in the present thesis, those initial conditions are considered to be zero. Eqs. (3.117 – 3.122) are transferred to the Laplace domain by using Eqs. (3.123 – 3.126). The transferred governing ordinary differential equations of the dynamic response of the problems to be tackled are presented as follows:

$$\frac{d\bar{u}}{dr} = \frac{D_{11}\bar{N}_{rr} - B_{11}\bar{M}_{rr}}{A_{11}D_{11} - B_{11}^2} - \nu \frac{\bar{u}}{r_i + r} \quad (3.132)$$

$$\frac{d\bar{w}}{dr} = \frac{\bar{Q}_{rz}}{A_{55}} - \bar{\chi} \quad (3.133)$$

$$\frac{d\bar{\chi}}{dr} = \frac{A_{11}\bar{M}_{rr} - B_{11}\bar{N}_{rr}}{A_{11}D_{11} - B_{11}^2} - v \frac{\bar{\chi}}{r_i + r} \quad (3.134)$$

$$\begin{aligned} \frac{d\bar{N}_{rr}}{dr} = & \frac{1 - v^2}{(r_i + r)^2} (A_{11} \bar{u} + B_{11} \bar{\chi}) + \frac{v - 1}{r_i + r} \bar{N}_{rr} - \bar{p}_r + I_{11}s^2\bar{u} \\ & + I_{12}s^2\bar{\chi} \end{aligned} \quad (3.135)$$

$$\frac{d\bar{Q}_{rz}}{dr} = -\frac{1}{r_i + r} \bar{Q}_{rz} - \bar{p}_z + I_{11}s^2\bar{w} \quad (3.136)$$

$$\begin{aligned} \frac{d\bar{M}_{rr}}{dr} = & \bar{Q}_{rz} + \frac{1 - v^2}{(r_i + r)^2} (B_{11} \bar{u} + D_{11} \bar{\chi}) + \frac{v - 1}{r_i + r} \bar{M}_{rr} + I_{12}s^2\bar{u} \\ & + I_{22}s^2\bar{\chi} \end{aligned} \quad (3.137)$$

3.3.3. Application of the CFM

To examine the dynamic response of the considered structure the CFM is applied to the governing equations in the Laplace space. The governing Eqs. (3.132 - 3.137) can be rewritten in matrix form in Eq (3.138). In the following equation $[\Psi]$ is the differential transition matrix, $\{\bar{\mathbf{Y}}\}$ is the state vector and $\{\bar{\mathbf{F}}\}$ is the load vector for the considered problem.

$$\frac{d}{dr} \{\bar{\mathbf{Y}}(r, s)\} = [\bar{\Psi}(r, s)] \{\bar{\mathbf{Y}}(r, s)\} + \{\bar{\mathbf{F}}(r, s)\} \quad (3.138)$$

The CFM transforms the solution of this BVPs to the solution of some IVPs. The boundary conditions are given in Eqs. (3.68 - 3.83). The general solution for the system of Eqs. (3.138) is:

$$\{\bar{\mathbf{Y}}(r, s)\} = \sum_{m=1}^6 C_m [\bar{\mathbf{U}}^{(m)}(r, s)] + \{\bar{\mathbf{V}}(r, s)\} \quad (3.139)$$

where $[\mathbf{U}^{(m)}]$ are linearly independent complementary solutions. For IVPs m^{th} component is equal to 1, whereas all the others are 0. $\{\mathbf{V}(r, s)\}$ is the particular solution with all 0 initial conditions. For the numerical solution of the above system of equations the RK5 algorithm is chosen. The solutions can be calculated for any desired number of collocation points through the radial direction.

Free vibration analysis is considered as a special case of forced vibration. In order to carry out the natural frequencies of the considered structures external loads and $\{\mathbf{V}(r, s)\}$ are assumed to be zero and the Laplace parameter is replaced with “ $i\omega$ ”. To obtain the values of C_m from the boundary conditions, simultaneous equations are carried out and the matrix of their coefficients is performed. Since the mass and stiffness matrix of the system are not obtained separately by the presented procedure the eigenvalues and eigenvectors of the problem are not calculated. Thus, the values of ω which make the determinant of coefficient's matrix zero are the natural frequencies of the structure.

3.3.4. Effect of Damping

To determine the viscoelastic behavior of the 2D-FG thick circular and annular plates the Kelvin damping model is used. The elastic viscoelastic analogy Boley and Weiner (2012) is used to treat the internal viscoelastic damping case. The relationship between deviatoric components of stress (σ_{ij}) and strain (e_{ij}) for the Kelvin viscoelastic model is:

$$\sigma_{ij} = 2G \left(e_{ij} + g \frac{de_{ij}}{dt} \right) \quad (3.140)$$

In order to investigate the viscoelastic transient response of the considered structures, elastic constant E is as follows:

$$E_v(r, z) = E(r, z)(1 + gs) \quad (3.141)$$

In this equations, E_v is viscoelastic constant, g is the coefficient of damping given by Temel et al. (2004).

In ANSYS, many forms of damping are available. In this thesis, mass damping is ignored. The coefficient of damping, g , is calculated from values of ξ and ω_1 by $g = \beta = 2 \xi / \omega_1$. ω_1 is the first fundamental frequency of the structure.

3.3.5. Numerical Inverse Laplace Transform Algorithm

To retransfer the obtained results from the Laplace domain to the time domain the modified Durbin's algorithm is employed. This algorithm is developed from Durbin's numerical inverse Laplace transform method (Durbin (1974), Temel and Şahan (2013), Eratlı et al. (2014)). The equations for Durbin's algorithm are given by:

$$f(t_j) \cong \frac{2e^{aj\Delta t}}{T} \left[-\frac{1}{2} \text{Re}\{\bar{F}(a)\} + \text{Re} \left\{ \sum_{k=0}^{N-1} (A(k) + i B(k)) e^{(i\frac{2\pi}{N})jk} \right\} \right] \quad (3.142)$$

$$A(k) = \sum_{l=0}^L \text{Re} \left\{ \bar{F} \left(a + i (k + l N) \frac{2\pi}{T} \right) \right\} \quad (3.143)$$

$$B(k) = \sum_{l=0}^L \text{Im} \left\{ \bar{F} \left(a + i \left(k + lN \right) \frac{2\pi}{T} \right) \right\} \quad (3.144)$$

where, i is the complex number, T is sampling time interval, N is the total number of equidistant sampling points ($N=2^m$: m being integer), $s_k = a + ik2\pi/T$ is k th Laplace transform parameter, $t_j = j\Delta t = jT/N$, ($j=0,1,2,\dots,N-1$). In Eq. (3.142), the second part of the equality between the brackets is

$$\left\{ \sum_{k=0}^{N-1} (A(k) + i B(k)) e^{i \left(\frac{2\pi}{N} \right) jk} \right\} \quad (3.145)$$

calculated by using a Fast Fourier Transform (FFT) sub-program ((Brigham, 1974)). Eq. (3.142) can also be modified as:

$$f(t_j) \cong \frac{2e^{aj\Delta t}}{T} \left[-\frac{1}{2} \text{Re} \{ \bar{F}(a) \} + \text{Re} \left\{ \sum_{k=0}^{N-1} (\bar{F}(s_k) L_k) e^{i \left(\frac{2\pi}{N} \right) jk} \right\} \right] \quad (3.146)$$

where, each term of discrete values that is calculated in the Laplace domain is modified by multiplying them with Lanczos (L_k) factor. These factors are given by:

$$L_k : \begin{cases} = 1 & , \quad k = 0 \\ = \text{Sin} \left(\frac{k\pi}{N} \right) / \left(\frac{k\pi}{N} \right) & , \quad k > 0 \end{cases} \quad (3.147)$$

In the modified inverse Laplace transform (Eq. (3.146)) which is obtained by multiplying the L_k factor, calculating the $A(k)$ and $B(k)$ terms are not required.

Therefore, this method requires less computation. Also, the second part of Eq. (3.146) is calculated with the aid of the FFT algorithm.

It should be noted that the selection of the appropriate values of parameters N , a and T are critical in order to achieve the desired accuracy in the inverse transform. In the literature, it is indicated that setting the value of T and choosing the value of a multiplied by $T(aT)$ in between $5 \leq aT \leq 10$ yields the value of a necessary for the required precision. For the numerical examples presented in this paper the value of ' aT ' is taken as '6'.





4. RESULTS AND DISCUSSIONS

In this section, numerical results of the axisymmetric bending, free vibration, damped and undamped transient response of 2D-FG solid circular and annular plates are presented for various boundary conditions, volume fraction indices and thickness functions. Comparisons are presented with available literature and ANSYS (2013) in order to validate the results of the suggested method.

4.1. Axisymmetric Bending of 2D FG Mindlin-Reissner Circular Plates

4.1.1. FG through the Thickness Direction

Consider a solid FG circular plate of constant thickness h and radius r_o subjected to uniform transverse load (p_z). To verify the efficiency and accuracy of the model proposed, FG solid circular plate made of Aluminum/Zirconi ($E_r = 0.396$; $\nu = 0.288$) is considered as in Reddy et al. (1999) and Saidi et al. (2009). E_r describes the ratio of the modulus of elasticity of Aluminum and Zirconi. The boundary conditions are as in Eqs. (3.68 – 3.73). Non-dimensional maximum vertical displacement of clamped, simply supported and roller supported circular plates can be obtained by:

$$\tilde{w} = \frac{64D_c}{p_z r_o^4 w_{max}}; D_c = \frac{E_c h^3}{12(1 - \nu^2)} \quad (4.1)$$

Maximum vertical displacements are presented for various boundary conditions, thickness radius ratios and several values of λ_z . Obtained results are compared with exact results which were given by Reddy et al. (1999), those of Saidi et al. (2009) and results of ANSYS in Tables (4.1 – 4.3). To model this problem in ANSYS, 100 layers are defined through the thickness of the plate. Mechanical properties of those layers vary gradually through the thickness direction based on power law form.

Table 4.1. Comparison of the non-dimensional deflection, \bar{w} , $\nu = 0.288$, $E_r = 0.396$ ($E_r = E_m/E_c$) and $\lambda_r = 0$

Support Type	λ_z	References	Thickness-radius Ratio		
			0.05	0.1	0.2
Clamped	0	Exact ^a	2.5540	2.6390	2.9790
		Saidi et al. (2009)	2.5535	2.6382	2.9748
		ANSYS	2.5536	2.6387	2.9793
		Present Study	2.5541	2.6400	2.9804
		RE	3.92E-05	3.79E-04	4.70E-04
	2	Exact ^a	1.4020	1.4440	1.6130
		Saidi et al. (2009)	1.4020	1.4429	1.6063
		ANSYS	1.4048	1.4469	1.6149
		Present Study	1.4035	1.4458	1.6147
		RE	1.07E-03	1.25E-03	1.05E-03
	6	Exact ^a	1.2200	1.2570	1.4040
		Saidi et al. (2009)	1.2196	1.2552	1.3969
		ANSYS	1.2229	1.2592	1.4045
		Present Study	1.2213	1.2581	1.4059
		RE	1.07E-03	8.75E-04	1.35E-03

a: Reddy et al. (1999)

In this problem, the shear correction factor k_s is taken to be 5/6. It can be clearly observed in Tables (4.1 – 4.3) that the results of the presented method are in excellent agreement with those of the literature for any type of boundary condition. Relative error (RE) is calculated by:

$$RE = \left| \frac{\text{Exact} - \text{Present Study}}{\text{Exact}} \right| \quad (4.2)$$

Table 4.2 Comparison of the non-dimensional deflection, \bar{w} , $\nu = 0.288$, $E_r = 0.396$ ($E_r = E_m/E_c$) and $\lambda_z = 0$

Support Type	λ_z	References	Thickness-radius Ratio		
			0.05	0.1	0.2
Simply Supported	0	Exact ^a	10.3960	10.4810	10.8220
		Saidi et al. (2009)	10.3940	10.4790	10.8200
		ANSYS	10.3960	10.4812	10.8216
		Present Study	10.3985	10.4818	10.8231
		RE	2.40E-04	7.63E-05	1.02E-04
	2	Exact ^a	5.4970	5.5390	5.7080
		Saidi et al. (2009)	5.4969	5.5382	5.7028
		ANSYS	5.4588	5.5001	5.6994
		Present Study	5.5025	5.5452	5.7158
		RE	1.00E-03	1.12E-03	1.37E-03
	6	Exact ^a	4.8970	4.9460	5.0940
		Saidi et al. (2009)	4.8968	4.9445	5.0874
		ANSYS	4.8749	4.9158	5.0612
		Present Study	4.9140	4.9510	5.0990
		RE	3.47E-03	1.01E-03	9.82E-04

a: Reddy et al. (1999)

Analyzing these results reveals that the displacement values obtained by the present study are closer to exact values than those by ANSYS. For high values of thickness-radius ratio and λ_z accuracy of the results of ANSYS decreases. The influence of the thickness to radius ratio on the vertical deflection of clamped plate is greater than simply and roller supported plates. Shear correction factor, k_s , is proposed as $5/6$ by Reissner and $\pi^2/12$ by Mindlin (see Washizu (1975)).

Table 4.3 Comparison of the non-dimensional deflection, \bar{w} , $\nu = 0.288$, $E_r = 0.396$ ($E_r = E_m/E_c$) and $\lambda_r = 0$

Support Type	λ_z	References	Thickness-radius Ratio		
			0.05	0.1	0.2
Roller Supported	0	Exact ^a	10.3960	10.4810	10.8220
		Saidi et al. (2009)	10.3960	10.4810	10.8220
		ANSYS	10.3960	10.4812	10.8216
		Present Study	10.3985	10.4818	10.8231
		RE	2.40E-04	7.63E-05	1.02E-04
	2	Exact ^a	5.7140	5.7560	5.9250
		Saidi et al. (2009)	5.7133	5.7546	5.9194
		ANSYS	5.6845	5.7265	5.8945
		Present Study	5.7184	5.7611	5.9297
		RE	7.70E-04	8.86E-04	7.93E-04
	6	Exact ^a	4.9700	5.0070	5.1550
		Saidi et al. (2009)	4.9700	5.0058	5.1489
		ANSYS	4.9484	4.9847	5.1299
		Present Study	4.9557	5.0127	5.1599
		RE	2.88E-03	1.14E-03	9.51E-04

a: Reddy et al. (1999)

To model the considered plate in ANSYS, SHELL209 element is used. The plate is meshed into 200 elements in radial direction. This shell element has three nodes with three degrees of freedom (translation in x and y directions and rotation about the z- axis) in each node. The y-axis is the symmetry axis.

4.1.2. FG through the Radial Direction

Consider a RFG circular plate of uniform thickness and $r_o = 5$ m subjected to transverse uniform load of $p_z = 10$ N/m². The material properties are assumed to be graded only in the radial direction according to Eq. (3.7). Maximum vertical deflection results of clamped, simply supported and roller supported plate are

carried out for various values of λ_r and several thickness to radius ratios. Since there are no available results in the literature for the bending response of RFG thick circular plates, obtained results are compared with those of ANSYS. Comparison is tabulated in Table (4.4.).

Table 4.4 Comparison of the maximum deflection, $w_{max} \times 10^{-7}$ (m), of clamped, simply and roller supported moderately thick RFG circular plates ($\lambda_z=0$)

Support Type	λ_r	References	Thickness-radius Ratio		
			0.05	0.1	0.2
Clamped	1	ANSYS	7.7970	1.0310	0.1463
		Present Study	8.0130	1.0370	0.1470
	2	ANSYS	7.4820	0.9673	0.1369
		Present Study	7.5340	0.9740	0.1379
	3	ANSYS	7.2400	0.9355	0.1322
		Present Study	7.2990	0.9432	0.1333
Simply Supported	1	ANSYS	29.9200	3.7750	0.4892
		Present Study	30.0600	3.7930	0.4916
	2	ANSYS	27.4000	3.4570	0.4482
		Present Study	27.5300	3.4750	0.4504
	3	ANSYS	26.3300	3.3230	0.4306
		Present Study	26.4400	3.3360	0.4324
Roller Supported	1	ANSYS	29.9200	3.7750	0.4892
		Present Study	30.0600	3.7930	0.4916
	2	ANSYS	27.4000	3.4570	0.4482
		Present Study	27.5300	3.4740	0.4504
	3	ANSYS	26.3300	3.3230	0.4306
		Present Study	26.4400	3.3360	0.4324

In this case, the plate is also divided into 200 SHELL209 elements in the radial direction. To define the RFG materials 200 layers are defined in the radial direction. Variation form of the mechanical properties of these layers is as in Eq.

(3.7). In this problem, the shear correction factor k_s is taken to be $\pi^2/12$. The boundary conditions are given in Eqs. (3.68 – 3.73).

It is seen in Table 4.4. that the results of the present model are in excellent agreement with the results of ANSYS. The effect λ_r index on the vertical displacement of the clamped plate is less than on simply and roller supported RFG plates. As may be expected, comparison of results shows that increasing the λ_r index and thickness of the RFG plates, decrease the vertical deflection.

4.1.3. 2D-FG Circular Plate with Variable Thickness

The axisymmetric bending response of a 2D-FG circular plates is investigated. The plate is considered to have non-uniform thickness. Mechanical properties of the plate are considered to vary both in radial and thickness direction by a power law as given in Eq. (3.7). The radial coordinate dependent function of the thickness is given by Eq. (3.9). The radius of the plate, shear correction factor and the transverse load values are as in previous cases. Maximum vertical deflection values of the plate are obtained for various boundary conditions, λ_r , λ_z and λ_h values. The thickness of the plate is considered to be ($h_i = 2$ m) in inner radii and ($h_o = 1$ m) at outer radius.

The presented results for maximum vertical deflection are listed in Tables (4.5 – 4.6) for different volume fraction exponents. Furthermore, the influence of thickness variation functions on the axisymmetric response of 2D-FG solid circular plates is investigated. As expected, tabulated results demonstrate that material gradient indices and geometric constant has significant effects on the deflection of 2D-FG plates.

Table 4.5 Maximum deflection $w_{max} \times 10^{-9}$ (m) of clamped moderately thick 2D-FG circular plate.

λ_r	λ_z	Geometric constant (λ_h)			
		1	2	3	10
0	0	8.2880	8.2690	8.7470	8.9160
	2	2.4270	2.5300	2.5660	2.6170
	4	2.0820	2.1690	2.2000	2.2430
	6	1.9330	2.0140	2.0420	2.0820
1	0	6.7690	7.0480	7.1450	7.2840
	2	2.2330	2.3280	2.3600	2.4070
	4	1.9350	2.0170	2.0450	2.0860
	6	1.8050	1.8810	1.9070	1.9450
2	0	6.3290	6.5900	6.6810	6.8100
	2	2.2170	2.2610	2.3300	2.3390
	4	1.8870	1.9660	1.9940	2.0330
	6	1.7630	1.8370	1.8620	1.8990
3	0	6.1150	6.3670	6.4540	6.5790
	2	2.1380	2.2280	2.2600	2.3040
	4	1.8630	1.9410	1.9680	2.0070
	6	1.7410	1.8140	1.8400	1.8760

Moreover, the variations of vertical deflection and rotation ($z = 0$) along the radial direction are depicted in Figures (4.1 – 4.2) only for the clamped 2D-FG circular plate. According to Figures (4.1) and Tables (4.5 – 4.6) the deflection of the plate decreases as λ_r and λ_z increase. This response of the plate is related to the resulting increase in Young's modulus. But increasing the geometric constant λ_h , gives rise to the increase of the deflection.

Table 4.6. Maximum deflection $w_{max} \times 10^{-8}$ (m) of simply supported moderately thick 2D-FG circular plate.

λ_r	λ_z	Geometric constant (λ_i)			
		1	2	3	10
0	0	2.0430	2.1780	2.2260	2.2960
	2	0.5665	0.6040	0.6174	0.6367
	4	0.5054	0.5391	0.5510	0.5683
	6	0.5759	0.5076	0.5188	0.5351
1	0	1.5670	1.6710	1.7070	1.7600
	2	0.5117	0.5458	0.5578	0.5753
	4	0.4607	0.4914	0.5023	0.5181
	6	0.4356	0.4647	0.4750	0.4899
2	0	1.4320	1.5260	1.5390	1.6080
	2	0.4932	0.5260	0.5376	0.5544
	4	0.4453	0.4749	0.4855	0.5007
	6	0.4217	0.4497	0.4597	0.4741
3	0	1.3700	1.4600	1.4920	1.5390
	2	0.4844	0.5166	0.5280	0.5445
	4	0.4379	0.4671	0.4774	0.4924
	6	0.4150	0.4426	0.4524	0.4667

As it can be observed in Figure (4.2), plates with higher volume fraction exponents through radial and thickness directions have smaller rotation angles. Furthermore, the impact of λ_r on the axisymmetric response of 2D-FG solid circular plates is less noticeable than λ_z .

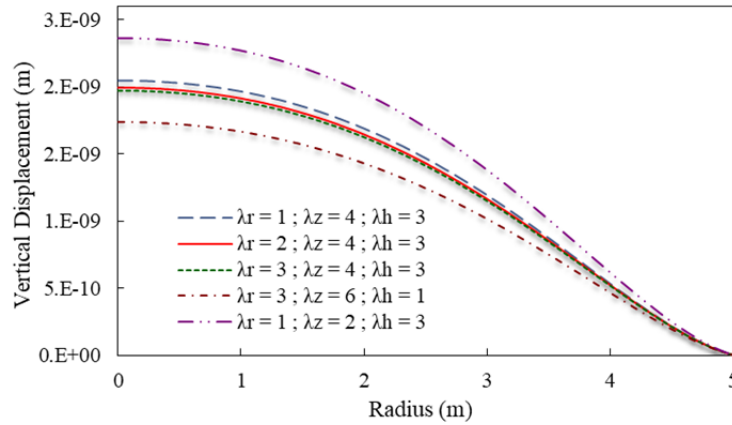


Figure 4. 1 Deflection of the clamped plate

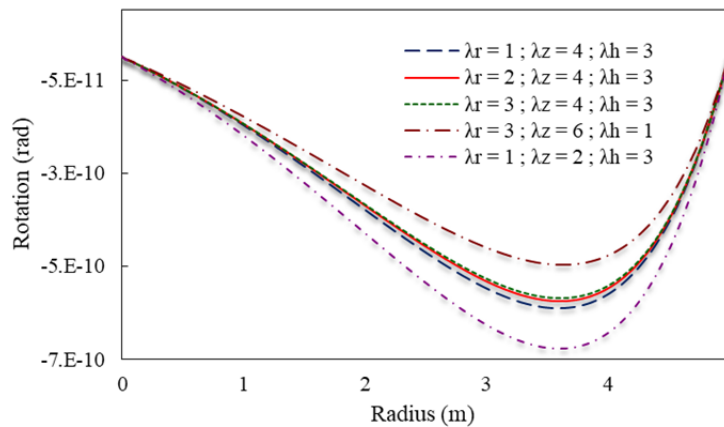


Figure 4. 2. Rotation of the clamped plate

4.2. Axisymmetric bending of 2D-FG Mindlin-Reissner Annular Plates

4.2.1. 2D-FG Annular Plate with Uniform Thickness

Consider a 2D-FG annular plate with inner radii of $r_i = 1$ m, outer radius of $r_o = 5$ m and constant thickness of $h(r) = 1$ m, subjected to uniform transverse load of $p_z = 10$ N/m². Properties of constituent materials, two different metal and two different ceramics, are given in Table (3.1). The influence of power law exponents (λ_r, λ_z) and boundary conditions on the axisymmetric bending behavior

of the annular plates is investigated. By virtue of the fact that there is lack of results in the available literature for the axisymmetric bending response of 2D-FG annular plates, analysis results are compared with those of ANSYS. To investigate the applicability of the presented model axisymmetric bending response is studied for several cases.

Table 4.7. Comparison of the maximum deflection, shear force and bending moment of C – C supported moderately thick 2D-FG annular plate.

λ_r	λ_z	Method	Results		
			$w_{max} \times 10^{-10}$ (m)	Q_{max} (N)	M_{max} (N.m)
1	2	ANSYS (20 x 100 layers)	5.215	38.69	21.40
		ANSYS (40 x 200 layers)	5.269	38.71	21.43
		Present Study	5.257	38.63	21.34
	4	ANSYS (20 x 100 layers)	4.539	38.56	21.26
		ANSYS (40 x 200 layers)	4.601	38.60	21.28
		Present Study	4.577	38.49	21.17
6	ANSYS (40 x 200 layers)	3.987	37.65	20.04	
	Present Study	4.117	38.38	21.03	
2	4	Present Study	5.125	38.63	21.15
		Present Study	4.475	38.49	21.01
		Present Study	4.069	37.96	20.40
3	4	Present Study	5.062	38.56	21.01
		Present Study	4.427	38.43	20.88
		Present Study	4.018	37.85	20.32

To model the 2D-FG annular plates in ANSYS, a large number of layers are required through the thickness and radial directions. In this study, two different models are generated in ANSYS. In the first model, the considered plate is divided into 20 layers through the thickness and 100 layers through the radial direction. In

the second model, the plate is divided into 40 layers through the thickness and 200 layers through the radial direction. It must be noted that for each layer a different material is defined in ANSYS.

Table 4.8. Comparison of the maximum deflection, shear force and bending moment of C – S supported moderately thick 2D-FG annular plate.

λ_r	λ_z	Method	Results			
			$w_{max} \times 10^{-10}$ (m)	Q_{max} (N)	M_{max} (N.m)	
1	2	ANSYS (20 x 100 layers)	9.537	54.22	32.28	
		ANSYS (40 x 200 layers)	9.443	54.25	32.32	
		Present Study	9.471	54.21	33.23	
	4	ANSYS (20 x 100 layers)	8.445	54.51	33.78	
		ANSYS (40 x 200 layers)	8.322	54.52	33.80	
		Present Study	8.341	54.45	33.66	
	6	ANSYS (40 x 200 layers)	7.400	54.08	32.64	
		Present Study	7.526	54.51	33.75	
		2	Present Study	9.176	54.08	32.85
	2	4	Present Study	8.108	54.33	33.30
			Present Study	7.463	54.14	32.90
			Present Study	9.040	53.97	32.60
3	4	Present Study	8.000	54.22	33.07	
		Present Study	7.392	54.10	32.86	

Properties of materials are graded based on Eq. (3.7). The vertical deflection, bending moments and shear forces of the considered plate are carried out for clamped – clamped supported (C – C), clamped – simply supported (C – S), simply – clamped supported (S – C), simply – simply supported (S – S), and clamped – free (C - F) boundary conditions. The numerical results of the presented approach and ANSYS are listed in Tables (4.7 – 4.11). Boundary conditions are

given in Eqs. (3.74 – 3.83). In this problem, the shear correction factor k_s is taken to be $\pi^2/12$.

Table 4.9. Comparison of the maximum deflection, shear force and bending moment of S – C supported moderately thick 2D-FG annular plate.

λ_r	λ_z	Method	Results				
			$w_{max} \times 10^{-10}$ (m)	Q_{max} (N)	M_{max} (N.m)		
1	2	ANSYS (20 x 100 layers)	7.142	30.93	13.05		
		ANSYS (40 x 200 layers)	7.066	30.89	13.09		
		Present Study	7.080	30.87	13.10		
	4	ANSYS (20 x 100 layers)	6.280	30.62	13.24		
		ANSYS (40 x 200 layers)	6.183	30.58	13.27		
		Present Study	6.191	30.58	13.28		
	6	ANSYS (40 x 200 layers)	5.336	29.99	13.67		
		Present Study	5.563	30.41	13.37		
	2	2	Present Study	6.882	30.91	13.02	
			4	Present Study	6.037	30.61	13.20
				6	Present Study	5.466	30.15
	3	2	Present Study	6.788	30.88	13.01	
4			Present Study	5.963	30.58	13.91	
			6	Present Study	5.399	30.04	13.58

Table 4.10. Comparison of the maximum deflection, shear force and bending moment of S – S supported moderately thick 2D-FG annular plate.

λ_r	λ_z	Method	Results			
			$w_{max} \times 10^{-9}$ (m)	Q_{max} (N)	M_{max} (N.m)	
1	2	ANSYS (20 x 100 layers)	1.380	45.74	16.69	
		ANSYS (40 x 200 layers)	1.368	45.74	16.62	
		Present Study	1.366	45.73	16.59	
	4	ANSYS (20 x 100 layers)	1.250	45.79	16.62	
		ANSYS (40 x 200 layers)	1.248	45.80	16.68	
		Present Study	1.244	45.77	16.58	
	6	ANSYS (40 x 200 layers)	1.166	45.60	16.60	
		Present Study	1.110	45.77	16.58	
		Present Study	1.319	45.66	16.66	
	2	4	Present Study	1.185	45.70	16.64
			Present Study	1.094	45.53	16.69
			Present Study	1.298	45.58	16.70
3	4	Present Study	1.168	45.63	16.68	
		Present Study	1.084	45.49	16.69	

As can be seen in Tables (4.7 – 4.11), comparison of the maximum deflections, shear forces and bending moments show a very good agreement with those of ANSYS for several boundary conditions and volume fraction exponents.

To obtain reliable accurate results in ANSYS, an appropriate number of graded layers in thickness and radial direction of the plate is required. Distinct material properties should be defined for each layer. For instance, 2000 different materials are required to generate the model of the plate with 20 layers through the thickness and 100 layers through the axial direction (20 x 100 layers) and 8000 materials for the plate with (40 x 200) layer. Defining such a large number of

materials is a time-consuming process for examining the axisymmetric bending response of 2D-FG plates of uniform thickness.

Table 4.11. Comparison of the maximum deflection, shear force and bending moment of C – F supported moderately thick 2D-FG annular plate.

λ_r	λ_z	Method	Results				
			$w_{max} \times 10^{-8}$ (m)	Q_{max} (N)	M_{max} (N.m)		
1	2	ANSYS (20 x 100 layers)	1.502	120.00	155.86		
		ANSYS (40 x 200 layers)	1.482	120.00	155.83		
		Present Study	1.467	120.00	155.80		
	4	ANSYS (20 x 100 layers)	1.322	120.00	155.64		
		ANSYS (40 x 200 layers)	1.297	120.00	155.60		
		Present Study	1.279	120.00	155.60		
	6	ANSYS (40 x 200 layers)	1.121	120.00	150.81		
		Present Study	1.144	120.00	155.40		
	2	2	Present Study	1.423	120.00	155.10	
			4	Present Study	1.246	120.00	154.90
				6	Present Study	1.146	120.00
	3	2	Present Study	1.407	120.00	154.80	
4			Present Study	1.233	120.00	154.50	
			6	Present Study	1.138	120.00	153.70

By infusing the suggested procedure to the governing equations of the problem, axisymmetric bending behavior of 2D-FG plates can be carried out in a simple and efficient manner. Comparison of the results demonstrates that as the number of layers increases, results of ANSYS approaches to those of the presented procedure. This demonstrates the accuracy and applicability of the current method. As stated in the previous section, λ_z has a more significant effect on the considered problem. For this reason, then plates must be divided into much more

layers in the thickness direction for higher values of λ_z in ANSYS. It should be emphasized that the presented approach is equally suitable for arbitrary functions of FGMs.

4.2.2. 2D-FG Annular Plate with Variable Thickness

Consider an annular plate of the previous section once again with the same loading.

Table 4.12. Maximum deflection, $w_{max} \times 10^{-9}$, of C – C supported moderately thick 2D-FG annular plate.

λ_r	λ_z	Geometric constant (λ_h)			
		1	2	3	10
0	0	1.0630	1.0910	1.1010	1.1140
	2	0.2912	0.2994	0.3021	0.3061
	4	0.2514	0.2584	0.2608	0.2642
	6	0.2358	0.2423	0.2445	0.2476
1	0	0.8276	0.8494	0.8569	0.8675
	2	0.2638	0.2711	0.2736	0.2772
	4	0.2302	0.2365	0.2387	0.2418
	6	0.2081	0.2138	0.2158	0.2186
2	0	0.7804	0.8008	0.8078	0.8178
	2	0.2574	0.2646	0.2670	0.2705
	4	0.2253	0.2315	0.2336	0.2366
	6	0.2157	0.2113	0.2133	0.2160
3	0	0.7580	0.7758	0.7846	0.7942
	2	0.2544	0.2614	0.2638	0.2672
	4	0.2229	0.2290	0.2311	0.2341
	6	0.2032	0.2087	0.2106	0.2133

As mentioned above, the plate is assumed to be made of two different metals and two different ceramics as given in Table (3.1). The plate has a non-uniform thickness which varies through the radial direction according to a power law of a linear function as given by Eq. (3.9). The thickness of the plate is $h_i = 2$ m at the inner edge and $h_0 = 1$ m at the outer edge. By applying the current method, static analysis is performed to show the influences of λ_r , λ_z and λ_h exponents on the axisymmetric bending response of 2D-FG annular plates.

Table 4.13. Maximum deflection, $w_{max} \times 10^{-9}$, of C – S supported moderately thick 2D-FG annular plate.

λ_r	λ_z	Geometric constant (λ_h)			
		1	2	3	10
0	0	1.5820	1.6640	1.6650	1.6960
	2	0.4313	0.4491	0.4552	0.4639
	4	0.3750	0.3904	0.3957	0.4082
	6	0.3520	0.3663	0.3712	0.3782
1	0	1.1690	1.2140	1.2300	1.2520
	2	0.3841	0.3998	0.4052	0.4129
	4	0.3382	0.3518	0.3567	0.3634
	6	0.3063	0.3187	0.3229	0.3290
2	0	1.0900	1.1320	1.1470	1.1670
	2	0.3730	0.3882	0.3934	0.4008
	4	0.3294	0.3427	0.3473	0.3539
	6	0.3035	0.3157	0.3199	0.3259
3	0	1.0550	1.0950	1.1090	1.1290
	2	0.3678	0.3827	0.3878	0.3951
	4	0.3252	0.3383	0.3429	0.3493
	6	0.3004	0.3125	0.3167	0.3226

Obtained results are tabulated in Tables (4.12 – 4.16) for C – C, C – S, S – C, S – S and C – F plates. In this problem the shear correction factor k_s is taken to be $\pi^2/12$.

Table 4.14. Maximum deflection, $w_{max} \times 10^{-9}$, of S – C supported moderately thick 2D-FG annular plate.

λ_r	λ_z	Geometric constant (λ_i)			
		1	2	3	10
0	0	1.3030	1.3470	1.3620	1.3840
	2	0.3579	0.3706	0.3751	0.3814
	4	0.3106	0.3216	0.3255	0.3310
	6	0.2912	0.3015	0.3050	0.3101
1	0	1.0320	1.0670	1.0790	1.0960
	2	0.3272	0.3389	0.3429	0.3487
	4	0.2867	0.2968	0.3004	0.3054
	6	0.2587	0.2679	0.2711	0.2756
2	0	0.9676	1.0000	1.0120	1.0280
	2	0.3186	0.3299	0.3339	0.3394
	4	0.2799	0.2898	0.2932	0.2981
	6	0.2542	0.2632	0.2663	0.2707
3	0	0.9357	0.9672	0.9781	0.9981
	2	0.3142	0.3254	0.3293	0.3348
	4	0.2764	0.2862	0.2896	0.2945
	6	0.2509	0.2597	0.2628	0.2672

Table 4.15. Maximum deflection, $w_{max} \times 10^{-9}$, of S – S supported moderately thick 2D-FG annular plate.

λ_r	λ_z	Geometric constant (λ_h)			
		1	2	3	10
0	0	2.0190	2.1200	2.1550	2.2060
	2	0.5495	0.5780	0.5879	0.6022
	4	0.4850	0.5102	0.5190	0.5315
	6	0.4566	0.4803	0.4835	0.5003
1	0	1.5280	1.6030	1.6290	1.6660
	2	0.4947	0.5202	0.5290	0.5417
	4	0.4409	0.4636	0.4715	0.4829
	6	0.4000	0.4206	0.4277	0.4380
2	0	1.4150	1.4850	1.5090	1.5430
	2	0.4792	0.5038	0.5124	0.5246
	4	0.4283	0.4503	0.4580	0.4690
	6	0.3938	0.4141	0.4211	0.4312
3	0	1.3620	1.4290	1.4520	1.4850
	2	0.4716	0.4957	0.5041	0.5161
	4	0.4420	0.4437	0.4512	0.4620
	6	0.3696	0.4096	0.4166	0.4266

Moreover, distributions of vertical displacement and rotations along the radial direction of the C – C and S – S supported plates are plotted in Figures (4.3 – 4.6) for several volume fraction exponents and geometric constants. In order to demonstrate the impact of boundary conditions on the axisymmetric response of 2D-FG plates the displacement and bending moment variations along the radial direction of the S – S, C – S, S – C and C – C supported plates are presented in Figures (4.7 – 4.8) for $\lambda_r = 2$, $\lambda_z = 4$ and $\lambda_h = 10$.

Table 4.16. Maximum deflection, $w_{max} \times 10^{-8}$, of C – F supported moderately thick 2D-FG annular plate.

λ_r	λ_z	Geometric constant (λ_h)			
		1	2	3	10
0	0	1.4380	1.5010	1.5240	1.5580
	2	0.4222	0.4412	0.4482	0.4584
	4	0.3617	0.3799	0.3839	0.3926
	6	0.3357	0.3507	0.3562	0.3642
1	0	1.0010	1.0460	1.0630	1.0870
	2	0.3630	0.3795	0.3855	0.3944
	4	0.3170	0.3314	0.3367	0.3444
	6	0.2846	0.2975	0.3022	0.3091
2	0	0.9319	0.9735	0.9886	1.0160
	2	0.3515	0.3674	0.3732	0.3817
	4	0.3082	0.3221	0.3271	0.3346
	6	0.2845	0.2973	0.3019	0.3087
3	0	0.9077	0.9480	0.9626	0.9841
	2	0.3473	0.3629	0.3686	0.3770
	4	0.3049	0.3187	0.3237	0.3310
	6	0.2828	0.2954	0.3000	0.3068

Remarkable effects of the volume fraction exponents and thickness variation constant on the axisymmetric bending behavior of the 2D-FG thick annular plates can be clearly observed in Tables (4.12 – 4.16). Gradually increasing of the λ_r and λ_z values decrease the deflection of the plate, but the deflection of the plate increases as λ_h increases. The decrease of vertical displacement describes that increasing the power law exponents will raise the rigidity of the plate.

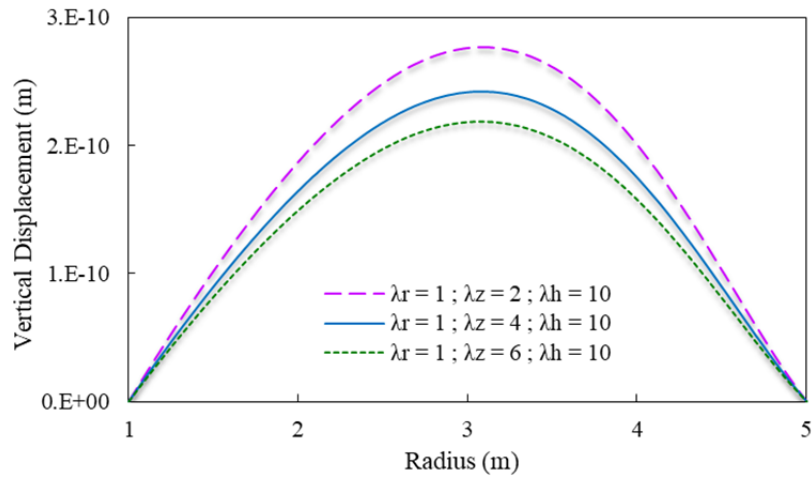


Figure 4. 3. Vertical deflection of C-C supported annular plate

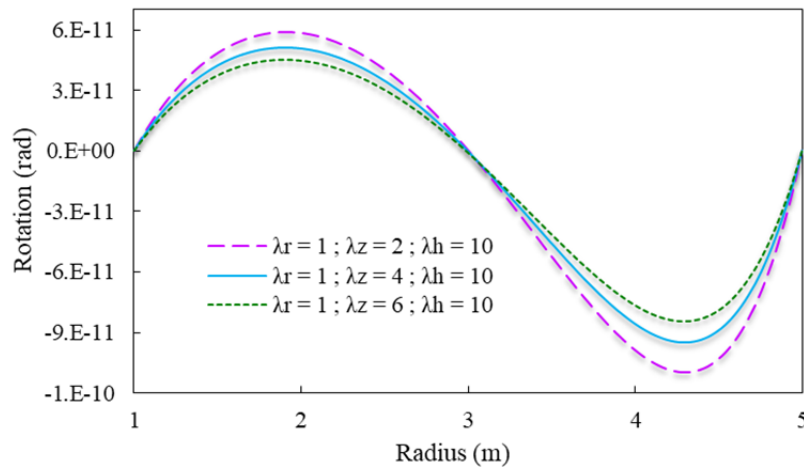


Figure 4. 4. Rotation of C – C supported annular plate

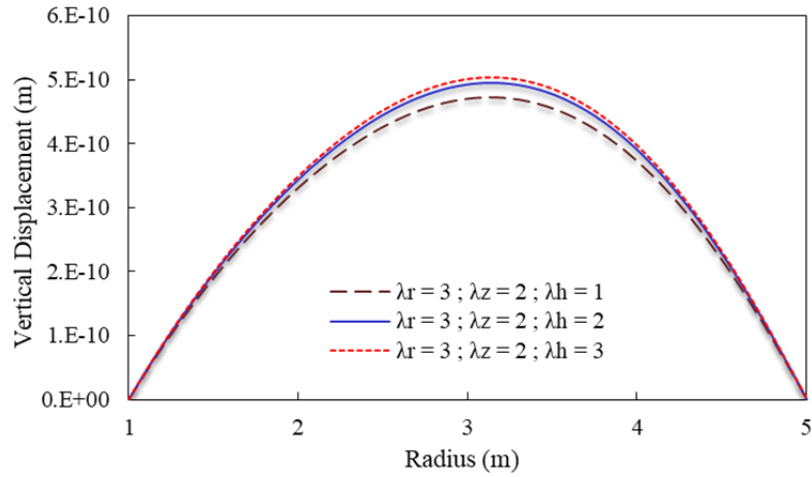


Figure 4. 5. Vertical deflection of S – S supported annular plate

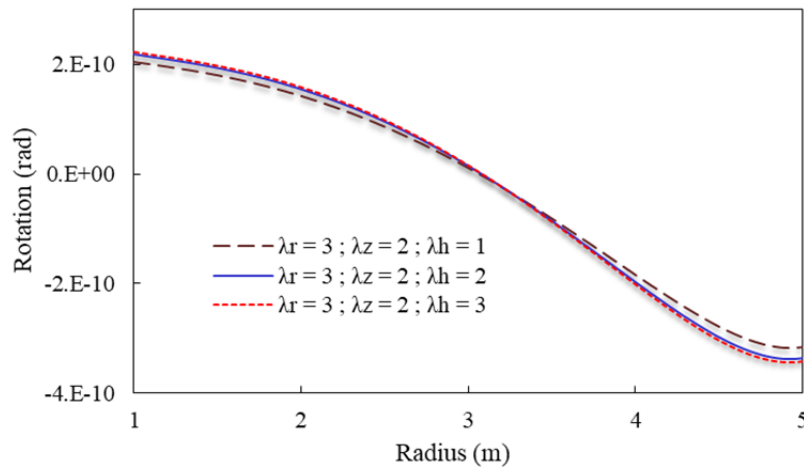


Figure 4. 6. Rotation of S – S supported annular plate

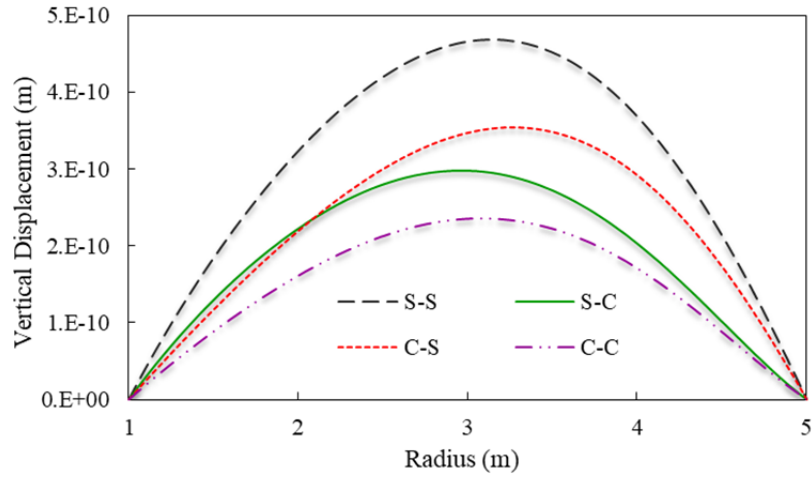


Figure 4. 7. Vertical deflection for various boundary conditions

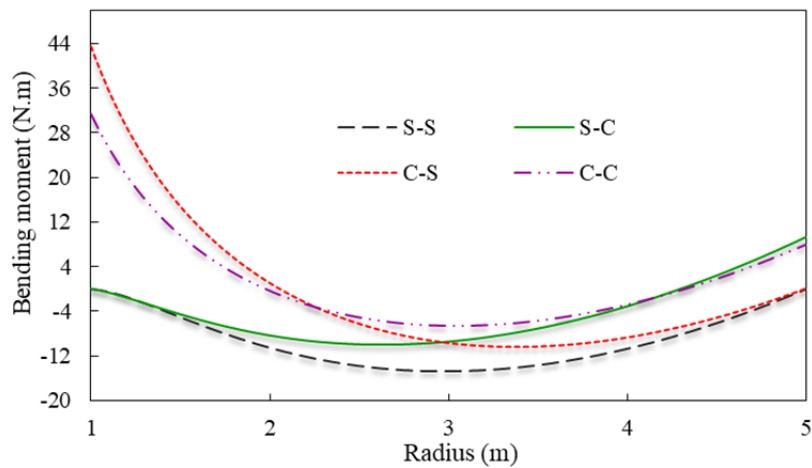


Figure 4. 8. Bending moment for various boundary conditions

As shown in Figures (4.3 – 4.4) the effect of λ_z on the static response of plates is more noticeable. Furthermore, the influence of thickness variation on the static response of 2D-FG axisymmetric plates is illustrated in Figures (4.5 – 4.6). It can be carried out from these figures that increasing the λ_h values leads to larger deflections and rotations. Figures (4.7 – 4.8) demonstrate that boundary conditions

have a remarkable impact on the axisymmetric response of 2D-FG annular plates. As may be expected, comparison of the results for various boundary conditions reveals that C – C supported plate has the minimum deflection and C – S supported has the maximum bending moment value.

4.3. Free Vibration Analysis of 2D-FG Circular Plates

4.3.1. Verification

In order to verify the presented procedure for free vibration analysis of the 2D-FG circular plates, two comparison studies are presented in this section.

As a first case study, dimensionless free vibration characteristics of isotropic and FG circular plates of uniform thickness are obtained and compared with those of Gupta et al. (2007), Liew et al. (1998) and Alipour et al. (2010). Comparisons are presented in Table (4.17) for various thickness ratios, material gradient exponents and different boundary conditions. Material distribution is assumed to be exponential (Eqs. (3.1 – 3.2)).

The dimensionless natural frequencies (Ω) are derived by

$$\Omega = \sqrt{\frac{\rho_0 h_i r_o^4}{D_0}} \omega^2 ; D_0 = \frac{E_0 h_i^3}{12(1 - \nu)} \quad (4.3)$$

It can be clearly seen in Table (4.17) that the dimensionless natural frequencies carried out by the presented approach are in excellent agreement with those of Gupta et al. (2007), Liew et al. (1998) and Alipour et al. (2010). In this case, the shear correction factor k_s is taken to be $\pi^2/12$.

Table 4.17. Comparison of non-dimensional natural frequencies (Ω) of FG circular plate ($\lambda_z = 0$)

Edge Condition	λ_r	$\frac{h_i}{r_o}$	Alipour et al. (2010)	Present Study	Exact
Clamped	-0.5	0.1	9.2457	9.2451	9.2457 ^a
	-0.5	0.2	8.5944	8.5936	8.5944 ^a
	0	0.001	10.216	10.2155	10.216 ^b
	0	0.15	9.6290	9.6283	9.6290 ^b
	0	0.25	8.8070	8.8066	8.8070 ^b
	1	0.1	11.5285	11.5289	11.5285 ^a
	1	0.2	10.6954	10.6944	10.6954 ^a
Simply Supported	-0.5	0.1	4.7943	4.7938	4.7943 ^a
	-0.5	0.2	4.6748	4.6744	4.6748 ^a
	0	0.001	4.9350	4.9350	4.9350 ^b
	0	0.15	4.8440	4.8438	4.8440 ^b
	0	0.25	4.6960	4.6962	4.6960 ^b
	1	0.1	5.0784	5.0775	5.0784 ^a
	1	0.2	4.9623	4.9614	4.9623 ^a
Free	-0.5	0.1	9.1418	9.1431	9.1418 ^a
	-0.5	0.2	8.7607	8.7612	8.7607 ^a
	0	0.001	9.0030	9.0028	9.0030 ^b
	0	0.15	8.7100	8.7092	8.7100 ^b
	0	0.25	8.2670	8.2671	8.2670 ^b
	1	0.1	8.4697	8.4689	8.4697 ^a
	1	0.2	8.1251	8.1250	8.1251 ^a

a: Gupta et al. (2007)

b: Liew et al. (1998)

As the second part of verification, the natural frequencies of radially FG, FG in the thickness direction and 2D-FG circular plate with clamped boundary condition are calculated and compared with the results of Liu and Lee (2000), Nie and Zhong (2007) and Kermani et al. (2012). Comparisons are presented in Table

(4.18). The circular plate is considered with a radius of 1 m, and a thickness of 0.2 m. The modulus of elasticity and mass density of the plate are assumed to have an exponential distribution (Eqs. (3.1 – 3.2)). Poisson's ratio is considered to be constant. In this case, the shear correction factor k_s is taken to be $\pi^2/12$.

Table 4.18. Comparison of non-dimensional natural frequencies (Ω) of FG circular plate.

λ_z	λ_r	Ω	Liu and Lee (2000)	Nie and Zhong (2007)	Kermani et al. (2012)	Present Study
0	0	Ω_1	0.097	---	0.097	0.097
		Ω_2	0.320	---	0.320	0.316
	1	Ω_1	---	---	0.113	0.112
		Ω_2	---	---	0.335	0.331
1	0	Ω_1	---	0.096	0.095	0.095
		Ω_2	---	---	0.314	0.311
	1	Ω_1	---	---	0.110	0.109
		Ω_2	---	---	0.329	0.327

A good agreement of the present results and those of Liu and Lee (2000), Nie and Zhong (2007) and Kermani et al. (2012) in all cases can be seen from the Table 4.18.

4.3.2. Free vibration of 2D-FG Circular Plates with Variable Thickness

Free vibration behavior of 2D-FG circular plates is investigated. The plate is assumed to have variable thickness as shown in Figure 4.9. Mechanical properties of the plate is considered to vary both in radial and thickness direction by a power law form Eq. (3.7). The radial coordinate dependent function of the thickness is given by Eq. (3.9). The radius of the plate is 5 m, and the shear correction factor is as in the previous case. Natural frequencies of the plate are

carried out for various boundary conditions, λ_r , λ_z and λ_h values. The thickness of the plate is considered to be ($h_i = 2$ m) in inner radii and ($h_o = 1$ m) at outer radius. Shear correction factor, k_s , is proposed as $5/6$ by Reissner and $\pi^2/12$ by Mindlin (see Washizu (1975)).

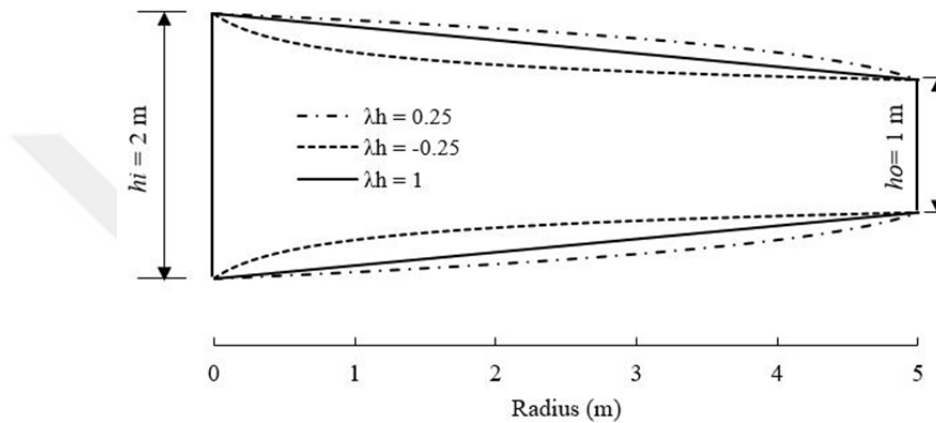


Figure 4. 9. Illustration of thickness profile

The calculated results of free vibration characteristics are listed in Tables (4.19 – 4.21) for different volume fraction exponents. Furthermore, the influence of thickness variation functions on the free vibration response of 2D-FG solid circular plates is investigated in details. As expected, tabulated results show that material gradient indices and geometric constant have significant influences on the natural frequencies of 2D-FG circular plates.

Table 4.19. Natural frequencies of 2D-FG circular plate (Clamped).

λ_r	λ_z	λ_h	Natural Frequencies (Hz)				
			ω_1	ω_2	ω_3	ω_4	ω_5
		-0.25	97.7654	321.7721	593.5375	655.4763	882.6572
	0	0.25	108.7406	358.5332	629.9787	644.7632	939.1016
		1	101.7386	346.5102	630.2576	640.3068	924.2638
		-0.25	154.5728	534.8401	999.0538	1146.9089	1498.9431
0	2	0.25	178.8480	601.0351	1078.4434	1113.0296	1606.4530
		1	166.9131	578.8720	1064.2245	1119.3151	1577.2374
		-0.25	163.7741	566.4712	1057.7519	1210.4915	1585.7969
	4	0.25	189.2995	636.5980	1146.5897	1172.2365	1699.2189
		1	176.6907	613.1693	1127.6311	1181.9823	1668.3239
		-0.25	87.7786	314.7163	586.2521	649.8939	875.1949
	0	0.25	101.0838	350.5478	625.2137	637.1889	931.7423
		1	94.5790	339.3342	623.0793	636.1949	916.9671
		-0.25	157.8469	552.0312	1032.2885	1180.3303	1549.4577
1	2	0.25	182.5225	619.4841	1111.4336	1148.5054	1659.5663
		1	170.4844	597.2185	1098.8439	1153.9274	1629.8080
		-0.25	171.1172	593.8744	1109.4800	1265.0511	1664.3195
	4	0.25	197.5045	666.2320	1199.9322	1227.6035	1782.9145
		1	184.5621	642.3051	1182.2240	1236.8756	1750.7120
		-0.25	86.8850	312.3453	583.8808	639.0107	873.0649
	0	0.25	99.9174	348.0186	614.6437	635.2434	930.1598
		1	93.5821	336.8240	621.0421	625.6035	915.2645
		-0.25	159.3229	557.8773	1043.5124	1189.3253	1566.2845
	2	0.25	184.1330	625.8195	1122.3908	1158.5248	1677.5588
		1	172.0623	603.4088	1110.8607	1162.9074	1647.5437
		-0.25	173.9392	603.8072	1127.6895	1285.3811	1691.3852
	4	0.25	200.7084	677.0574	1219.6944	1246.9831	1811.8860
		1	187.6198	652.8661	1201.6452	1256.8002	1779.2333

Table 4.20. Natural frequencies of 2D-FG circular plate (Simply Supported).

λ_r	λ_z	λ_h	Natural Frequencies (Hz)				
			ω_1	ω_2	ω_3	ω_4	ω_5
		-0.25	54.1022	272.8022	556.9002	655.4763	858.9251
	0	0.25	72.1165	327.1340	626.4580	629.9787	931.3211
		1	64.8330	306.6038	602.3207	640.3068	907.5765
		-0.25	91.1040	448.0931	924.5472	1141.1407	1451.5566
0	2	0.25	121.7538	541.6626	1034.4994	1111.1201	1587.0368
		1	109.4286	505.6470	1001.7619	1118.5235	1541.3087
		-0.25	94.4780	474.8749	981.8837	1207.5408	1535.6572
	4	0.25	126.3946	574.5159	1105.6864	1169.4427	1679.5705
		1	113.5140	536.2968	1066.0435	1181.6113	1631.1718
		-0.25	52.5114	270.2822	552.9950	649.8639	853.8595
	0	0.25	69.9446	322.7501	621.0573	625.2137	925.0150
		1	62.7935	303.5259	597.9575	636.1949	902.1114
		-0.25	94.0752	465.1475	958.1530	1174.6864	1503.5060
1	2	0.25	125.6682	560.8964	1068.7717	1146.1650	1641.8393
		1	112.8994	524.3048	1036.7963	1153.2928	1595.3958
		-0.25	99.6668	500.1531	1033.0662	1262.0606	1615.4680
	4	0.25	133.3237	603.6431	1160.4692	1223.9267	1765.2900
		1	119.6649	564.0479	1120.4094	1236.5618	1715.0622
		-0.25	52.5028	270.4200	553.0199	639.0107	853.6918
	0	0.25	69.8373	322.3127	614.6437	620.8085	924.5218
		1	62.7466	303.3287	597.9990	625.6035	902.0105
		-0.25	95.3231	471.4881	970.3583	1183.5868	1521.4530
2	2	0.25	127.2824	567.9688	1081.1023	1155.7154	1660.7627
		1	114.3758	531.1078	1049.6895	1162.2862	1614.1862
		-0.25	101.7563	509.6091	1051.5648	1282.2575	1643.3494
	4	0.25	135.9854	614.5275	1180.6931	1243.4243	1795.1050
		1	122.1398	574.3928	1140.2505	1256.4216	1744.3995

Table 4.21. Natural frequencies of 2D-FG circular plate (Roller Supported).

λ_r	λ_z	λ_h	Natural Frequencies (Hz)				
			ω_1	ω_2	ω_3	ω_4	ω_5
		-0.25	54.1022	272.8022	365.4292	556.9002	858.9251
	0	0.25	72.1165	327.1340	373.9717	626.4580	928.9249
		1	64.8330	306.6038	377.8451	602.3207	907.5765
		-0.25	87.0727	447.1738	643.7305	927.8732	1448.7271
0	2	0.25	116.6527	541.4631	657.2710	1055.9367	1578.3006
		1	104.7098	505.2650	664.5933	1010.3442	1541.1996
		-0.25	92.3944	474.4192	677.0620	983.6415	1534.2352
	4	0.25	123.7560	574.4286	692.1207	1118.3731	1678.4874
		1	111.0750	536.1159	699.5498	1070.6453	1631.0732
		-0.25	52.5114	270.2822	387.5779	552.9950	853.8595
	0	0.25	69.9446	322.7501	395.9788	621.0573	925.0150
		1	62.7935	303.5259	400.4014	597.9575	902.1114
		-0.25	90.4572	464.0172	669.1775	961.8985	1500.7932
1	2	0.25	121.1131	560.5365	683.8342	1092.8707	1634.8213
		1	108.6698	523.7339	691.3837	1046.4392	1595.2924
		-0.25	97.7181	499.5974	708.6503	1035.0899	1614.0377
	4	0.25	130.7794	603.4965	725.6216	1175.3025	1764.1150
		1	117.3663	563.7887	733.1391	1125.6579	1714.9556
		-0.25	52.5028	270.4200	389.1729	553.0199	853.6918
	0	0.25	69.8373	322.3127	396.8769	620.8085	924.5218
		1	62.7466	303.3287	401.5838	597.9990	902.0105
		-0.25	91.8651	470.4271	677.9909	974.0098	1518.6518
2	2	0.25	122.9346	567.6574	692.8641	1105.9289	1655.1957
		1	110.3358	530.5853	700.5160	1059.3120	1614.0216
		-0.25	99.8665	509.0713	721.8479	1053.5277	1641.8449
	4	0.25	133.6050	614.3919	739.3582	1195.5598	1794.2549
		1	119.9311	574.1442	746.9499	1145.4067	1744.2585

The suggested scheme is applied to study the influences of various thickness profiles and the power law indices and different boundary conditions. Influences of the volume fraction exponents and thickness variation profile on the natural frequencies of the 2D-FG thick circular plates can be clearly seen in Tables (4.19 – 4.21). As may be expected, the circular plate with convex thickness profile ($\lambda_h = 0.25$) has the highest natural frequencies while the plate with concave thickness profile ($\lambda_h = -0.25$) has the lowest natural frequencies among compared cases. When the plate is radially FG ($\lambda_z = 0$), it is revealed that increasing the value of λ_r decreases natural frequencies of the structure for the considered FGM model. When the plate is FG only through the thickness direction ($\lambda_r = 0$), It can be concluded that an increase in the value of λ_z leads to an increase in the natural frequencies of the structure. In 2D-FG circular plates gradually increasing of the λ_r and λ_z values increase the natural frequencies of the plate.

4.4. Free Vibration Analysis of 2D-FG Annular Plates

4.4.1. Verification

This section contains two parts; firstly, results of the presented approach are validated with some available results in the literature. A simply supported – clamped 2D-FG annular plate is considered. ($h_i = 0.1$; $r_o = 1$; $\lambda_r = \lambda_z = 1$). Natural frequencies of the considered plate are carried out for several ratios of inner radii/outer radii and compared with those results given by Kermani et al. (2012) based on 3D elasticity theory. Comparisons are presented in Table (4.22). The modulus of elasticity and mass density of the plate vary exponentially (Eqs. (3.1 – 3.2)). Poisson's ratio is considered to be constant. In this case, the shear correction factor k_s is taken to be $\pi^2/12$. Boundary conditions are given by Eqs. (3.76 – 3.77). Non-dimensional natural frequencies of the problem are carried out by Eq. (4.3).

Table 4.22. Comparison of non-dimensional natural frequencies (Ω) of FG annular plate.

$\frac{r_i}{r_o}$	Ω	Kermani et al. (2012)	Present Study
0.1	Ω_1	0.057	0.056
	Ω_2	0.151	0.149
0.2	Ω_1	0.068	0.067
	Ω_2	0.182	0.180
0.3	Ω_1	0.084	0.083
	Ω_2	0.226	0.224

From Table (4.22), it is evident that the results of the proposed method are in a good agreement with the existing results.

As the second part of verification, the free vibration response of the 2D-FG annular plates is examined and compared with the results of ANSYS to validate the efficiency and accuracy of the suggested approach.

Consider a 2D-FG annular plate with inner radii of $r_i = 1$ m, outer radius of $r_o = 5$ m and uniform thickness of $h(r) = 1$ m. The material properties, two different metal and two different ceramics, listed in Table (3.1) are used in the numerical computations. To investigate the applicability of the presented model, free vibration of the 2D-FG annular plates is examined for several cases.

To generate the model of the considered plate in ANSYS, a large number of layers are required through the thickness and radial directions. In this section, the plate is divided into 40 layers through the thickness and 200 layers through the radial direction. It must be noted that for each layer a different material is defined in ANSYS. Defining such a large number of materials is a time-consuming process. To generate the finite element model of the considered problem SHELL209 element is used which is suitable for analyzing moderately thick axisymmetric plates. In analysis, shear correction factor, k_s , is taken to be 5/6.

Several comparison studies are carried out and presented in Tables (4.23 – 4.28). Boundary conditions of clamped – clamped annular plate are given by Eqs. (3.74 – 3.75).

Table 4.23. Comparison of natural frequencies of 2D-FG annular plate (C – C).

λ_r	λ_z	Method	Natural Frequencies (Hz)					
			ω_1	ω_2	ω_3	ω_4	ω_5	
0	0	ANSYS	238.9200	526.1880	717.6680	863.3420	1218.0000	
		Present Study	238.9200	526.1885	717.6681	863.3419	1218.0000	
	2	ANSYS	399.0630	888.1480	1247.2100	1463.8200	2076.6400	
		Present Study	399.4540	889.0698	1258.9959	1465.2809	2077.0358	
	4	ANSYS	423.4630	945.2820	1318.5600	1559.9200	2212.9500	
		Present Study	422.3180	940.6610	1327.0234	1550.7501	2197.3500	
	1	0	ANSYS	235.7880	520.9700	708.8820	857.2960	1211.1600
			Present Study	235.8051	520.9927	708.9220	857.3143	1211.1767
2		ANSYS	414.4380	924.4470	1293.4700	1525.6900	2161.0200	
		Present Study	414.0554	920.5681	1296.9106	1517.0744	2149.4431	
4		ANSYS	445.6640	995.1370	1385.4600	1642.7500	2327.6400	
		Present Study	444.9982	989.5056	1390.9186	1630.5693	2309.2842	
2		0	ANSYS	230.1940	513.8470	694.2530	850.9420	1205.5800
			Present Study	230.0268	513.9429	694.4439	851.0209	1205.6423
	2	ANSYS	416.8330	932.6390	1302.1700	1541.4300	2184.4800	
		Present Study	416.4923	927.8085	1304.3378	1530.9283	2170.3069	
	4	ANSYS	451.8980	1009.8100	1405.5900	1667.7900	2363.6000	
		Present Study	451.4262	1003.8466	1410.8890	1658.8213	2344.3603	

It can be seen from Table (4.23), that current results of the natural frequencies of clamped - clamped circular plates concur well with those obtained by ANSYS.

Boundary conditions of clamped – simply supported annular plate are given by Eqs. (3.78 – 3.79).

Table 4.24. Comparison of natural frequencies of 2D-FG annular plate (C – S).

λ_r	λ_z	Method	Natural Frequencies (Hz)				
			ω_1	ω_2	ω_3	ω_4	ω_5
0	0	ANSYS	173.5800	477.3510	717.6680	830.0840	1201.5800
		Present Study	173.5798	477.3509	717.6681	830.0843	1201.5833
	2	ANSYS	289.6720	791.3760	1238.8600	1397.0800	2039.2600
		Present Study	290.2403	794.5349	1247.8620	1401.8038	2041.1460
	4	ANSYS	305.5120	844.2400	1314.3300	1487.7900	2172.3500
		Present Study	305.3697	843.1452	1321.3360	1482.8788	2159.6300
1	0	ANSYS	178.8260	477.8840	708.8820	828.2070	1197.4500
		Present Study	178.8000	477.8756	708.9222	828.2026	1197.4479
	2	ANSYS	304.7330	828.3680	1280.0500	1463.9300	2124.8200
		Present Study	304.8440	827.2943	128.5000	1456.3375	2116.1099
	4	ANSYS	324.4870	893.1280	1378.0600	1573.9100	2289.4700
		Present Study	324.7574	891.4167	1384.6194	1564.7139	2274.8480
2	0	ANSYS	175.8550	473.6970	694.2530	824.5830	1193.9200
		Present Study	175.8528	473.7253	694.4439	824.6060	1193.9442
	2	ANSYS	307.5060	837.9290	1287.4000	1481.2800	2149.5100
		Present Study	307.6683	835.6043	1292.5874	1471.3202	2138.5071
	4	ANSYS	329.9900	908.1200	1397.0700	1600.1900	2326.6800
		Present Study	330.4043	905.8564	1404.5206	1589.7810	2311.3669

We can observe from Table (4.24), that free vibration characteristic results of the presented approach and those of ANSYS are consistent.

Boundary conditions of simply supported – clamped annular plate are given by Eqs. (3.76 – 3.77).

Table 4.25. Comparison of natural frequencies of 2D-FG annular plate (S – C).

λ_r	λ_z	Method	Natural Frequencies (Hz)				
			ω_1	ω_2	ω_3	ω_4	ω_5
0	0	ANSYS	207.4760	503.0360	717.6680	848.9070	1212.6700
		Present Study	207.4765	503.0356	717.6681	848.9069	1212.6693
	2	ANSYS	344.3350	838.8930	1243.6600	1430.8900	2062.4900
		Present Study	345.2990	841.6073	1253.8509	1434.1850	2063.6941
	4	ANSYS	363.9030	893.4320	1316.7400	1524.8300	2197.3000
		Present Study	363.9830	891.5533	1324.3640	1518.2931	2183.2511
1	0	ANSYS	200.9040	495.4230	708.8820	841.2750	1205.0700
		Present Study	200.9377	495.4563	708.9220	841.3000	1205.0847
	2	ANSYS	355.3830	872.4230	1289.8900	1489.2200	2146.3700
		Present Study	355.8811	870.4682	1293.4114	1483.3804	2135.1586
	4	ANSYS	381.5630	939.1610	1383.4600	1603.1400	2310.2400
		Present Study	382.2569	936.3630	1389.0295	1594.2640	2293.2071
2	0	ANSYS	197.2160	490.0030	694.2530	836.1190	1200.2000
		Present Study	197.2906	490.0957	694.4439	836.1954	1200.2528
	2	ANSYS	358.0810	881.5470	1297.6900	1506.0300	2170.6600
		Present Study	358.5947	878.5034	1300.7741	1498.0900	2156.7959
	4	ANSYS	387.4860	954.2030	1403.0000	1628.8700	2347.1100
		Present Study	388.3395	950.9621	1408.9010	1619.0999	2329.0859

Table (4.25), demonstrates that current results and those of ANSYS are in a good agreement.

Boundary conditions of simply supported – simply supported annular plate are given by Eqs. (3.80 – 3.81).

Table 4.26. Comparison of natural frequencies of 2D-FG annular plate (S – S).

λ_r	λ_z	Method	Natural Frequencies (Hz)				
			ω_1	ω_2	ω_3	ω_4	ω_5
0	0	ANSYS	143.8670	449.7930	717.6670	814.4240	1195.1800
		Present Study	143.8674	449.7927	717.6681	814.4241	195.1752
	2	ANSYS	242.4230	733.7110	1238.1200	1357.9000	2023.2300
		Present Study	243.1304	738.4166	1246.6384	1363.5960	2026.5600
	4	ANSYS	252.4330	784.0040	1313.9100	1447.7000	2154.4000
		Present Study	252.9180	785.5360	13206.3840	1445.2113	2143.6929
1	0	ANSYS	145.7010	447.9970	708.8820	811.0000	1190.3000
		Present Study	145.6914	447.9988	708.9220	811.0017	1190.3020
	2	ANSYS	253.5295	768.3659	1284.5035	1416.4658	2100.3310
		Present Study	253.0400	767.4590	1279.6400	1420.8300	2108.6300
	4	ANSYS	267.0510	828.2190	1377.8200	1528.8300	2269.8400
		Present Study	268.0153	829.3824	1384.3238	1523.4963	2256.6813
2	0	ANSYS	144.1780	445.8930	694.2530	808.7460	1187.6600
		Present Study	144.1816	445.9140	694.4439	808.7635	1187.6778
	2	ANSYS	255.7900	777.8370	1286.6400	1438.9000	2134.5600
		Present Study	256.3203	777.5170	1291.9686	1432.5270	2123.5854
	4	ANSYS	272.0900	843.3820	1396.6300	1555.5100	2308.2600
		Present Study	273.1764	843.9909	1404.1741	1549.2213	2294.0745

It is apparent from Table (4.26) that results of the presented scheme matches with those of finite element method.

Boundary conditions of clamped – free annular plate are given by Eqs. (3.82 – 3.83).

Table 4.27. Comparison of natural frequencies of 2D-FG annular plate (C – F).

λ_r	λ_z	Method	Natural Frequencies (Hz)				
			ω_1	ω_2	ω_3	ω_4	ω_5
0	0	ANSYS	47.0814	232.9450	373.4140	560.6510	914.7920
		Present Study	47.0814	232.9449	373.4142	560.6508	914.7918
	2	ANSYS	75.6516	380.3310	659.5840	926.9050	1528.5500
		Present Study	76.1606	383.0451	661.5248	931.8354	1534.8980
	4	ANSYS	80.3169	405.8760	691.9370	989.3450	1632.6900
		Present Study	80.7684	406.9116	693.7867	989.1787	1628.8288
1	0	ANSYS	53.3090	243.7600	400.7230	567.0110	918.8750
		Present Study	53.2742	243.7002	400.5698	566.9655	918.8325
	2	ANSYS	81.9138	404.0048	691.6611	972.2130	1594.8987
		Present Study	81.5164	402.4500	690.9740	972.0830	1593.6300
	4	ANSYS	86.1643	432.1970	729.3580	1047.7100	1721.2900
		Present Study	86.7146	433.5191	731.0863	1046.9957	1718.2516
2	0	ANSYS	53.0251	242.7810	399.8640	567.2220	920.0880
		Present Study	52.9869	242.7133	399.6913	567.1520	920.0060
	2	ANSYS	82.4247	407.9620	697.7440	985.2730	1613.8300
		Present Study	82.8205	409.0267	699.1777	984.0336	1613.8694
	4	ANSYS	87.4632	440.1680	741.0190	1066.3000	1750.3600
		Present Study	88.0368	441.3088	743.4840	1064.9939	1747.1716

Table 4.28. Comparison of natural frequencies of 2D-FG annular plate (F – C).

λ_r	λ_z	Method	Natural Frequencies (Hz)				
			ω_1	ω_2	ω_3	ω_4	ω_5
0	0	ANSYS	92.7847	315.3700	559.5560	627.6540	971.8230
		Present Study	92.7847	315.3696	559.5557	627.6539	971.8233
	2	ANSYS	149.3060	515.9140	976.8940	1040.7900	1626.9400
		Present Study	150.3153	519.0491	984.3466	1045.7440	1633.1726
	4	ANSYS	158.5880	549.7180	1030.6600	1110.0200	1737.1200
		Present Study	159.4364	550.8570	1036.1362	1109.2837	1732.3256
1	0	ANSYS	84.3015	303.2610	539.4860	615.7940	960.0110
		Present Study	84.3415	303.3170	539.5772	615.8415	960.0495
	2	ANSYS	153.3993	535.4695	1013.4141	1080.6959	1689.7330
		Present Study	152.5130	535.4060	1011.4300	1083.4800	1697.8100
	4	ANSYS	165.8440	577.8860	1087.5200	1167.0700	1827.3000
		Present Study	167.1301	578.5291	1091.6471	1163.9194	1817.6124
2	0	ANSYS	83.9201	301.7910	533.7330	614.0020	958.5630
		Present Study	83.9708	301.8714	533.8956	614.0747	958.6188
	2	ANSYS	153.9220	541.7240	1018.8000	1096.7800	1718.4800
		Present Study	154.7038	541.4431	1020.5838	1092.7922	1708.4355
	4	ANSYS	168.2430	587.5700	1103.0200	1186.4300	1857.3000
		Present Study	169.5908	588.1563	1107.4078	1182.8630	1846.8551

As outlined in the previous section, as the number of layers increases, results of ANSYS approaches to those of the presented procedure. To obtain accurate results in ANSYS, the plate needs to be divided to a large number of layers in the thickness and radial directions. Increasing material gradient indices increases the required number of layers to obtain accurate results.

By infusing the suggested procedure to the Eqs. (3.133 – 3.137) and substituting the Laplace parameter with “ $i\omega$ ”, free vibration behavior of 2D-FG thick annular plates can be carried out in a simple and efficient manner. This

demonstrates the accuracy and applicability of the current method. It should be emphasized that the presented approach is equally suitable for arbitrary functions of FGMs. By using the suggested approach considerable saving in computation time can be provided.

4.3.2. Free vibration of 2D-FG Annular Plates with Variable Thickness

Numerical computations given in the previous sections showed the validity, applicability and accuracy of the presented procedure. In this section, the suggested model will be applied to free vibration response of 2D-FG annular plate of variable thickness. Also, effects of the geometrical and material properties on the frequency parameters of the 2D-FG annular plates will be discussed in details.

The plate is assumed to have variable thickness as shown in Figure 4.9. Mechanical properties of the plate is considered to vary both in radial and thickness direction by a power law form Eq. (3.7). The radial coordinate dependent function of the thickness is given by Eq. (3.9).

Consider a 2D-FG annular plate with inner radii of $r_i = 1$ m, outer radius of $r_o = 5$ m. The shear correction factor k_s is taken to be $\pi^2/12$. The thickness of the plate is considered to be ($h_i = 2$ m) in inner radii and ($h_o = 1$ m) at outer radius. Natural frequencies of the plate are carried out for various boundary conditions, λ_r , λ_z and λ_h values.

The obtained natural frequencies are listed in Tables (4.29 – 4.34) for different volume fraction exponents. Furthermore, the influence of thickness variation functions on the free vibration response of 2D-FG annular plates is investigated in details. Boundary conditions are given by Eqs. (3.74 – 3.83).

Table 4.29. Natural frequencies of 2D-FG annular plate (C – C).

λ_r	λ_z	λ_h	Natural Frequencies (Hz)					
			ω_1	ω_2	ω_3	ω_4	ω_5	
0	0	-0.25	267.5424	560.9236	732.7283	904.4027	1259.7803	
		0.25	270.6771	574.4984	695.5696	938.1162	1172.8981	
		1	269.4255	570.2079	708.1353	927.4146	1250.8238	
	2	0	-0.25	452.7248	953.0053	1279.3945	1541.0834	2158.0747
			0.25	462.5909	972.4833	1217.5203	1599.3529	2066.6968
			1	459.0705	967.1279	1237.3299	1580.9449	2162.6577
		4	-0.25	477.9948	1008.3786	1351.7538	1630.9341	2281.9811
			0.25	487.8244	1033.2953	1284.5974	1695.6533	2170.3219
			1	484.2931	1025.6934	1306.7387	1674.7360	2285.5361
1	0	-0.25	266.5758	557.4399	727.6532	899.5442	1253.9463	
		0.25	269.6450	570.4844	691.0494	933.1827	1170.8247	
		1	268.8230	567.1233	704.7205	922.7980	1247.4019	
	2	0	-0.25	469.8388	987.1593	1321.4775	1595.2174	2232.6339
			0.25	479.7167	1007.1664	1257.1653	1655.3870	2122.1888
			1	476.5199	1002.3668	1279.2616	1636.4277	2235.1584
		4	-0.25	504.0411	1061.0023	1419.3242	1714.4811	2397.0421
			0.25	514.2826	1085.9213	1348.7457	1781.4401	2254.6846
			1	510.9813	1079.2144	1373.6652	1759.9377	2391.0981
2	0	-0.25	260.2049	549.7878	712.8224	893.1091	1248.3209	
		0.25	263.0513	562.2464	676.5315	927.4578	1164.5235	
		1	262.3024	559.1899	690.1237	916.8506	1241.1455	
	2	0	-0.25	472.4702	994.6068	1329.3791	1609.6126	2254.0265
			0.25	482.1094	1014.1750	1264.5689	1670.5854	2137.5133
			1	478.9985	1009.6136	1286.8665	1651.3794	2254.2993
		4	-0.25	511.2132	1076.0521	1439.9359	1739.8073	2433.3409
			0.25	521.3008	1100.4356	1368.0218	1807.6811	2282.9358
			1	518.0633	1094.0310	1393.4669	1785.9063	2424.2919

Table 4.30. Natural frequencies of 2D-FG annular plate (C – S).

λ_r	λ_z	λ_h	Natural Frequencies (Hz)					
			ω_1	ω_2	ω_3	ω_4	ω_5	
0	0	-0.25	208.8338	519.1056	732.7283	876.2541	1248.6174	
		0.25	228.4862	554.6279	695.5696	926.5669	1136.3471	
		1	222.5540	539.6703	708.1353	906.3655	1247.9275	
	2	0	-0.25	352.5242	869.6100	1273.3604	1483.1961	2132.8660
			0.25	390.7615	925.5517	1214.7484	1571.8185	2013.8710
			1	378.7486	902.0736	1234.5241	1534.7757	2162.5994
		4	-0.25	371.0052	923.0998	1348.5533	1348.5533	1571.0812
			0.25	410.4111	987.4686	1283.0633	1668.3267	2118.5183
			1	398.1522	960.3865	1305.1944	1628.2464	2285.5319
1	0	-0.25	215.6809	520.9072	727.6532	875.1556	1244.8736	
		0.25	234.5959	554.0303	691.0494	923.7110	1137.7312	
		1	228.9335	540.9005	704.7205	904.7787	1245.0234	
	2	0	-0.25	369.8673	905.2896	1314.4178	1540.3216	2209.7793
			0.25	409.0573	962.3661	1253.6196	1630.0756	2060.8098
			1	396.8016	939.0012	1275.6241	1592.7390	2234.2460
		4	-0.25	394.1258	975.7607	1415.5185	1656.8265	2373.6779
			0.25	435.7919	1041.7347	1346.7769	1755.9372	2190.4493
			1	4228.5879	1014.5832	1371.6642	1715.1131	2389.1661
2	0	-0.25	211.8965	515.9439	712.8224	871.1155	1240.9239	
		0.25	230.0074	547.6733	676.5315	919.5152	1132.6553	
		1	224.5481	535.2835	690.1237	900.8694	1238.2193	
	2	0	-0.25	373.0805	913.8649	1322.2859	1555.9815	2232.6403
			0.25	412.0903	970.5624	1260.8698	1646.3716	2074.9650
			1	399.8666	947.4188	1283.1244	1608.8713	2252.6391
		4	-0.25	400.7554	991.1098	1436.0378	1683.0455	2411.4397
			0.25	442.6798	1057.0097	1365.9344	1783.1389	2216.1423
			1	429.6408	1029.9405	1391.3725	1741.9266	2421.0434

Table 4.31. Natural frequencies of 2D-FG annular plate (S – C).

λ_r	λ_z	λ_h	Natural Frequencies (Hz)				
			ω_1	ω_2	ω_3	ω_4	ω_5
0	0	-0.25	232.0806	544.1074	732.7283	897.3647	1240.8515
		0.25	248.3341	571.8121	695.5696	937.8031	1023.9417
		1	242.1310	565.2771	708.1353	927.0864	1075.3170
	2	-0.25	389.7596	915.3153	1276.6780	1525.3038	2152.8839
		0.25	421.6583	962.7783	1216.1509	1598.7481	1808.0192
		1	409.7068	952.4298	1235.4469	1579.9183	1893.1502
4	-0.25	410.2514	969.6583	1350.2926	1614.0799	2277.6792	
	0.25	443.6027	1024.1808	1283.8198	1694.8871	1903.2602	
	1	431.0358	1011.3467	1305.6894	1673.6360	1995.5346	
1	0	-0.25	226.6945	537.9263	727.6532	890.7989	1230.8062
		0.25	242.7303	566.7649	691.0494	932.4954	1012.8405
		1	236.6617	560.6527	704.7205	922.0652	1063.9636
	2	-0.25	402.2638	946.7265	1319.6809	1577.0204	2229.6649
		0.25	434.6832	996.7752	1256.3525	1654.4598	1858.3771
		1	422.5522	986.3755	1278.0523	1634.9169	1951.1643
4	-0.25	431.1444	1017.9469	1418.3185	1694.1957	2394.6789	
	0.25	465.5386	1075.3919	1348.2750	1780.3092	1985.4476	
	1	452.6151	1062.5801	1372.9737	1758.1167	2088.8941	
2	0	-0.25	222.2431	532.1618	712.8222	885.7396	1229.8203
		0.25	237.8503	559.3964	676.5315	927.1446	1013.0344
		1	232.0171	553.8822	690.1237	916.5004	1064.7205
	2	-0.25	405.0447	955.2777	1327.5186	1592.5359	2247.2996
		0.25	437.5178	1004.5890	1263.6399	1669.9819	1871.2701
		1	425.4252	994.5850	1285.5539	1650.3045	1963.9929
4	-0.25	437.7317	1033.6080	1438.8857	1720.5518	2425.1973	
	0.25	472.5048	1090.6101	1367.4905	1806.9795	2006.5488	
	1	459.5001	1078.1806	1392.7193	1784.6312	2109.3788	

Table 4.32. Natural frequencies of 2D-FG annular plate (S – S).

λ_r	λ_z	λ_h	Natural Frequencies (Hz)				
			ω_1	ω_2	ω_3	ω_4	ω_5
0	0	-0.25	174.7248	497.2968	732.7283	869.2191	1240.6618
		0.25	206.0830	550.0819	695.5696	926.4358	1008.8635
		1	195.1535	531.9131	708.1353	906.3353	1070.5693
	2	-0.25	296.0055	821.2940	1272.0376	1465.2125	2132.8320
		0.25	352.1845	910.2399	1213.3533	1571.8120	1785.6608
		1	332.3177	880.0185	1232.8641	1534.2185	1887.1155
4	0	-0.25	308.4638	873.9258	1347.8149	1552.6064	2254.8742
		0.25	367.3416	973.3070	1282.2656	1668.3267	1881.5043
		1	346.5125	939.1326	1304.2589	1627.6080	1989.8759
	2	-0.25	177.3302	496.4549	727.6532	866.4435	1228.7325
		0.25	207.6900	548.3803	691.0494	923.7108	999.1938
		1	196.7958	531.5151	704.7205	904.5511	1059.4016
1	2	-0.25	308.6840	854.0797	1313.7761	1520.2459	2209.2225
		0.25	366.2507	946.3259	1252.7749	1630.0746	1832.7096
		1	345.6705	915.4978	1274.6166	1591.9070	1943.5180
	4	-0.25	326.7206	921.7935	1415.1410	1635.0805	2372.9353
		0.25	388.2759	1025.8491	1346.2839	1755.9298	1958.6087
		1	366.2753	990.5788	1371.0812	1714.1030	2081.0834
2	0	-0.25	174.9367	493.8873	712.8224	863.8476	1229.5063
		0.25	204.6146	543.2919	676.5315	919.4833	999.5972
		1	193.9999	527.5267	690.1237	900.8112	1060.2975
	2	-0.25	311.6781	863.8904	1321.5607	1537.1655	2232.3820
		0.25	369.5316	955.5993	1259.8859	1646.3470	1845.7555
		1	348.8715	925.1286	1281.9980	1608.3621	1956.4901
4	-0.25	322.5765	937.6972	1435.6166	1662.4238	2411.4395	
	0.25	395.0021	1041.9948	1365.3637	1783.1117	1979.8545	
	1	372.7099	1006.8279	1360.7229	1741.3295	2101.7136	

Table 4.33. Natural frequencies of 2D-FG annular plate (C – F).

λ_r	λ_z	λ_h	Natural Frequencies (Hz)				
			ω_1	ω_2	ω_3	ω_4	ω_5
		-0.25	70.3747	277.1798	402.0721	609.8991	964.8122
	0	0.25	86.0937	315.0212	405.5163	680.1548	1015.9010
		1	85.0119	304.5273	412.9435	649.6844	1001.7801
		-0.25	114.7747	460.2362	711.8073	1020.0036	1628.8129
0	2	0.25	141.9161	521.9434	723.5719	1138.1823	1734.1122
		1	139.7458	506.0531	733.1160	1086.3818	1698.5811
		-0.25	121.6335	488.7039	746.8060	1082.7031	1727.1490
	4	0.25	150.2760	556.5651	756.2502	1210.8519	1839.6829
		1	148.0020	538.2853	768.1037	1154.8627	1801.4326
		-0.25	79.4545	289.8792	431.2523	617.4968	969.8793
	0	0.25	96.9606	329.5091	434.1601	687.4903	1021.9370
		1	95.8267	318.2027	442.3653	657.3351	1007.2738
		-0.25	123.1341	484.5248	744.5073	1063.4599	1691.1457
1	2	0.25	152.4226	550.3797	756.8416	1185.8230	1798.8829
		1	150.0506	532.8846	767.2244	1131.9879	1762.4582
		-0.25	130.3217	519.9489	787.1044	1145.3119	1820.2738
	4	0.25	161.4586	593.1025	798.4395	1279.4956	1931.1837
		1	158.8889	572.9670	810.8048	1220.4642	1895.2813
		-0.25	79.3657	288.5259	430.6635	617.3439	970.9539
	0	0.25	96.1620	327.8543	432.3848	688.2570	1023.6919
		1	95.2935	316.8621	440.9256	657.6547	1008.8508
		-0.25	124.7164	490.3458	752.8335	1075.8906	1710.7631
2	2	0.25	154.0425	556.8384	764.6455	1199.9927	1819.1624
		1	151.7588	539.1996	775.4243	1145.2582	1782.6926
		-0.25	132.5077	529.1340	800.7303	1164.5659	1850.5251
	4	0.25	163.9676	603.2192	812.0332	1300.9544	1962.4681
		1	161.4242	582.8672	824.7259	1240.7516	1926.3841

Table 4.34. Natural frequencies of 2D-FG annular plate (F – C).

λ_r	λ_z	λ_h	Natural Frequencies (Hz)					
			ω_1	ω_2	ω_3	ω_4	ω_5	
0	0	-0.25	98.4547	339.5240	551.4558	658.0194	983.9485	
		0.25	111.8896	374.9097	534.0486	721.1034	989.5488	
		1	104.7315	361.2457	535.1673	703.1956	1003.4601	
	2	0	-0.25	160.5845	560.2452	966.5523	1100.7682	1659.7754
			0.25	183.5439	621.3332	941.3866	1207.3777	1716.3037
			1	171.5563	597.1128	942.4024	1177.0081	1718.1266
		4	-0.25	170.1181	595.1349	1019.3332	1167.1855	1761.6348
			0.25	194.3650	661.3166	989.8066	1284.2761	1812.4210
			1	181.6386	635.3041	991.4041	1250.6210	1820.0653
1	0	-0.25	90.5313	329.4329	535.1844	647.2040	971.5550	
		0.25	102.9642	361.9830	517.4835	709.5363	977.3569	
		1	96.6509	349.6769	519.5357	692.0462	990.7479	
	2	0	-0.25	164.5921	579.6083	999.3998	1137.2147	1717.4086
			0.25	187.7356	640.5988	970.0990	1247.6700	1768.9641
			1	175.8471	616.5987	972.7646	1216.0855	1775.4668
		4	-0.25	179.0519	626.0661	1078.6238	1223.7183	1847.1767
			0.25	203.9437	692.6861	1043.9076	1345.3611	1895.3885
			1	191.0486	666.5701	1047.5851	1310.0868	1906.8738
2	0	-0.25	90.0387	326.8759	529.2938	645.4225	971.6841	
		0.25	102.1945	359.3298	511.2328	708.6944	978.5038	
		1	96.0228	347.0239	513.5121	691.0291	992.2905	
	2	0	-0.25	165.9646	585.1749	1006.0933	1149.3513	1735.8711
			0.25	189.2171	646.8194	976.5171	1261.5612	1786.5710
			1	177.2881	622.5538	979.2133	1229.6127	1794.2818
		4	-0.25	181.5611	635.5185	1093.4223	1242.8503	1875.8218
			0.25	206.7987	703.1073	1058.4795	1366.7026	1923.0946
			1	193.7574	676.5963	1062.1327	1330.9463	1936.1193

The proposed method is applied to study the effect of different thickness profiles, the power law indices, and several boundary conditions on the free vibration response of the 2D-FG annular plates of variable thickness. Those remarkable influences can be clearly seen in Tables (4.29 – 4.34). As anticipated, the annular plates with convex thickness profiles ($\lambda_h = 0.25$) have the highest natural frequencies while the plates with concave thickness profiles ($\lambda_h = -0.25$) have the lowest natural frequencies among compared cases. when the plate is radially FG ($\lambda_z = 0$), it is revealed that increasing the value of λ_r decreases natural frequencies of the structure for the considered FGM model. When the plate is FG only through the thickness direction ($\lambda_r = 0$), It can be concluded that an increase in the value of λ_z leads to an increase in the natural frequencies of the structure. In 2D-FG annular plates gradually increasing of the λ_r and λ_z values increase the natural frequencies of the plate.

Boundary conditions have also a significant influence on the free vibration behavior of considered structures. Clamped – clamped boundary conditions lead to the highest natural frequencies and clamped – free boundary conditions lead to the smallest free vibration characteristics.

4.5. Forced Vibration Analysis of 2D-FG Annular Plates

4.5.1. Verification

To examine the forced vibration behavior of 2D-FG annular plates a computer program code is written in FORTRAN. To validate the suggested scheme, several 2D-FG annular plates of uniform thickness are considered. Transient responses of the considered structures are examined by the proposed method and ANSYS. Calculated results are compared and illustrated below. One type of dynamic uniformly distributed load, as shown in Figure (4.10) with an amplitude $P_{z0} = 100$ kN/m is applied to the plate. Constituent materials are two distinct metals and two distinct ceramics given in Table (3.1). Mechanical

properties of the plate is considered to vary both in radial and thickness direction by a power law form (Eq. (3.7)). The Poisson's ratio is assumed to be constant. Unified approach of the CFM and the Laplace transform is employed to solve the governing equations of the problem. The canonical Eqs. (3.132 - 3.137) are solved for a series of Laplace parameter. The results obtained in the Laplace domain, are transformed to the time domain with the help of modified Durbin's numerical inverse Laplace transform method. The damped forced vibration of the considered structures is investigated by the means of Kelvin damping model.

To examine the transient response of the considered structures in ANSYS, the plate is divided into 200 SHELL209 elements. Shear deformation is included in this element. Each element is divided into 40 layers in the thickness direction. It must be noted that for each layer a different material is defined in ANSYS. Whereas, geometric and material properties can be considered as a function of radial coordinates by using the suggested approach.

In this case, results obtained for fewer Laplace transform parameters (coarse time increment) overlap the results obtained with higher parameters (finer increments) (see Noori et al. (2018a)). While the validity of the ANSYS results depends on the appropriate selection of the optimum time step size. 64 steps of time (64 Laplace parameters) are used in the analysis by the presented procedure while 512 steps of time each are used in the ANSYS. By using the suggested approach considerable saving in computation time can be observed

A 2D-FG annular plates of uniform thickness ($h_i = h_o = 1\text{ m}$; $r_o = 5\text{ m}$; $r_i = 1\text{ m}$) is considered (Figure (4.10)). The plate is subjected to step dynamic load. The shear correction factor, k_s , is taken to be 5/6. For Laplace transform of the load see Appendix A.

The damped and undamped forced vibration analysis is performed. Comparisons for maximum vertical deflections, shear forces, bending moments and rotations of the plate are obtained and compared for various boundary

conditions, λ_r , λ_z and λ_h values. Comparisons are presented in the graphical form will be given below.

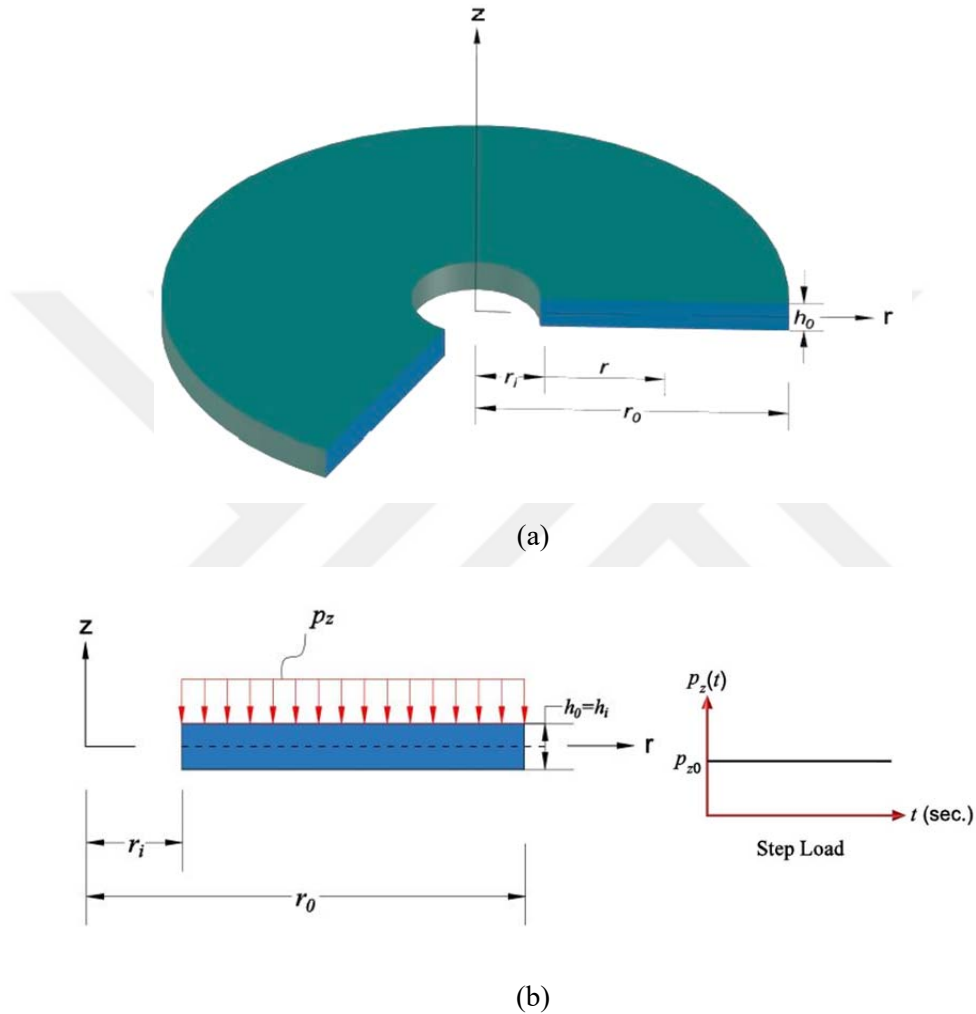


Figure 4.10. (a) Perspective view of the plate (b) Section and dynamic load

Figures (4.11 - 4.13) present the comparison of maximum vertical displacement, bending moment and shear force of clamped-clamped isotropic annular plate for $\lambda_r = 0$ and $\lambda_z = 0$.

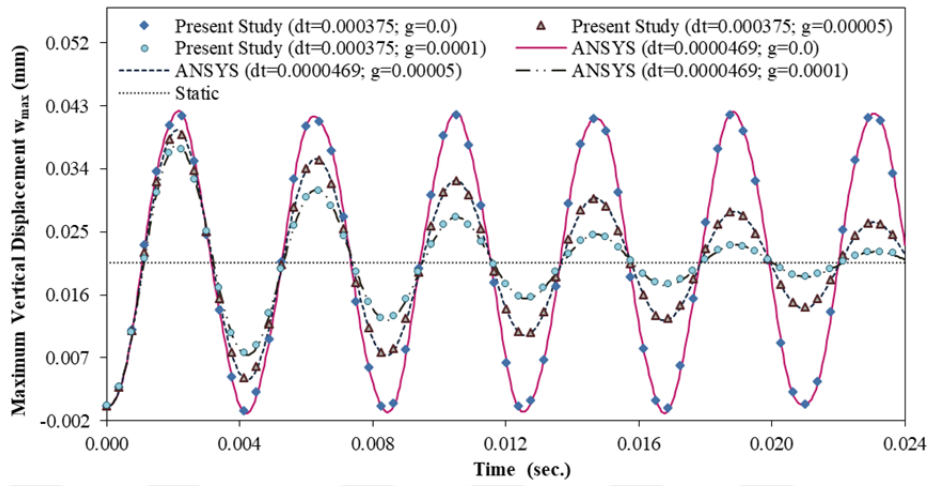


Figure 4.11. Comparison of the maximum vertical displacement.

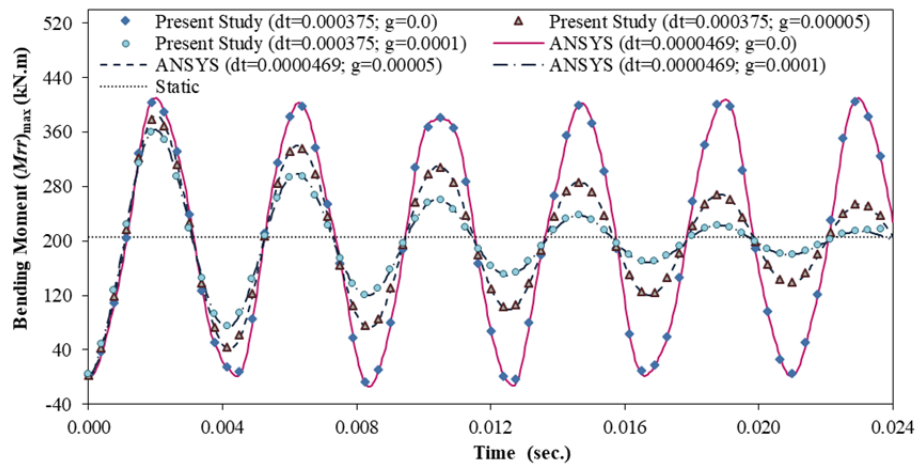


Figure 4.12. Comparison of the maximum bending moment.

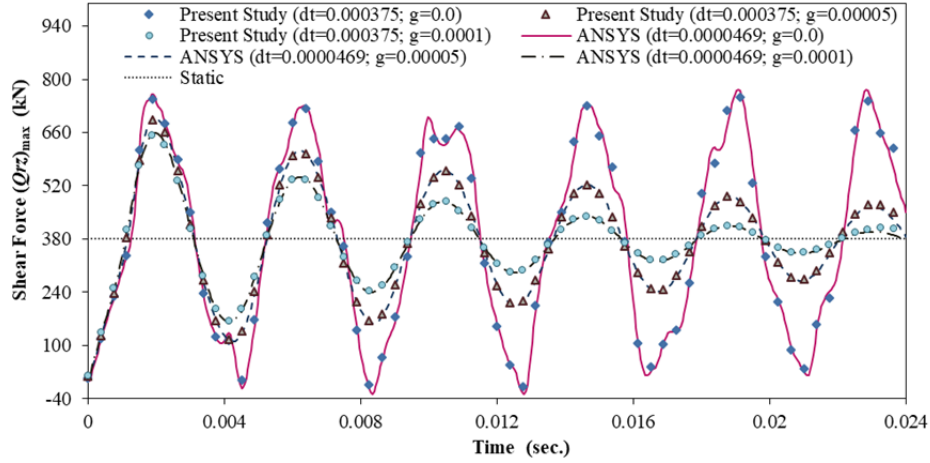


Figure 4.13. Comparison of the maximum shear force.

Figures (4.14 - 4.16) illustrate the comparison of maximum vertical displacement, bending moment and shear force of clamped-clamped supported annular plate. The plate is assumed to be FG only in the thickness direction for $\lambda_r = 0$ and $\lambda_z = 2$.

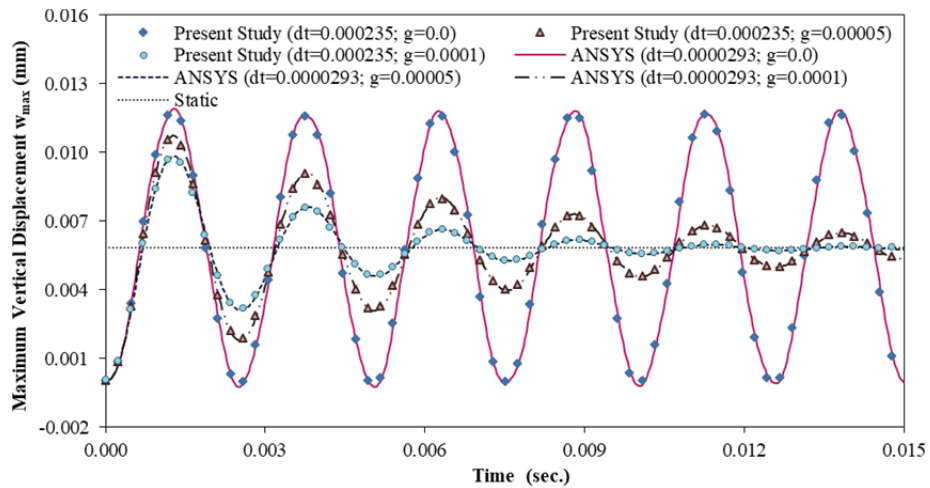


Figure 4.14. Comparison of the maximum vertical displacement.

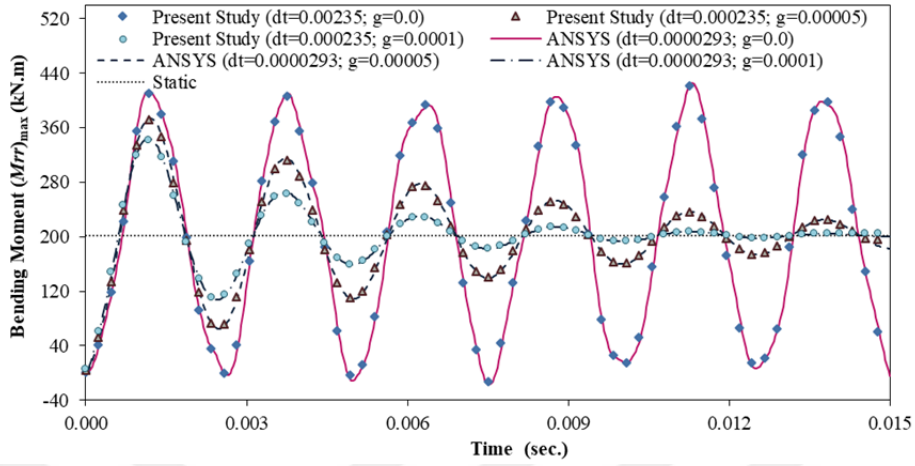


Figure 4.15. Comparison of the maximum bending moment.

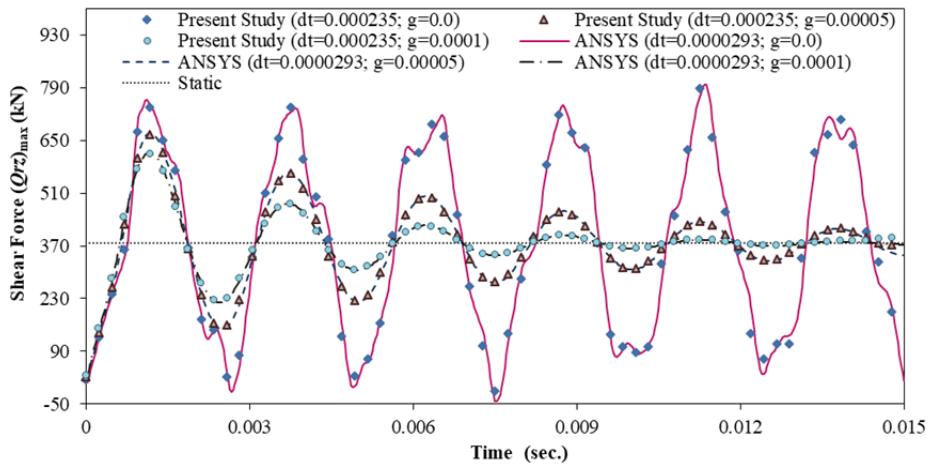


Figure 4.16. Comparison of the maximum shear force.

Figures (4.17 - 4.19) demonstrate the comparison of maximum vertical displacement, bending moment and shear force of clamped clamped supported FG annular plate. The plate is assumed to be FG only in the thickness direction for $\lambda_r = 0$ and $\lambda_z = 4$.

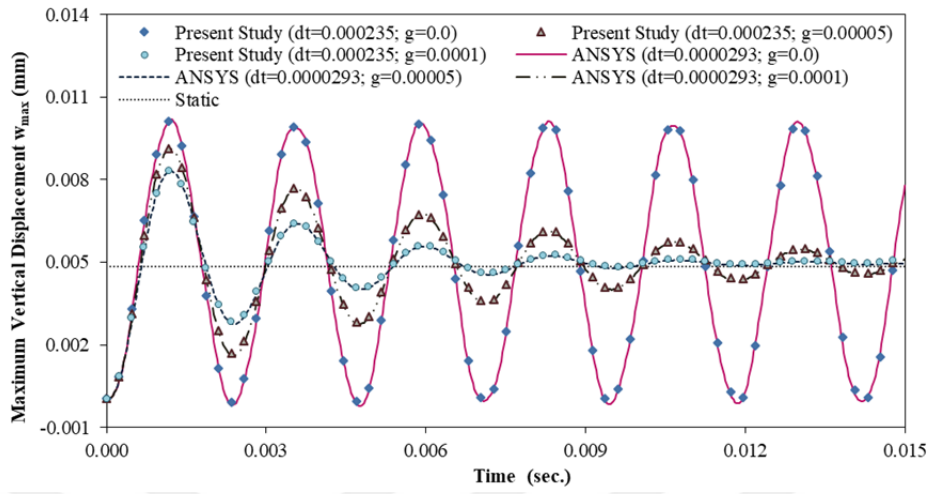


Figure 4.17. Comparison of the maximum vertical displacement.

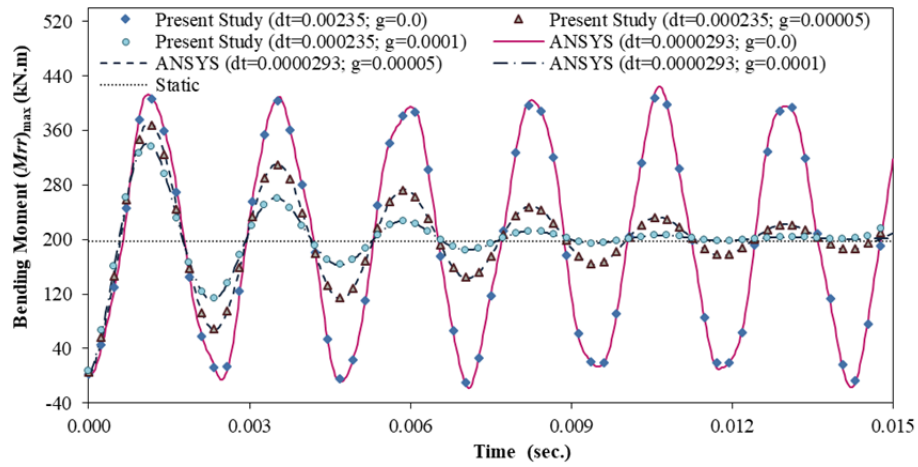


Figure 4.18. Comparison of the maximum bending moment.

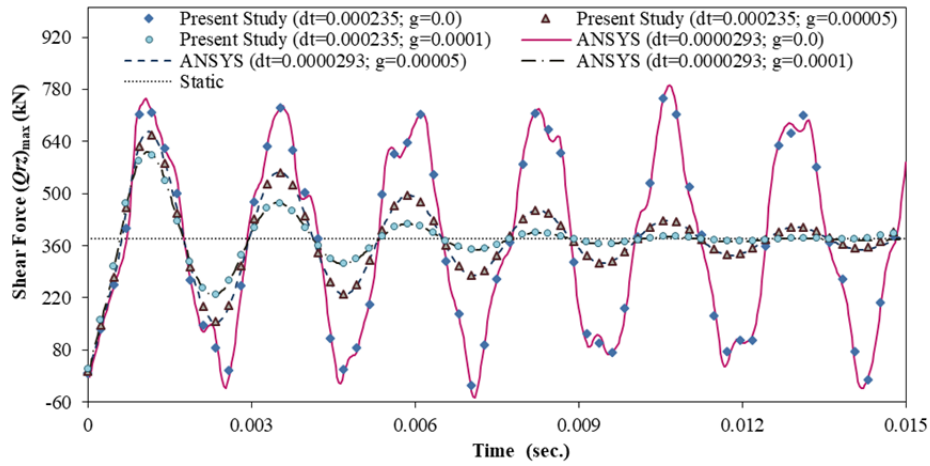


Figure 4.19. Comparison of the maximum shear force.

Figures (4.20 - 4.22) report the comparison of maximum vertical displacement, bending moment and shear force of clamped-clamped supported annular plate. The plate is assumed to be radially FG for $\lambda_r = 1$ and $\lambda_z = 0$.

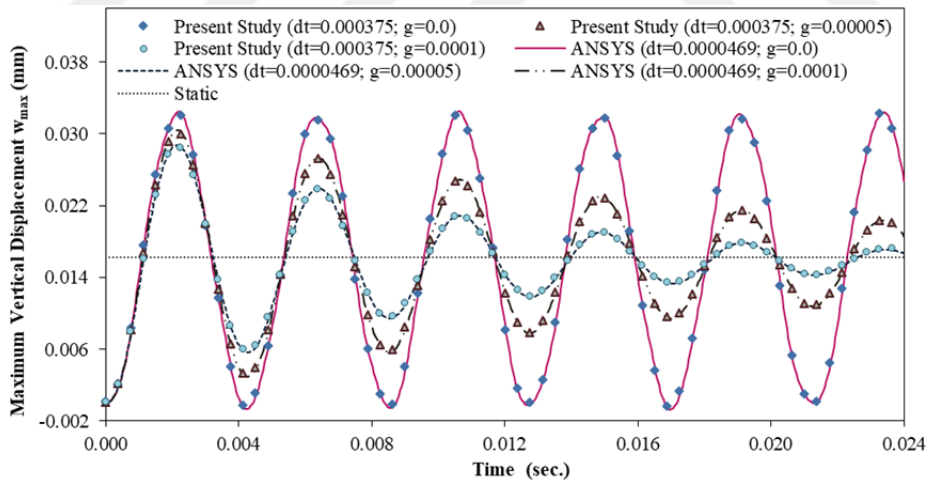


Figure 4.20. Comparison of the maximum vertical displacement.

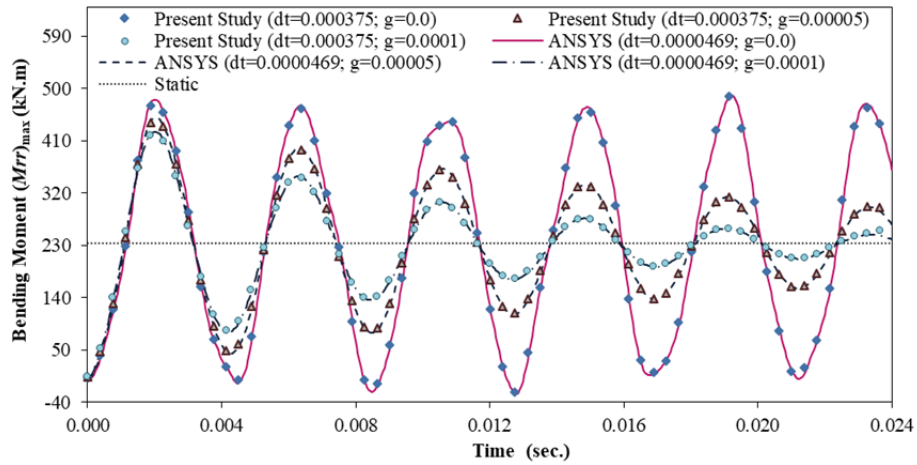


Figure 4.21. Comparison of the maximum bending moment.

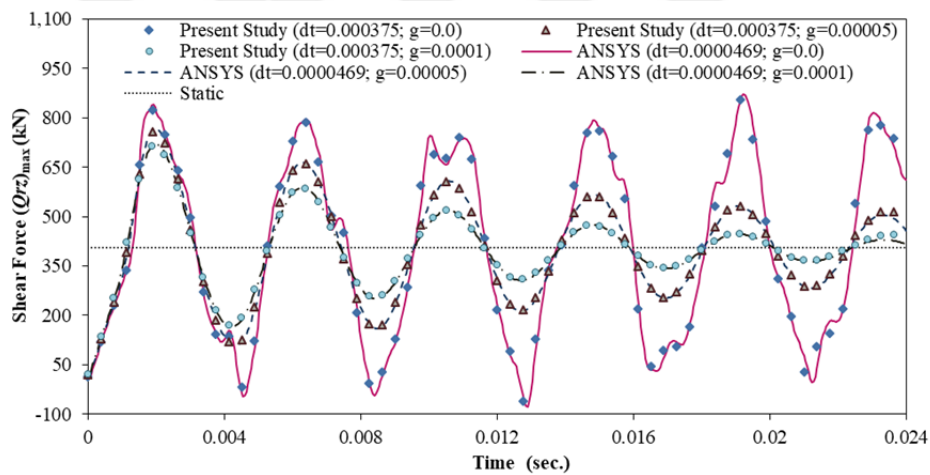


Figure 4.22. Comparison of the maximum shear force.

Figures (4.23 - 4.25) indicate the comparison of maximum vertical displacement, bending moment and shear force of clamped – simply supported annular plate. The plate is assumed to be functionally graded both in radial and thickness directions for $\lambda_r = 1$ and $\lambda_z = 2$.

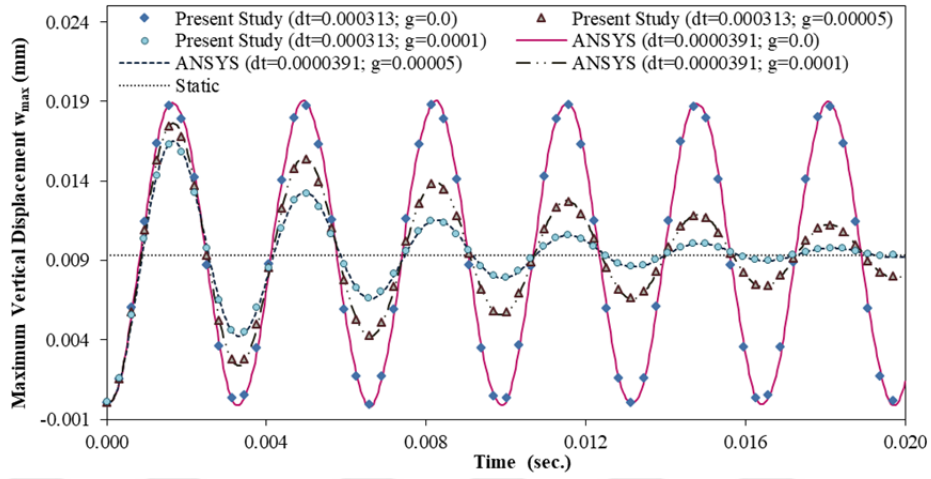


Figure 4.23. Comparison of the maximum vertical displacement.

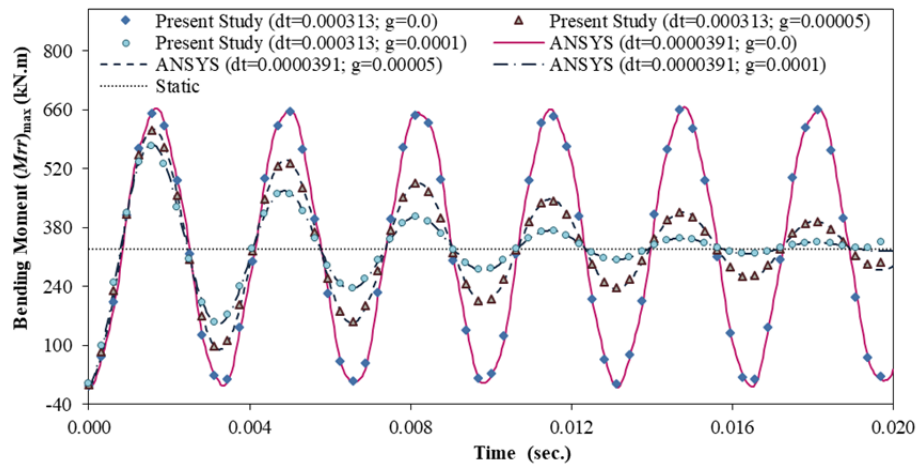


Figure 4.24. Comparison of the maximum bending moment.

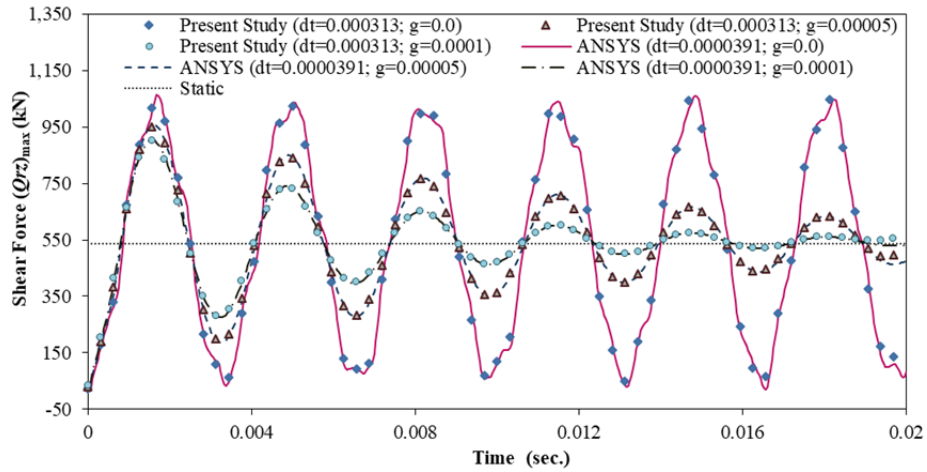


Figure 4.25. Comparison of the maximum shear force.

Figures (4.26 - 4.28) present the comparison of maximum vertical displacement, bending moment and shear force of clamped – simply supported annular plate. The plate is assumed to be 2D-FG for $\lambda_r = 1$ and $\lambda_z = 4$.

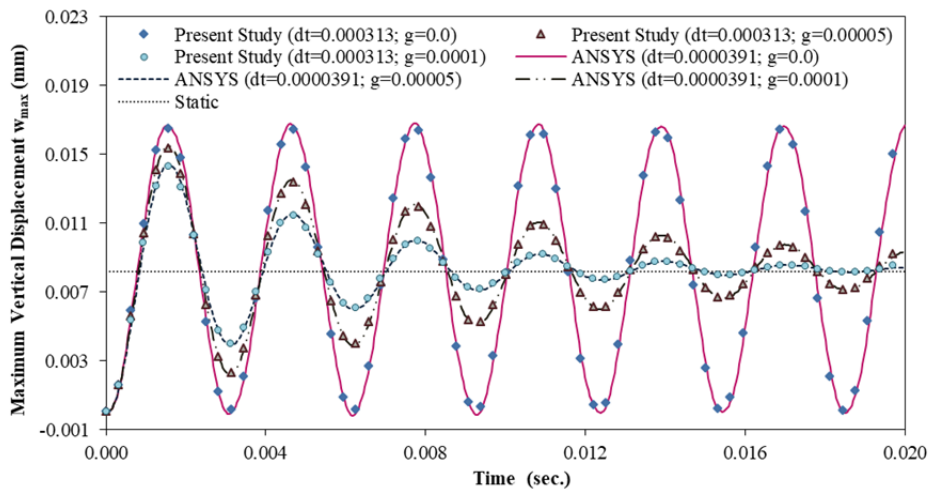


Figure 4.26. Comparison of the maximum vertical displacement.

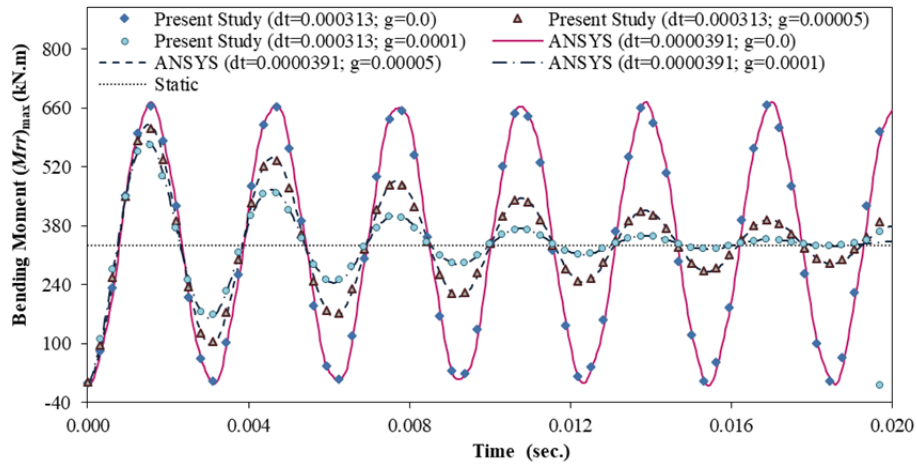


Figure 4.27. Comparison of the maximum bending moment.

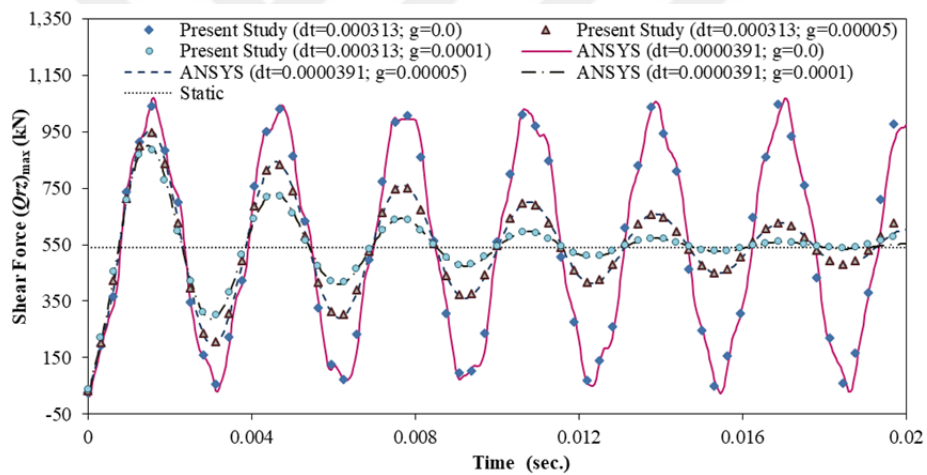


Figure 4.28. Comparison of the maximum shear force.

Figures (4.29 - 4.32) show the comparison of maximum vertical displacement, bending moment, rotation and shear force of clamped – free annular plate. The plate is assumed to be functionally graded only in radial direction for $\lambda_r = 2$ and $\lambda_z = 0$.

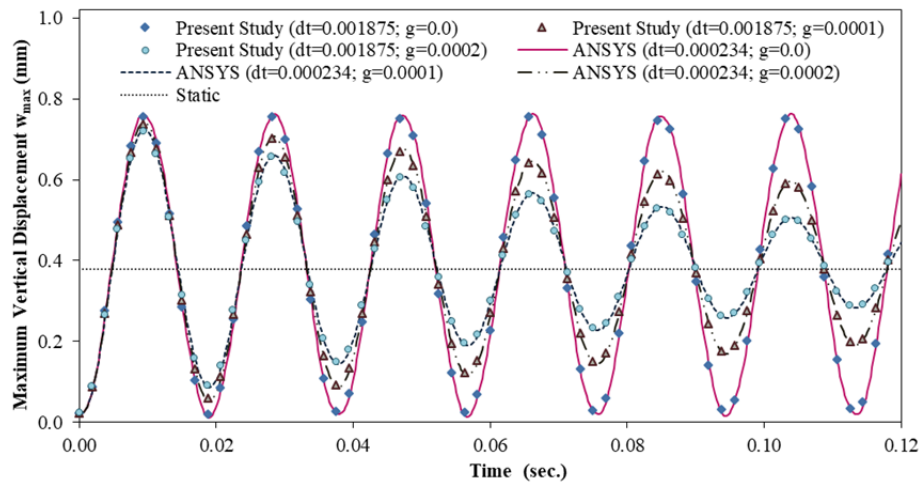


Figure 4.29. Comparison of the maximum vertical displacement.

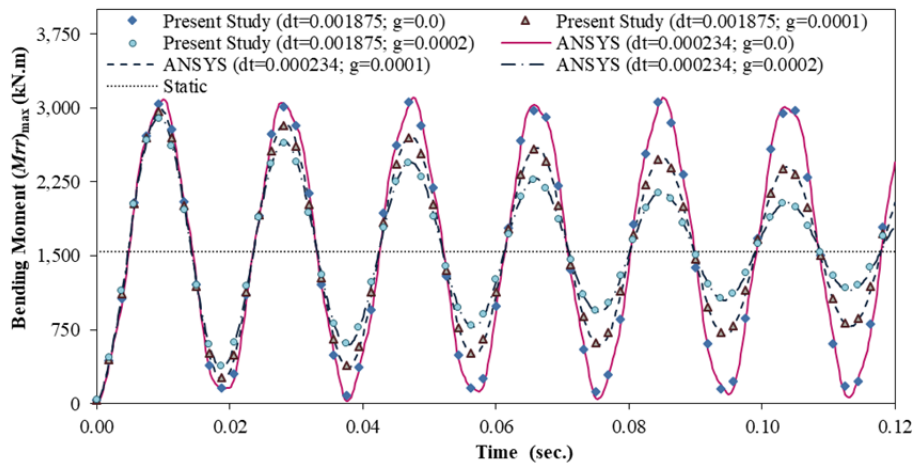


Figure 4.30. Comparison of the maximum bending moment.

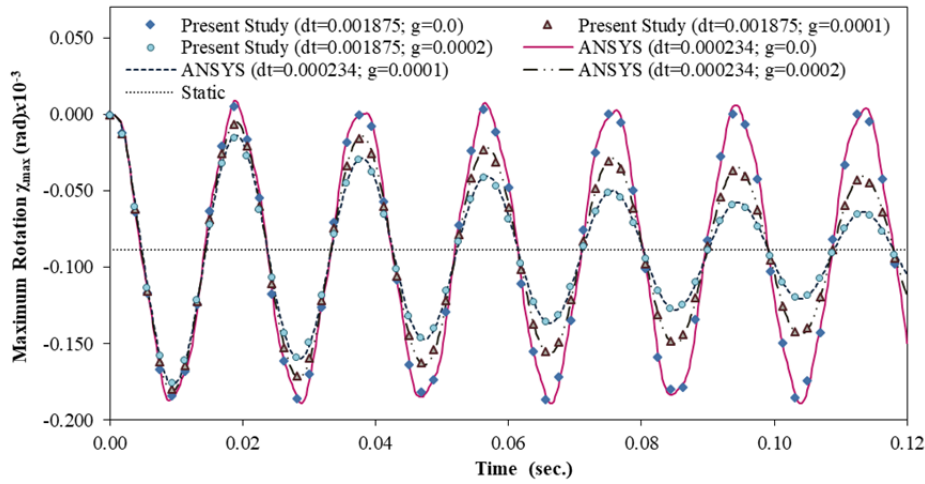


Figure 4.31. Comparison of the maximum rotation.

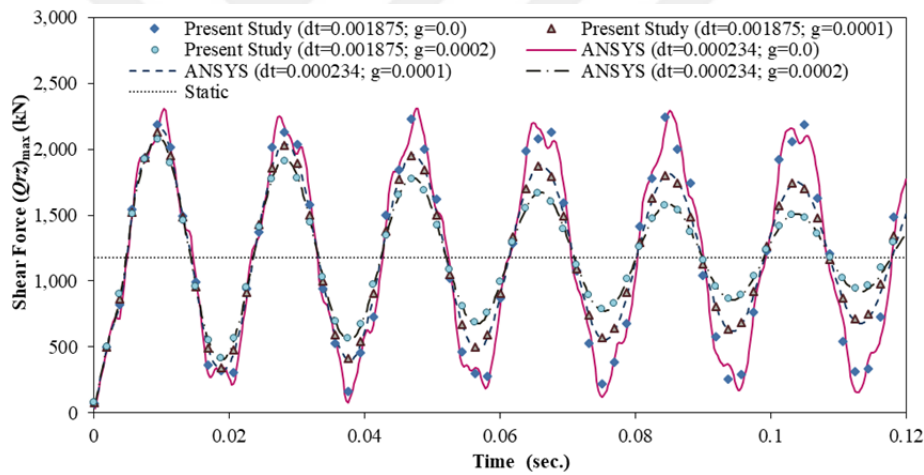


Figure 4.32. Comparison of the maximum shear force.

Figures (4.33 - 4.36) indicate the comparison of maximum vertical displacement, bending moment, rotation and shear force of clamped – free supported annular plate. The plate is assumed to be functionally graded both in radial and thickness directions for $\lambda_r = 2$ and $\lambda_z = 2$.

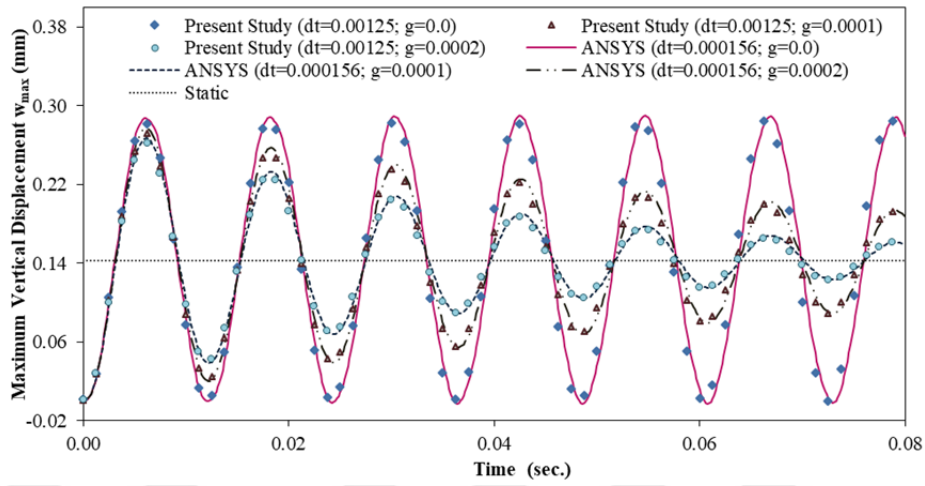


Figure 4.33. Comparison of the maximum vertical displacement.

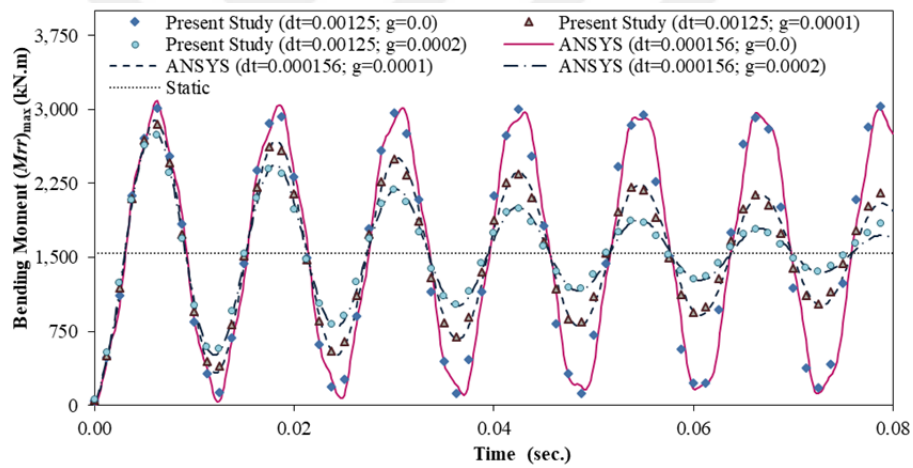


Figure 4.34. Comparison of the maximum bending moment.

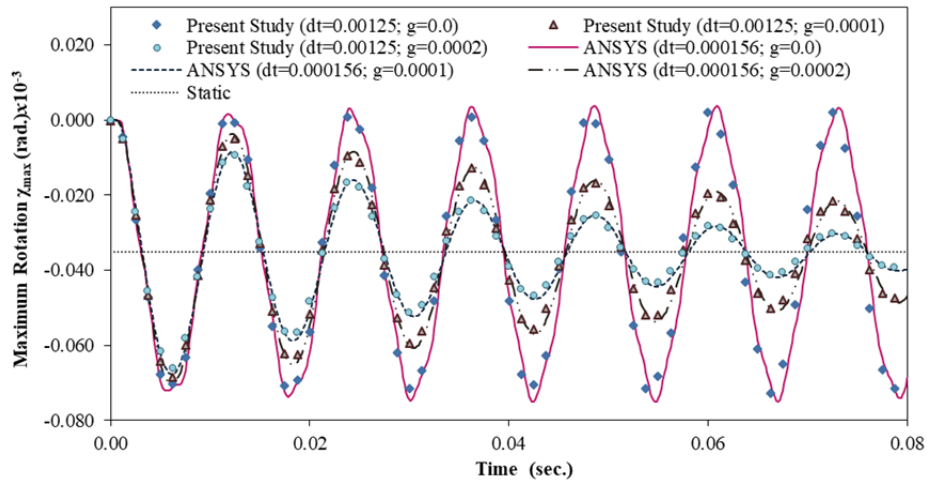


Figure 4.35. Comparison of the maximum rotation.

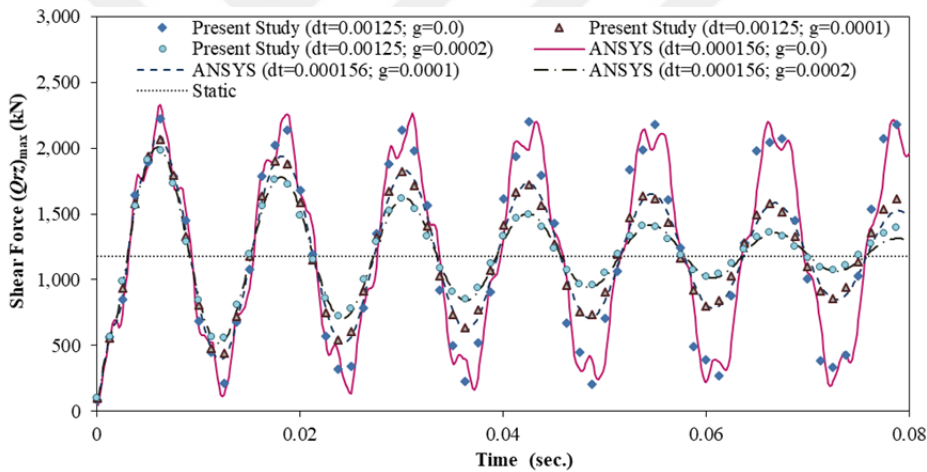


Figure 4.36. Comparison of the maximum shear force.

Figures (4.37 - 4.40) present the comparison of maximum vertical displacement, bending moment, rotation and shear force of clamped – free supported annular plate. The plate is assumed to be functionally graded both in radial and thickness directions for $\lambda_r = 2$ and $\lambda_z = 4$.

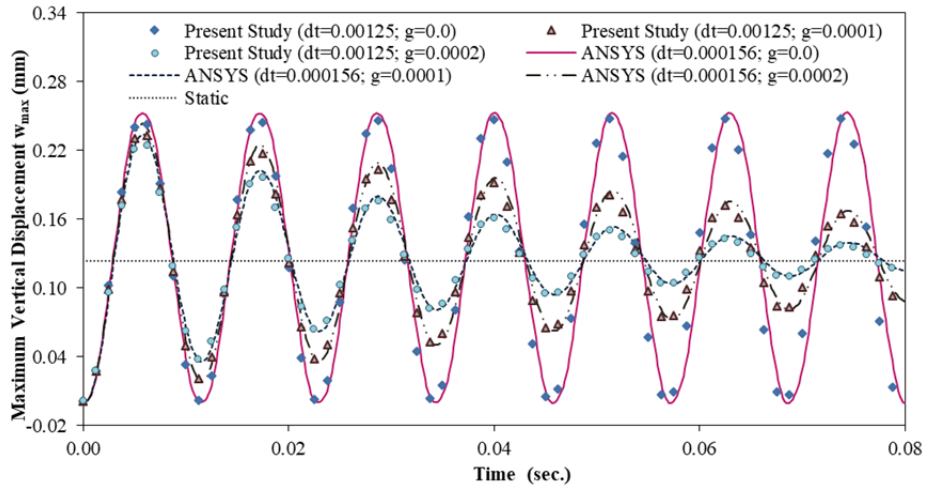


Figure 4.37. Comparison of the maximum vertical displacement.

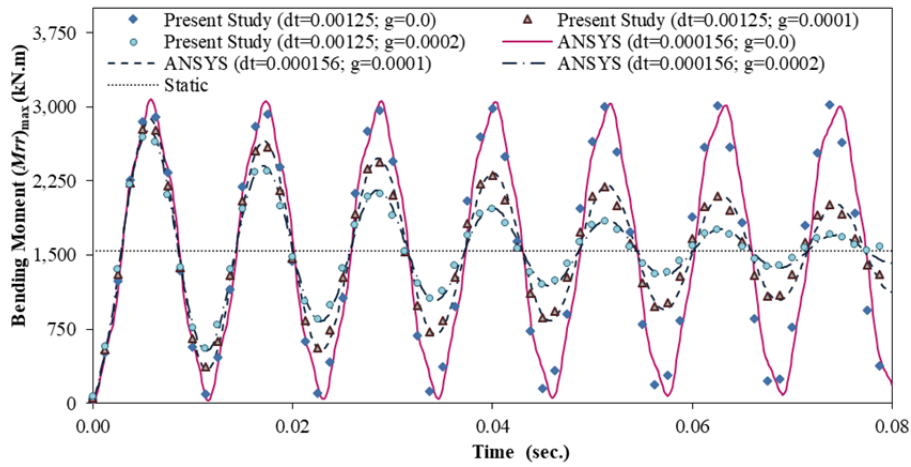


Figure 4.38. Comparison of the maximum bending moment.

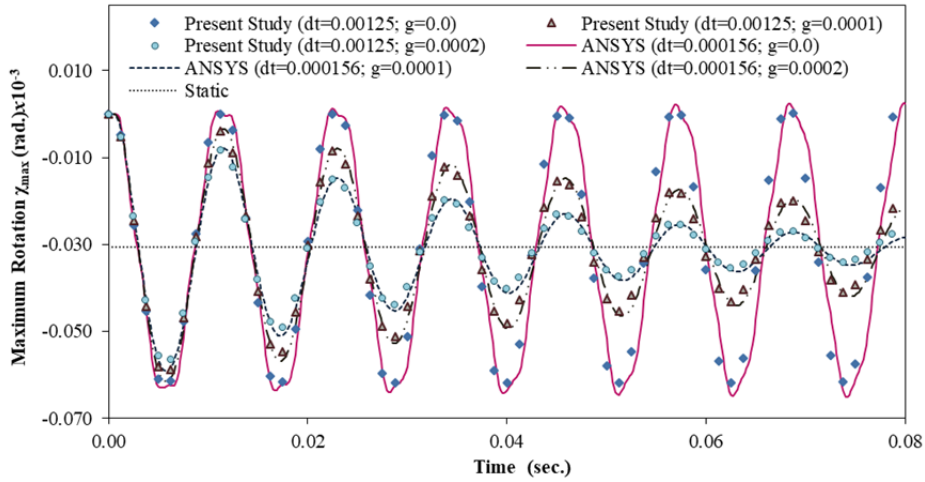


Figure 4.39. Comparison of the maximum rotation.

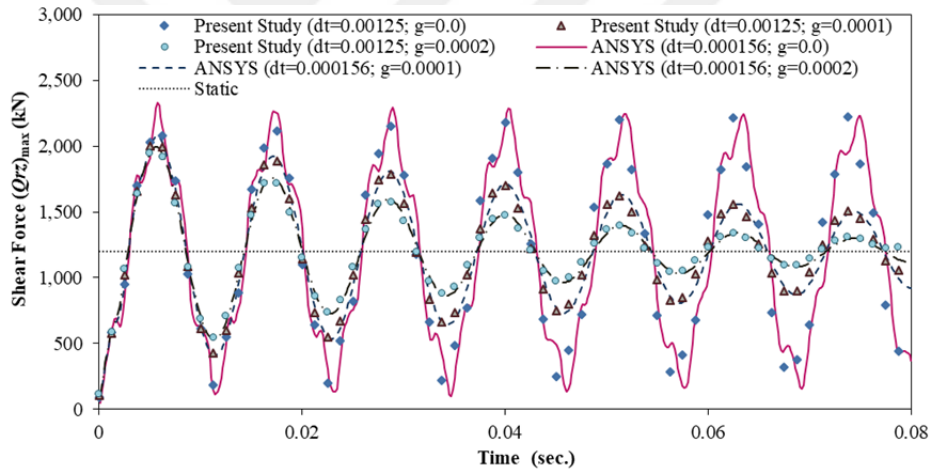


Figure 4.40. Comparison of the maximum shear force.

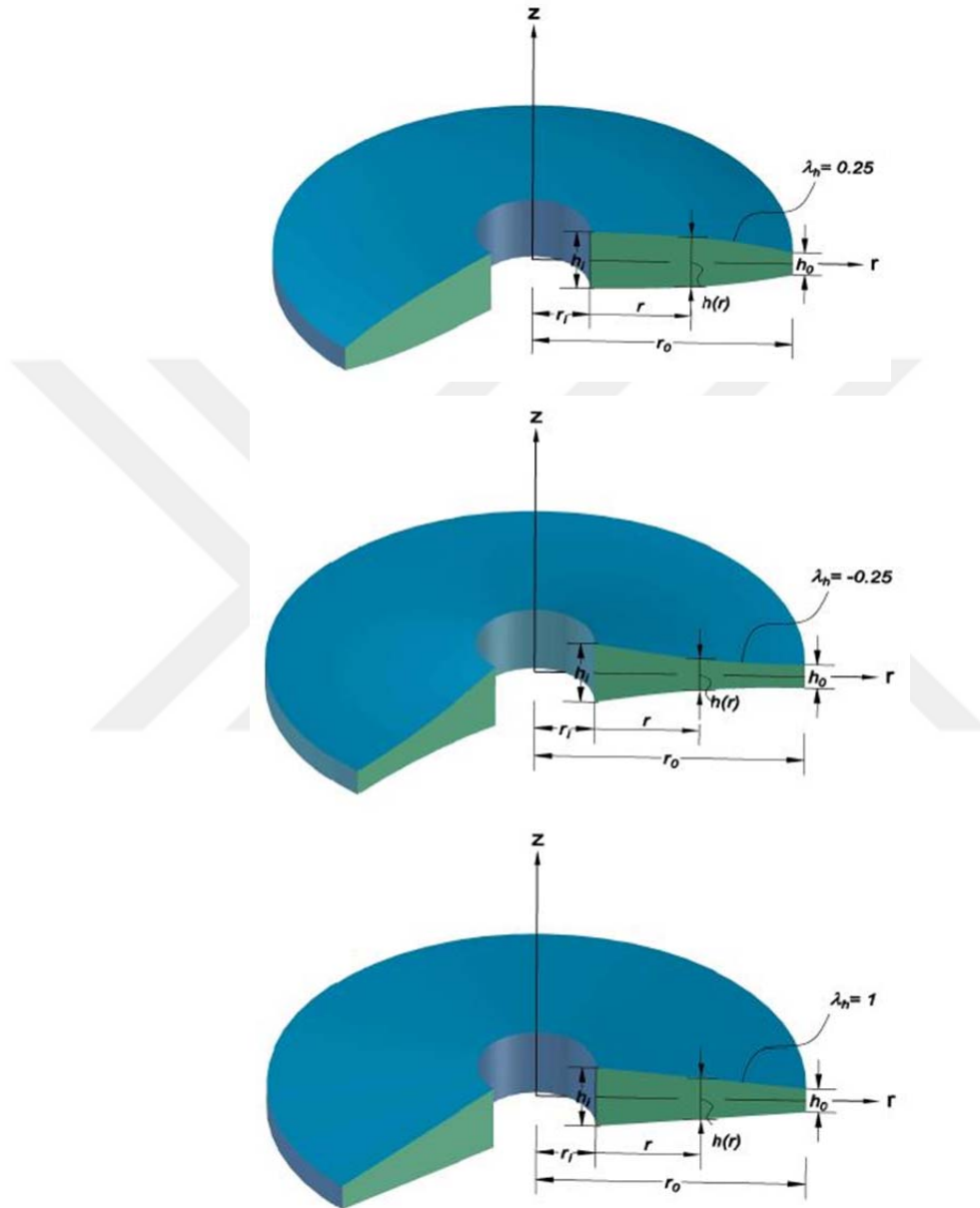
It is apparent in Figures (4.11 – 4.40), that current results show a very good agreement with those of ANSYS for several boundary conditions and volume fraction exponents. To obtain reliable accurate results for the damped and undamped transient response of 2D-FG circular and annular plates in ANSYS, an appropriate number of graded layers in thickness and radial direction of the plate is required. Not surprisingly, for higher values of λ_z and λ_r results of ANSYS start

to differ from those of the CFM, especially for higher values of λ_z . Because λ_z has a more significant influence on the static and dynamic response of the considered problem. For this reason, then plates must be divided into much more layers in the thickness direction for higher values of λ_z in ANSYS.

By infusing the suggested procedure to the governing equations of the problem damped and undamped transient response of 2D-FG plates can be carried out in a simple and efficient manner. Exactness of the results of the CFM does not depend on the number and size of the time steps, for this reason results obtained for a coarse time increment along with fewer Laplace transform parameters coincide with those obtained with finer increments and higher parameters. This reveals the effectiveness and superiority of the proposed method. The exactness of the results of the CFM does not depend on the number and size of the time steps, for this reason, results obtained for a coarse time increment along with fewer Laplace transform parameters coincide those obtained with finer time increments and higher parameters. This reveals the effectiveness and superiority of the proposed method.

When step by step time integration methods, for example the Newmark method, is applied to tackle time-dependent governing equations of present class of problems, the optimum time step size is required to obtain accurate results. In this thesis, 64 and 512 sub-steps of time have been used in the suggested method and in ANSYS, respectively.

4.5.2. Forced Vibration of 2D-FG Annular Plates with Variable Thickness

Figure 4. 41. Illustrations of thickness profiles ($\lambda_h = 0.25$; $\lambda_h = -0.25$; $\lambda_h = 1$)

In this section, forced vibration of 2D-FG annular plates with variable thickness is examined.

First, the influence of geometric constant on the transient response of the considered plate is studied. The radially varying thickness profiles are shown in Figure (4.41). A clamped – free annular plate is considered under the same dynamic loads as given in the previous section. The plate has inner radii of $r_i = 1$ m, outer radius of $r_o = 5$ m. The shear correction factor k_s is taken to be $\pi^2/12$. The thickness of the plate is considered to be ($h_i = 2$ m) in inner radii and ($h_o = 1$ m) at outer radius. Properties of materials are graded based on Eq. (3.7). The radial coordinate dependent function of the thickness is given by Eq. (3.9). Boundary conditions of the problem are given by Eqs. (3.82 – 3.83). Forced vibration of the plate is examined for $\lambda_r = 0$ and $\lambda_z = 0$ volume fraction exponents. The time histories for maximum vertical displacement and rotation are illustrated in Figures (4.42 - 4.43).

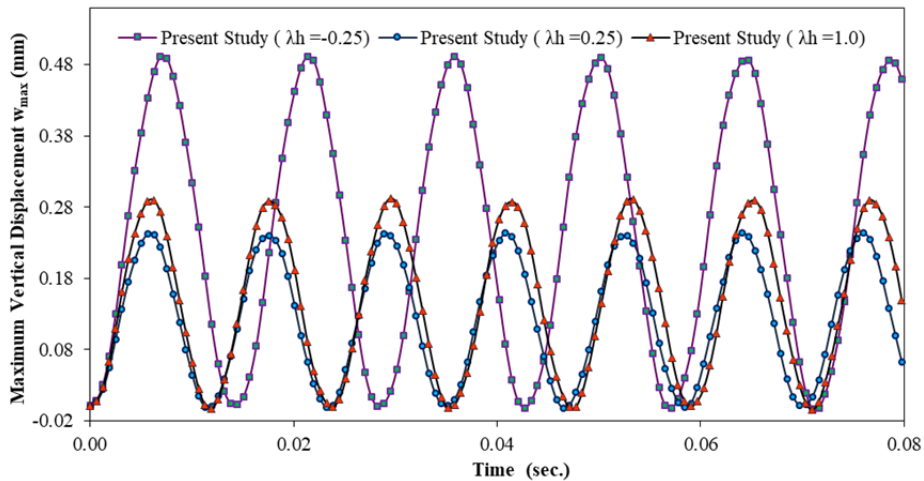


Figure 4.42. Comparison of the maximum vertical displacement.

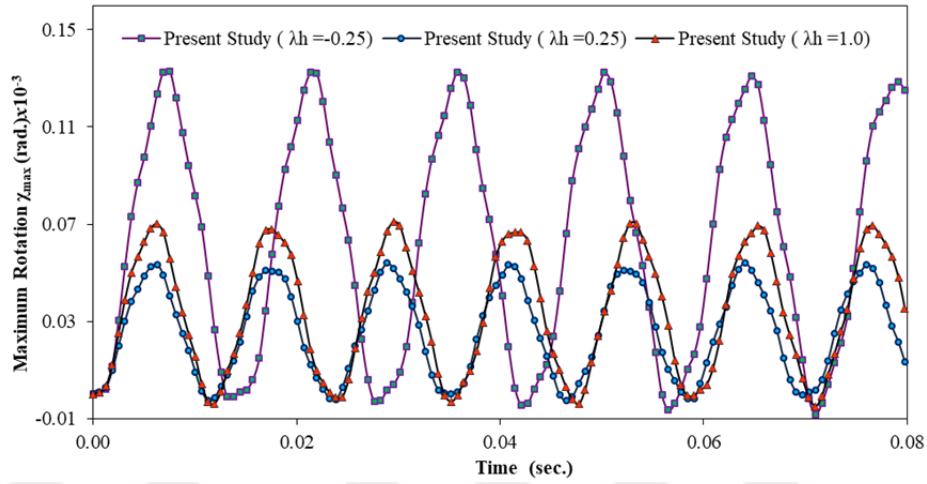


Figure 4.43. Comparison of the maximum rotation.

Transient response of the considered plate is studied for $\lambda_r = 0$ and $\lambda_z = 2$ values. The results for maximum vertical displacement and rotation are given in Figures (4.44 - 4.45).

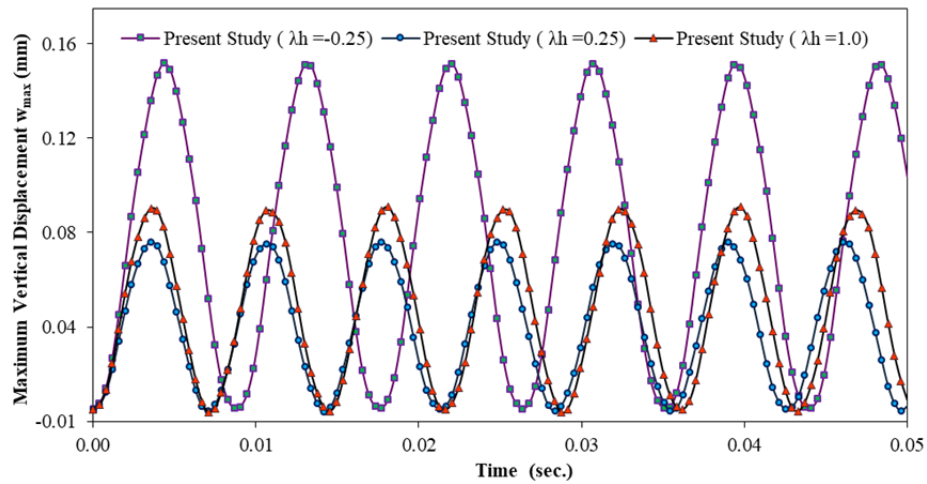


Figure 4.44. Comparison of the maximum vertical displacement.

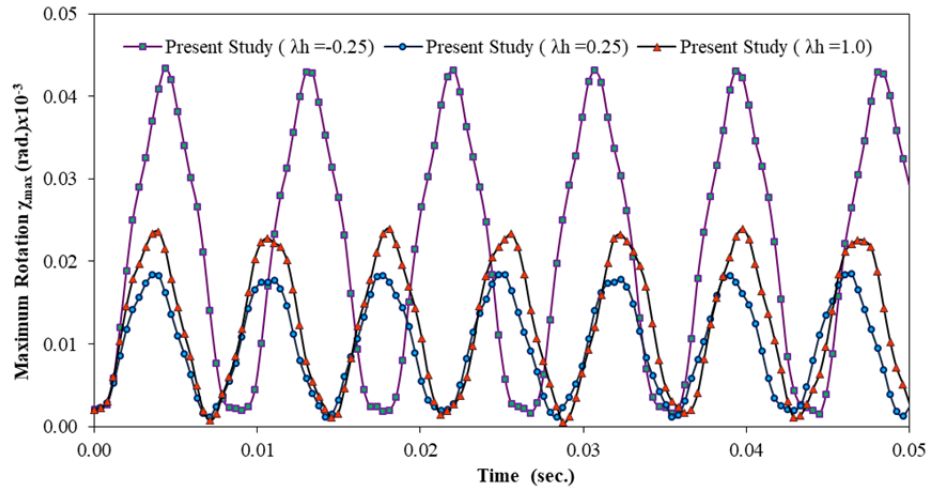


Figure 4.45. Comparison of the maximum rotation.

Undamped forced vibration behaviour of the considered structure is carried out for $\lambda_r = 0$ and $\lambda_z = 4$ values. Numerical values for maximum vertical displacement and rotation are presented in Figures (4.46- 4.47).

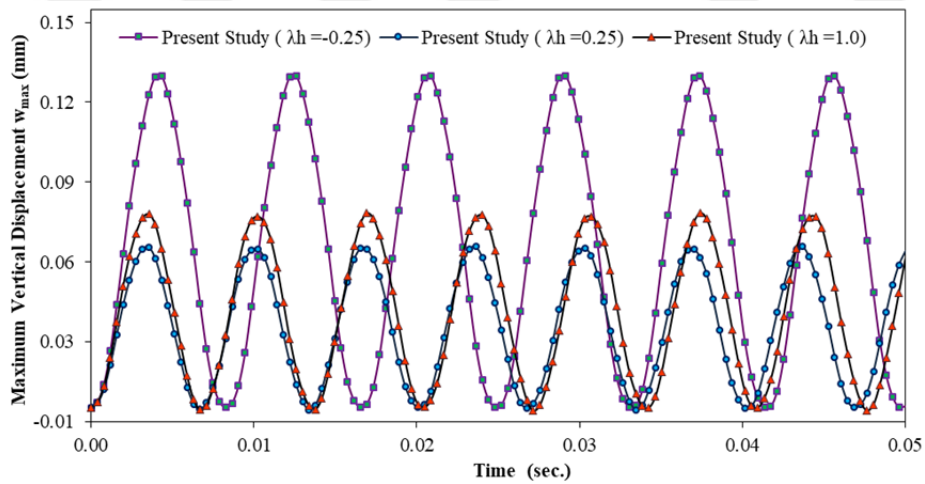


Figure 4.46 Comparison of the maximum vertical displacement.

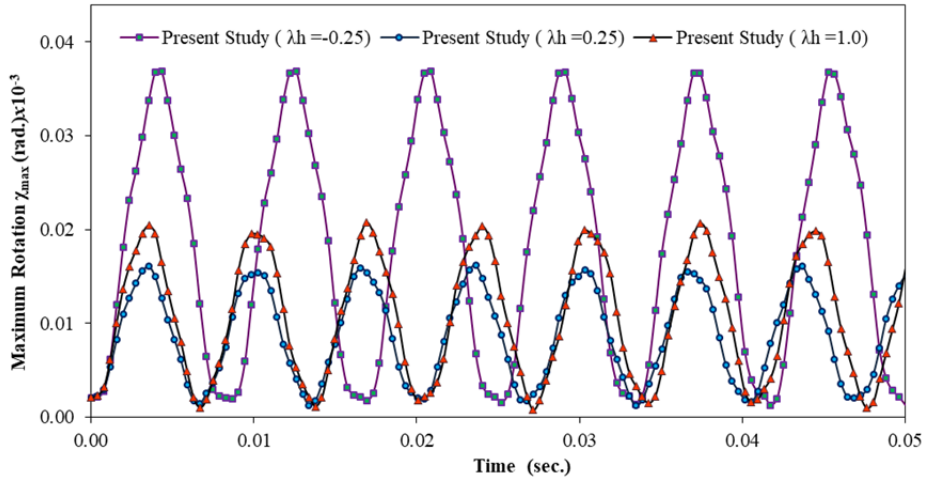


Figure 4.47. Comparison of the maximum rotation.

As expected, the thickness variation profile has a highly significant influence on the undamped forced vibration of the considered structures. According to Figures (4.42 - 4.47) the plate with a concave thickness variation profile ($\lambda_h = -0.25$) has the highest vibration amplitudes and periods for deflection and rotations. Contrary to this case, the annular plate with the convex thickness variation profile ($\lambda_h = 0.25$) has the lowest periods and amplitudes of vibration. This behavior is due to the resulting change in the flexural rigidity of the plate.

In the next step, the effect of variations of Young's modulus and the density in the radial direction on the forced vibration of the 2D-FG annular plates of variable thickness is examined. Thickness profiles are shown in Figure (4.40). A free – clamped supported annular plate is considered under the same dynamic loads as given in the previous section. The plate has inner radii of $r_i = 1$ m, outer radius of $r_o = 5$ m. Properties of materials are graded based on Eq. (3.7). The radial coordinate dependent function of the thickness is given by Eq. (3.9).

Forced vibration of the plate is examined for $\lambda_h = 1$ and $\lambda_z = 4$ values. The time histories for maximum vertical displacement and rotation are illustrated in Figures (4.48 - 4.49).

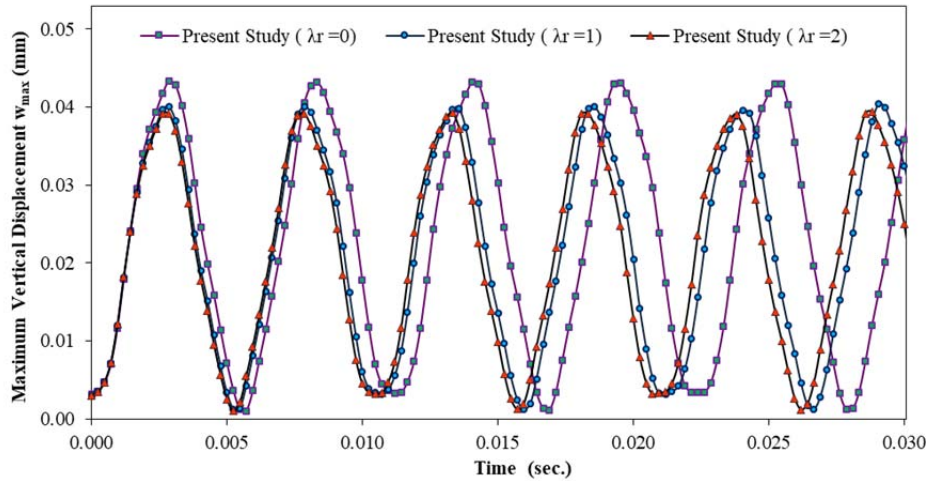


Figure 4.48. Comparison of the maximum vertical displacement.

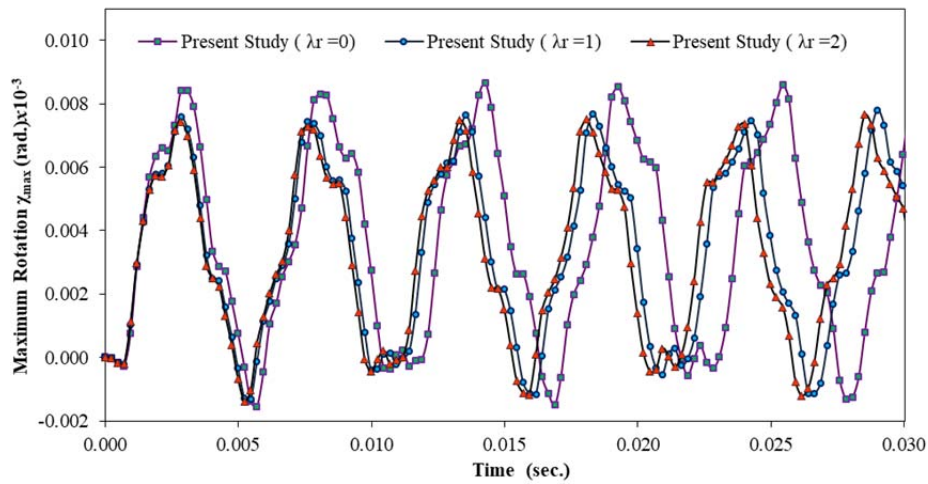


Figure 4.49. Comparison of the maximum rotation.

Figures (4.50-4.51) show the comparison of maximum vertical displacement and rotation for F – C annular plate ($\lambda_h = 0.25$ and $\lambda_z = 4$). Results are obtained for various λ_r values and compared in graphical form.

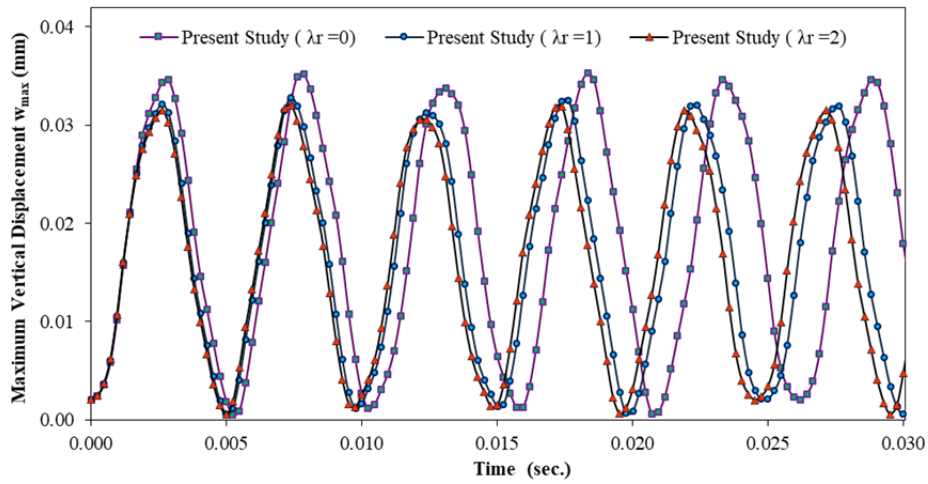


Figure 4.50. Comparison of the maximum vertical displacement.

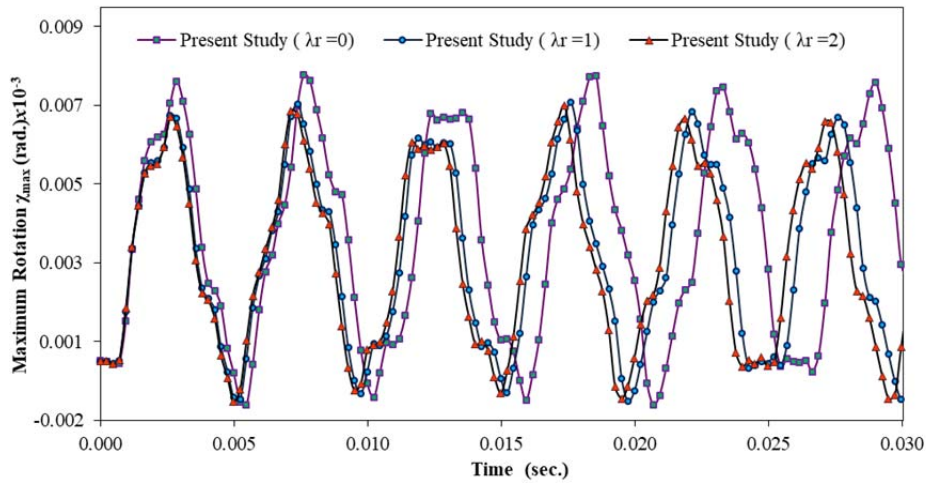


Figure 4.51. Comparison of the maximum rotation.

Figures (4.52 - 4.53) demonstrate the comparison of maximum vertical displacement and rotation for F – C supported annular plate ($\lambda_h = -0.25$ and $\lambda_z = 4$). Results are obtained for various λ_r values and compared in graphical form.

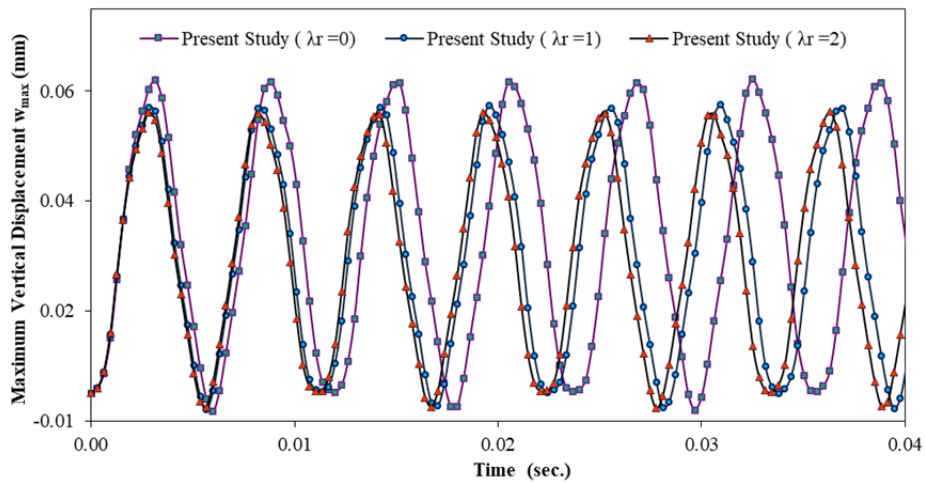


Figure 4.52. Comparison of the maximum vertical displacement.

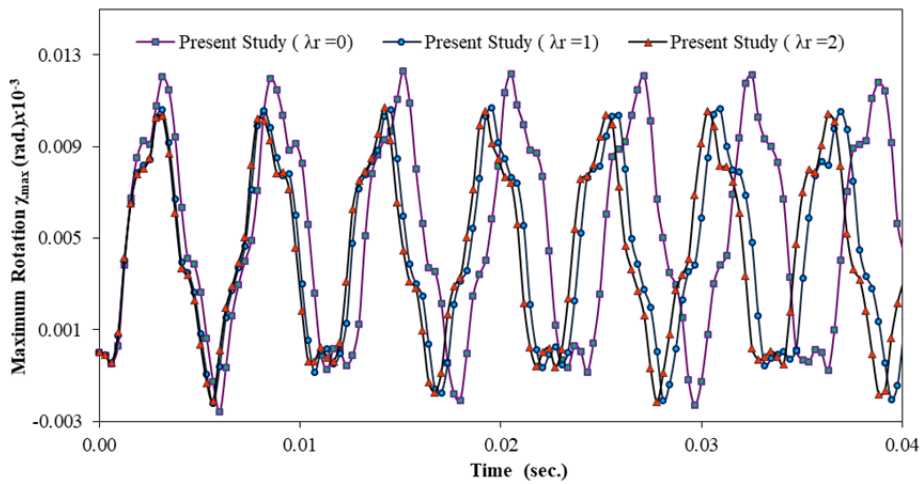


Figure 4.53 Comparison of the maximum rotation.

The results reveal that the λ_r has an insignificant effect on the transient response of the considered structures. It can be concluded from Figures (4.48 - 4.53) that an increase in the radial exponent of volume fractions leads to a decrease in the period and vibration amplitude of forced vibration results.

Furthermore, a comprehensive parametric study is carried out to highlight the effects of the volume fraction exponents of the thickness direction, λ_z , on the forced vibration response of the considered structures. Material properties, dynamic loads, and geometric properties of the plate are the same as the previous example. The plate is considered to be clamped in the inner edge and free at its outer edge. Results are depicted in Figures (4.54 - 4.55) for various λ_z values to compare the time history of maximum vertical displacement and rotation for C – F annular plate of variable thickness for $\lambda_r = 1$ and $\lambda_h = 1$ values.

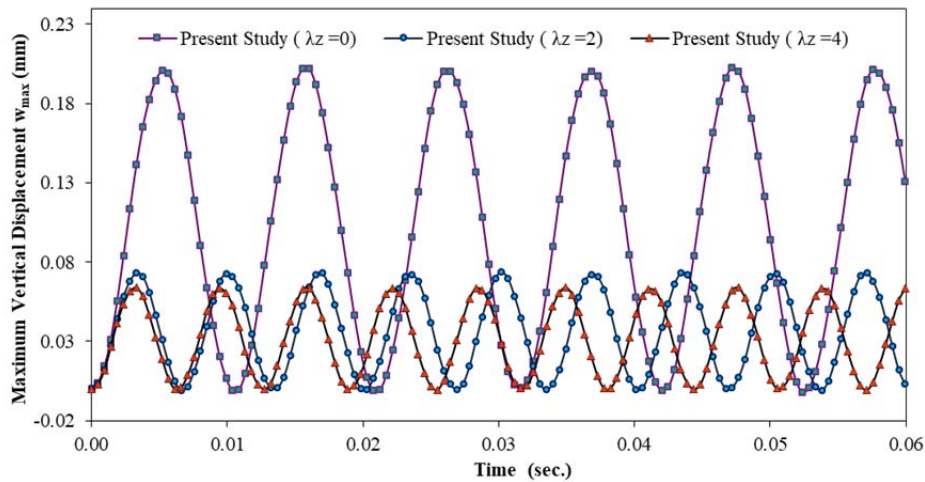


Figure 4.54. Comparison of the maximum vertical displacement.

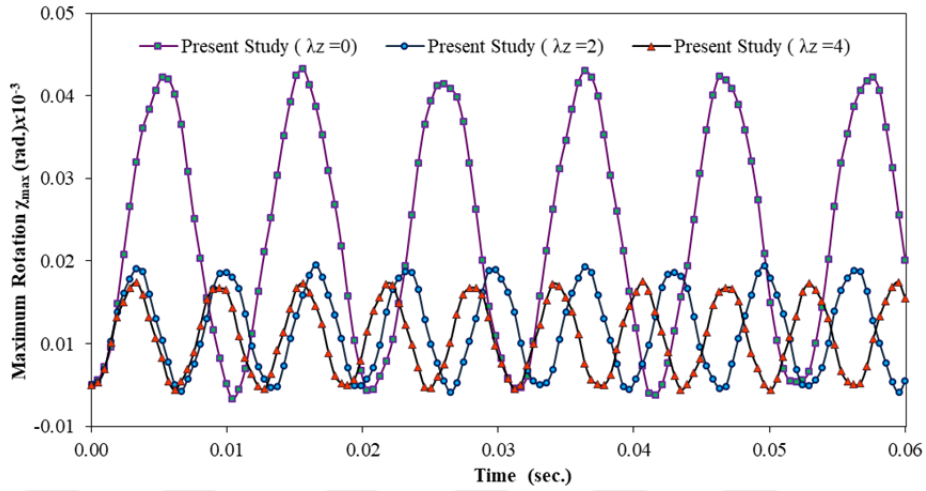


Figure 4.55. Comparison of the maximum rotation.

Figures (4.56 - 4.57) illustrate the influence of exponent of volume fraction index, λ_z , of thickness direction on the forced vibration of an annular plate with clamped-free boundary conditions for $\lambda_r = 1$ and $\lambda_h = -0.25$.

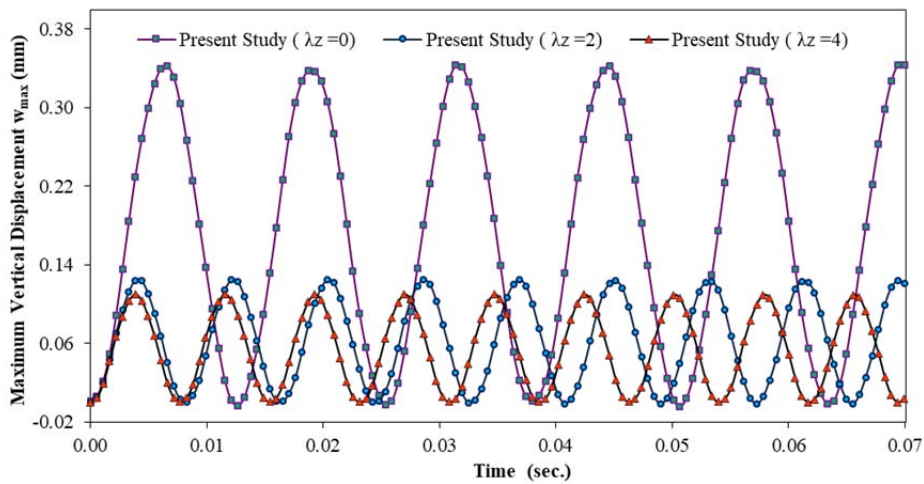


Figure 4.56. Comparison of the maximum vertical displacement.

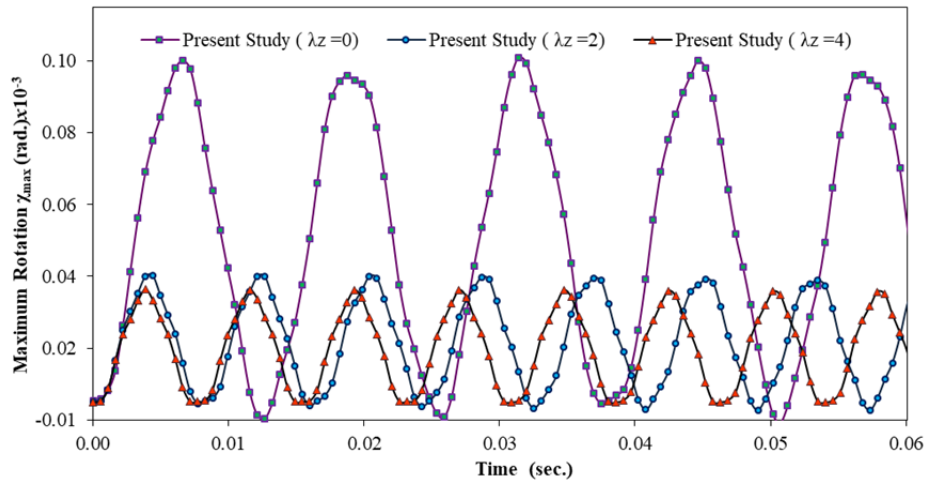


Figure 4.57. Comparison of the maximum rotation.

Figures (4.58 - 4.59) show the comparison of maximum vertical displacement and rotation for C – F annular plate ($\lambda_r = 1$ and $\lambda_h = 0.25$). Results are obtained for various λ_z values and compared in graphical form.

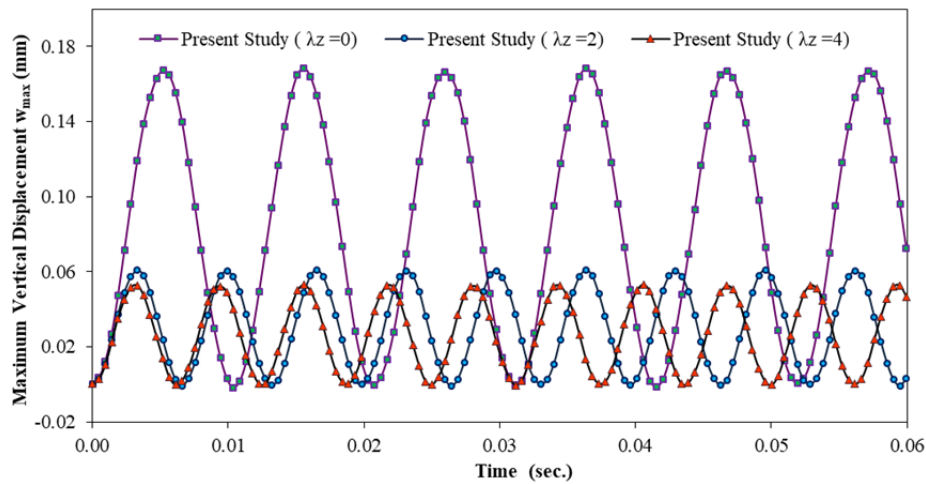


Figure 4.58. Comparison of the maximum vertical displacement.

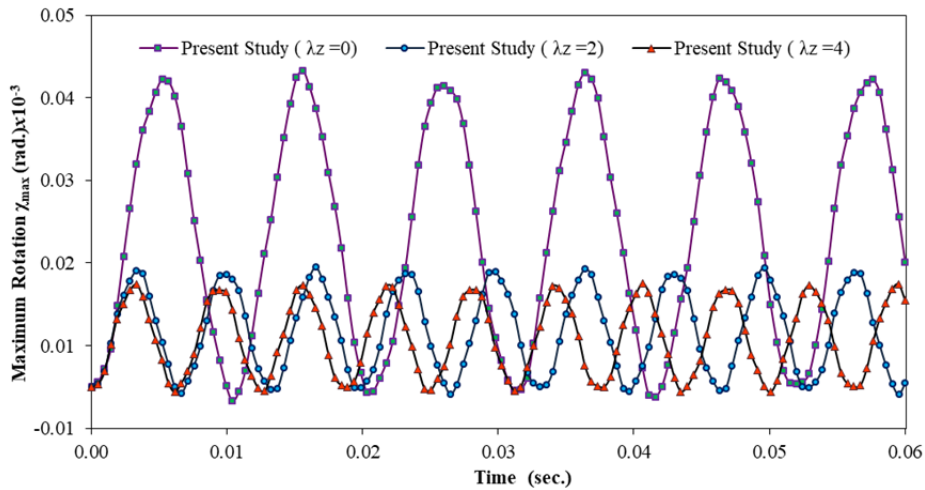


Figure 4.59 Comparison of the maximum rotation.

It is observed in Figures (4.54- 4.59) that volume fraction exponent of the thickness direction has a significant effect on the forced vibration response of the considered plate. It can be seen that with increasing λ_z values, periods and amplitudes of displacement reduce. It is worthwhile noting that the effect of λ_z on the transient response of the 2D-FG plate is more noticeable than the influence of λ_r and λ_h .

Finally, the half rectified sine wave function of a transverse uniform distributed load is considered. In this case, the beating phenomenon occurs Figure (4.61) in the considered structure. The magnitude of displacements depends on the period of the dynamic load and the vibration characteristics of the annular plate. As these quantities approach to each other, the amplitudes of displacement become larger. In this sample, the frequency of the load (e.g. 166.6 Hz) is close to the vibration characteristics of the considered plate (e.g. 158.8889 Hz for $\lambda_z=4$; 95.8267 Hz for $\lambda_z=0$; 150.0506 Hz for $\lambda_z=2$). The plate ($\lambda_r = 1$ and $\lambda_h = 1$) is given in Figure (4.60). The boundary conditions are considered to be C – F. For Laplace transform of the load see Appendix A.

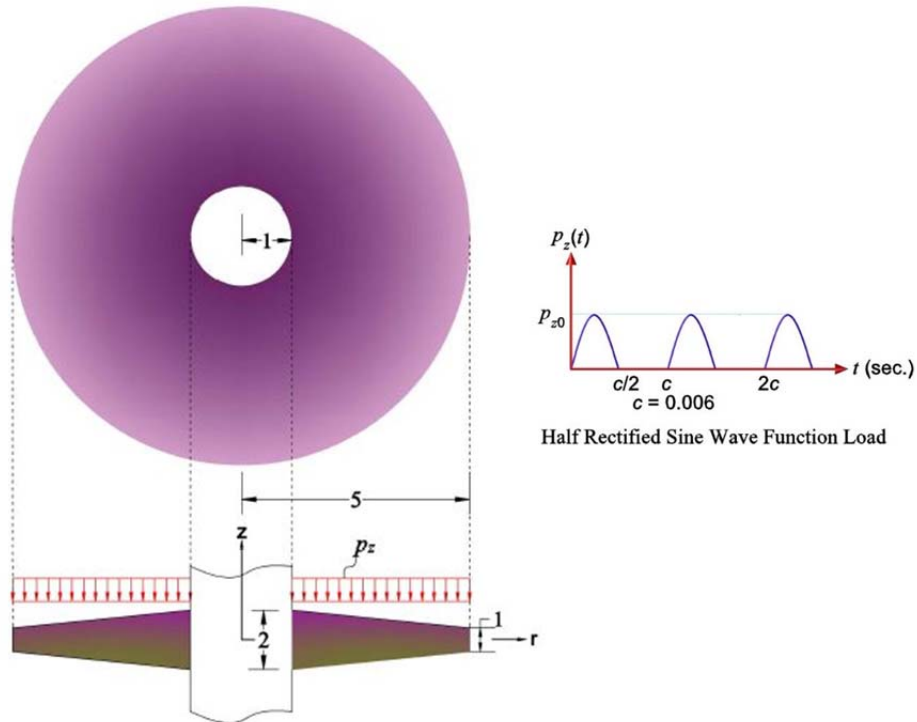


Figure 4.60. Geometry of the 2D-FG annular plate and dynamic load.

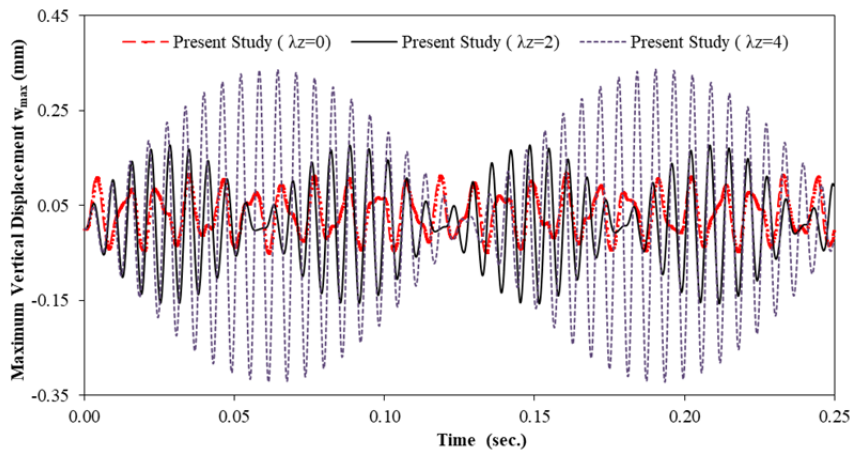


Figure 4.61. Comparison of the maximum vertical displacement.

4.6. Forced Vibration Analysis of 2D-FG Circular Plates

In this section, damped and undamped forced vibration response of 2D-FG circular plates with variable thickness is investigated.

4.6.1. Undamped Forced Vibration

First, the effects of geometric constant on the undamped forced vibration of the circular plate are examined for several boundary conditions. The radially varying thickness profiles are shown in Figure (4.9). The dynamic load is given in Figure (4.10). The plate has radius of $r_o = 5$ m. The shear correction factor k_s is taken to be $\pi^2/12$. The thickness of the plate is considered to be ($h_i = 2$ m) in inner radii and ($h_o = 1$ m) at outer radius. Properties of materials are graded based on Eq. (3.7). The radial coordinate dependent function of the thickness is given by Eq. (3.9).

Forced vibration of a clamped plate is studied. The time history for maximum vertical displacement is illustrated in Figures (4.62 – 4.64). For a clamped circular plate the boundary conditions are given by Eqs. (3.68 – 3.69).

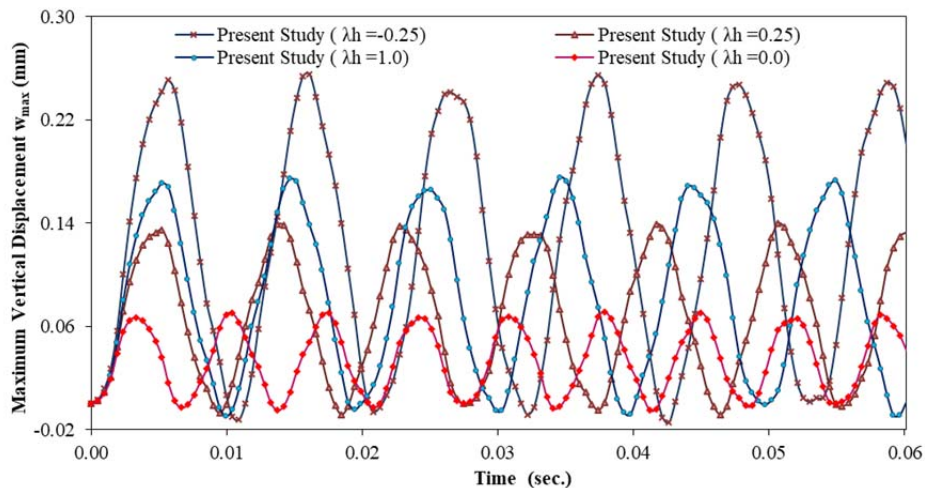


Figure 4.62. Comparison of the vertical displacement ($\lambda_r = 0$ and $\lambda_z = 0$).

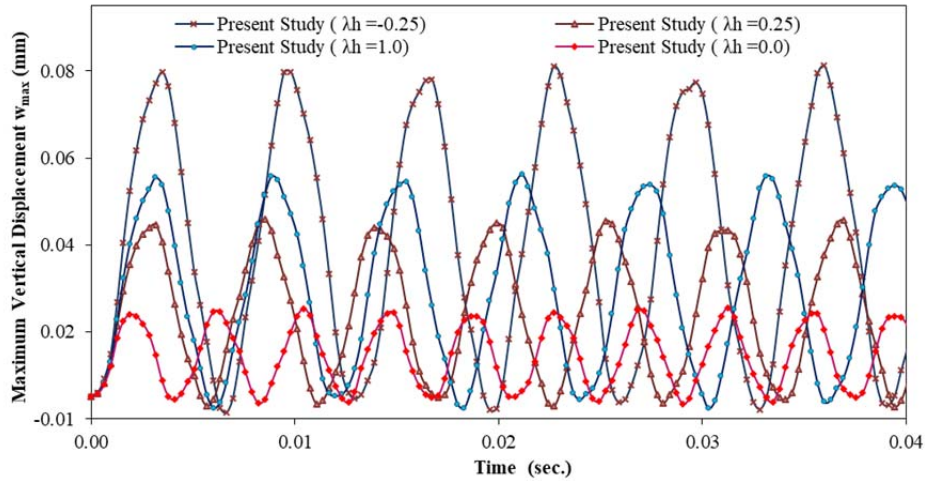


Figure 4.63. Comparison of vertical displacement ($\lambda_r = 0$ and $\lambda_z = 2$).

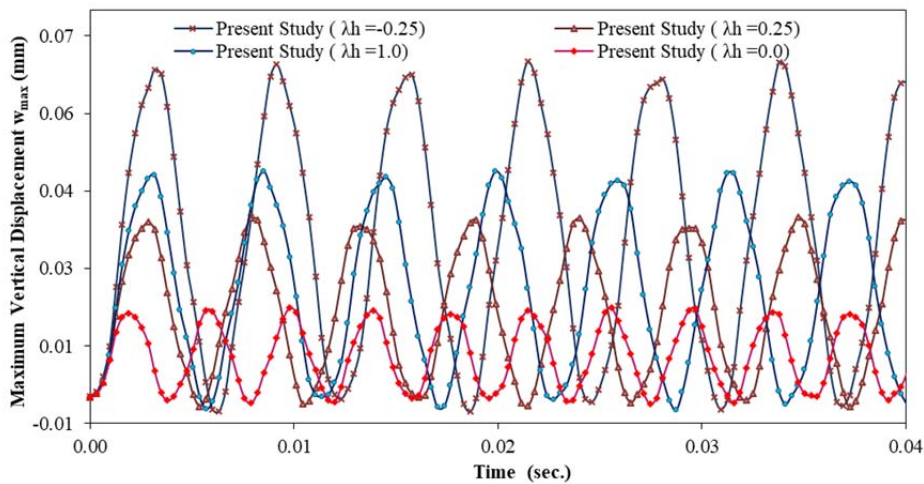


Figure 4.64. Comparison of vertical displacement ($\lambda_r = 0$ and $\lambda_z = 4$).

Forced vibration of a simply supported circular plate is examined by the suggested approach. The time history for maximum vertical displacement is illustrated in Figures (4.65 – 4.67). For a simply supported circular plate the boundary conditions are given by Eqs. (3.70 – 3.71).

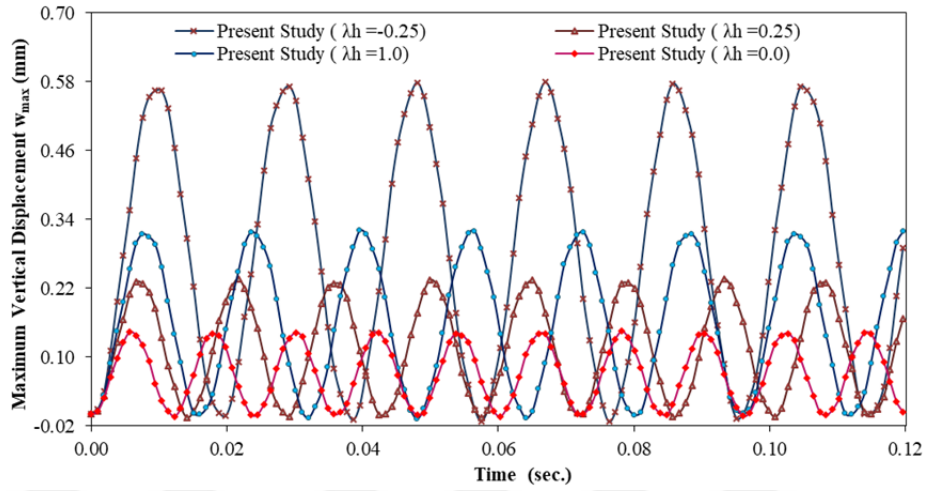


Figure 4.65. Comparison of the vertical displacement ($\lambda_r = 1$ and $\lambda_z = 0$).

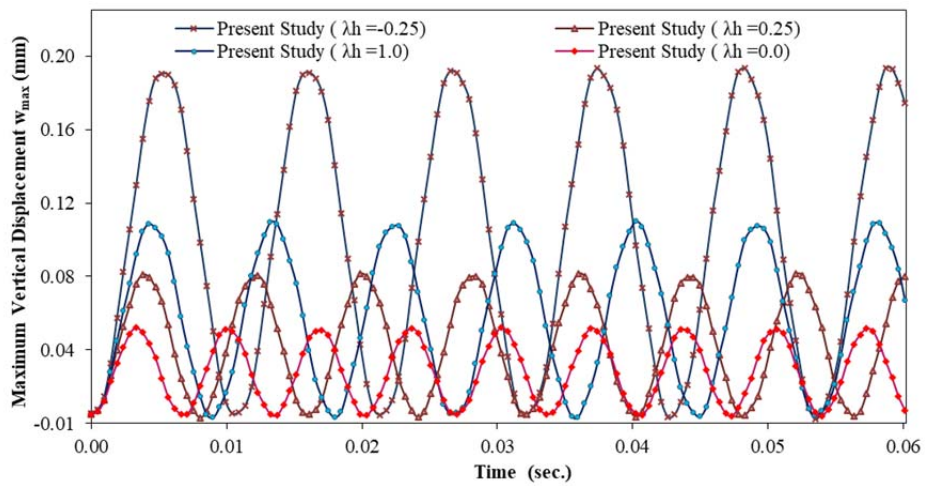


Figure 4.66. Comparison of the vertical displacement ($\lambda_r = 1$ and $\lambda_z = 2$).

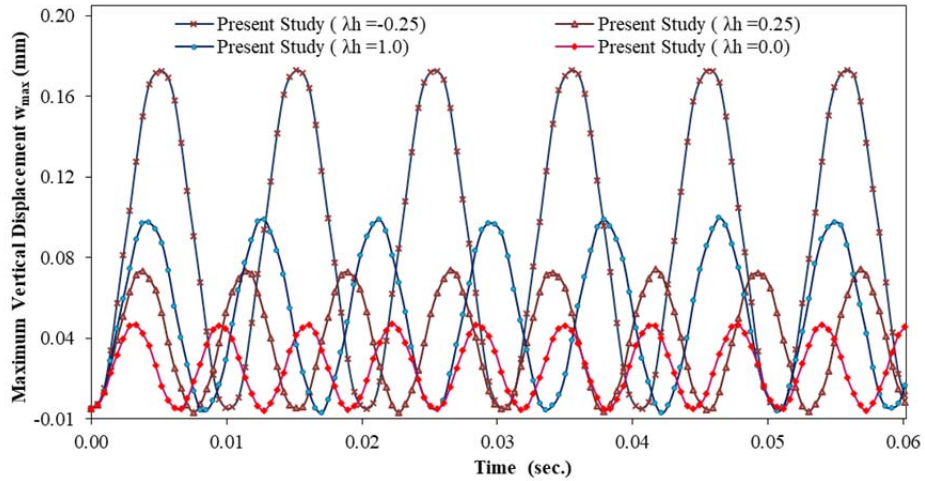


Figure 4.67. Comparison of the vertical displacement ($\lambda_r = 1$ and $\lambda_z = 4$).

Undamped transient response of a roller supported 2D FG circular plate is studied. Results of the maximum vertical displacement are showed in Figures (4.68 – 4.70).

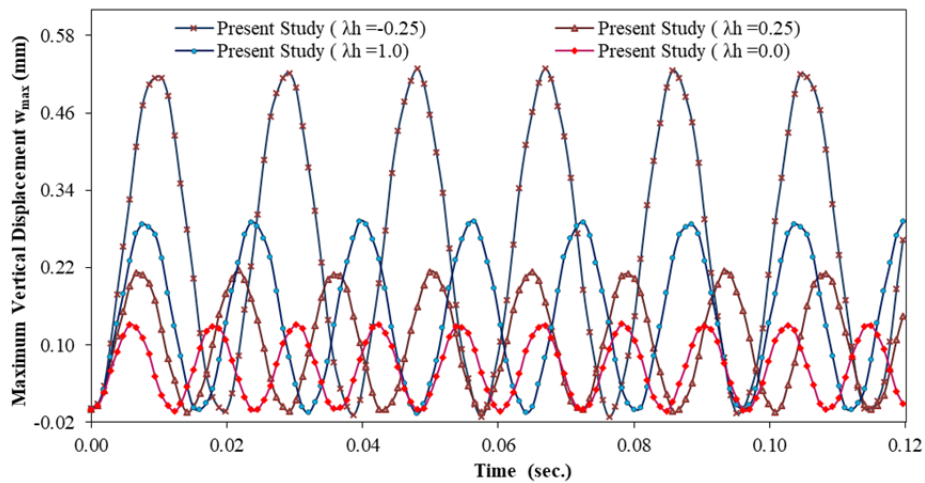


Figure 4.68. Comparison of the vertical displacement ($\lambda_r = 2$ and $\lambda_z = 0$).

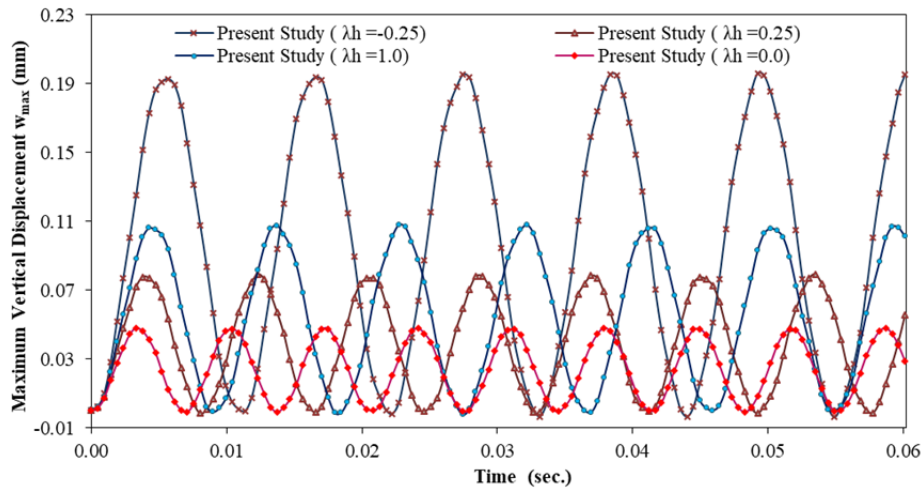


Figure 4.69. Comparison of the vertical displacement ($\lambda_r = 2$ and $\lambda_z = 2$).

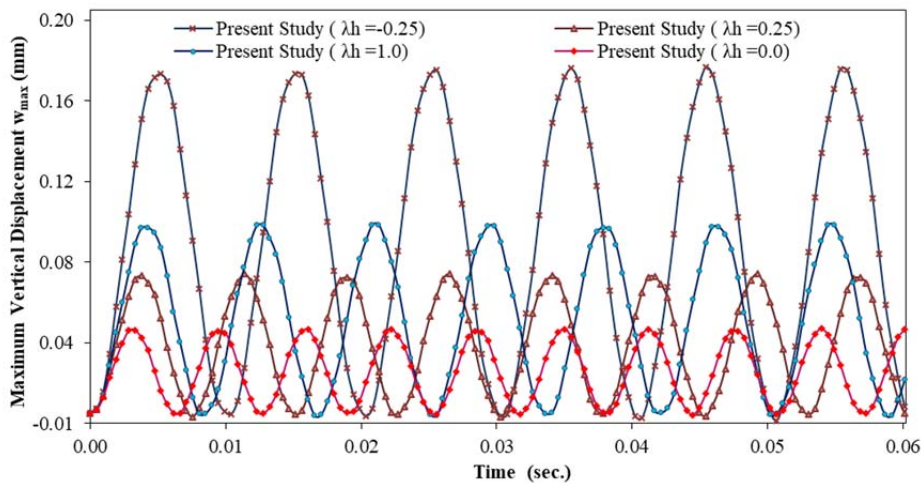


Figure 4.70. Comparison of the vertical displacement ($\lambda_r = 2$ and $\lambda_z = 4$).

We observe in Figures (4.62 - 4.70) that geometric constant (λ_h) has a significant effect on the forced vibration response of 2D-FG circular plates of variable thickness. Obtained results for various volume fraction exponents and boundary conditions reveal that the displacement components of the circular plate of uniform thickness ($\lambda_h = 0$) have the lowest periods and vibration amplitudes.

When the thickness of the plate has a concave variation ($\lambda_h = -0.25$), the vibration amplitudes and periods become the highest.

In the next step, the influences of variations of material properties in the radial direction on the transient response of the 2D-FG circular plates of variable thickness are studied. Thickness profiles are shown in Figure (4.9). Geometric and material properties are as in the previous section.

Undamped forced vibration of a clamped plate is studied. The plate is considered under the same step load as given in the previous section. The time histories for maximum vertical displacement of several cases are illustrated in Figures (4.71 – 4.73). For a clamped circular plate the boundary conditions are given by Eqs. (3.68 – 3.69).

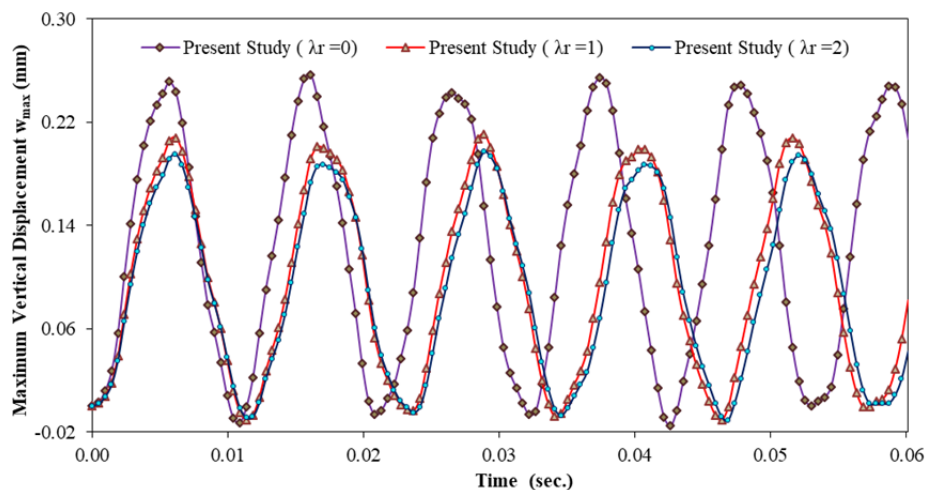


Figure 4.71. Comparison of the vertical displacement ($\lambda_z = 0$ and $\lambda_h = -0.25$).

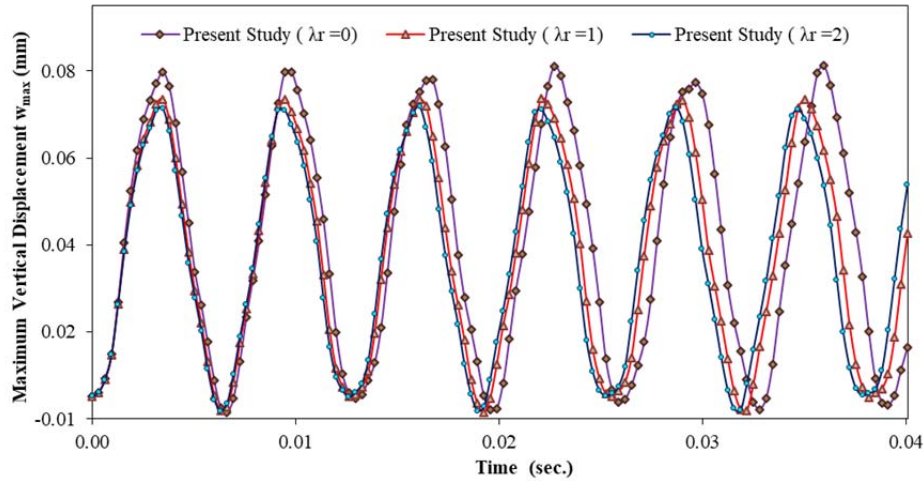


Figure 4.72. Comparison of the vertical displacement ($\lambda_z = 2$ and $\lambda_h = -0.25$).

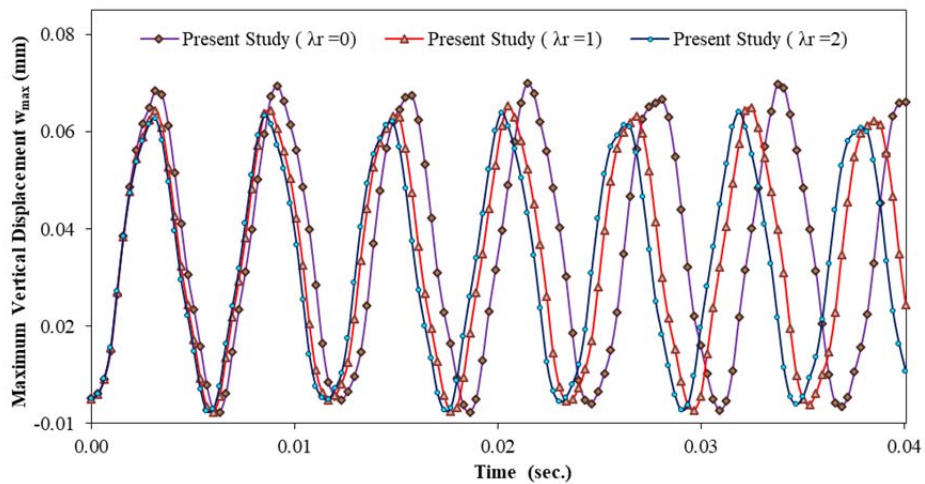


Figure 4.73. Comparison of the vertical displacement ($\lambda_z = 4$ and $\lambda_h = -0.25$).

Undamped transient response of a roller supported 2D-FG circular plate is studied. Results of the maximum vertical displacement are showed in Figures (4.74 – 4.76). For a roller supported circular plate the boundary conditions are given by Eqs. (3.72 – 3.73).

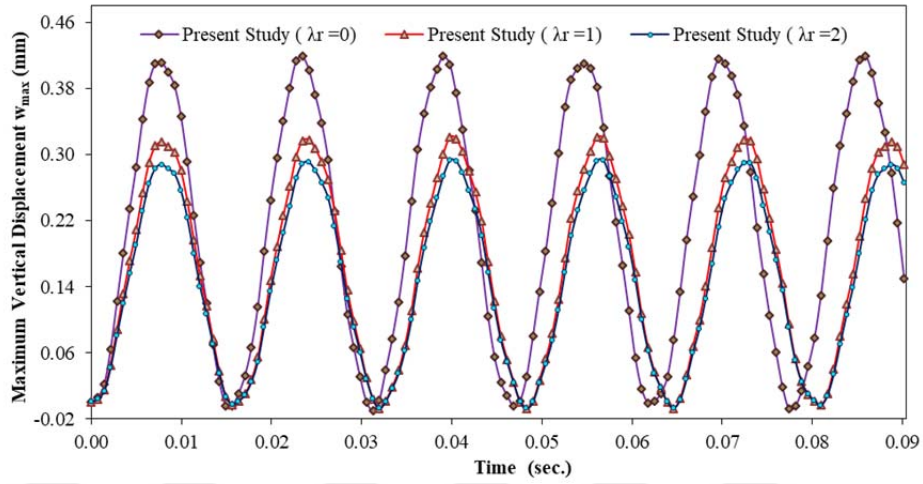


Figure 4.74. Comparison of the vertical displacement ($\lambda_z = 0$ and $\lambda_h = 1$).

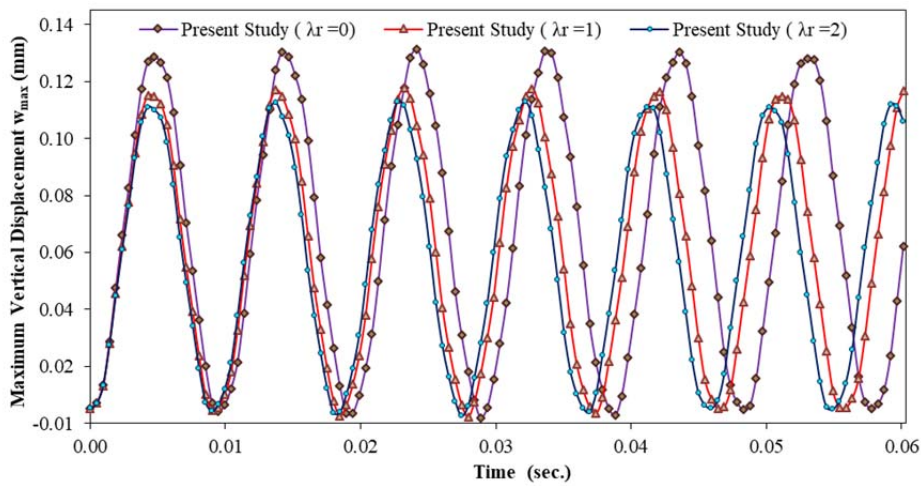


Figure 4.75. Comparison of the vertical displacement ($\lambda_z = 2$ and $\lambda_h = 1$).

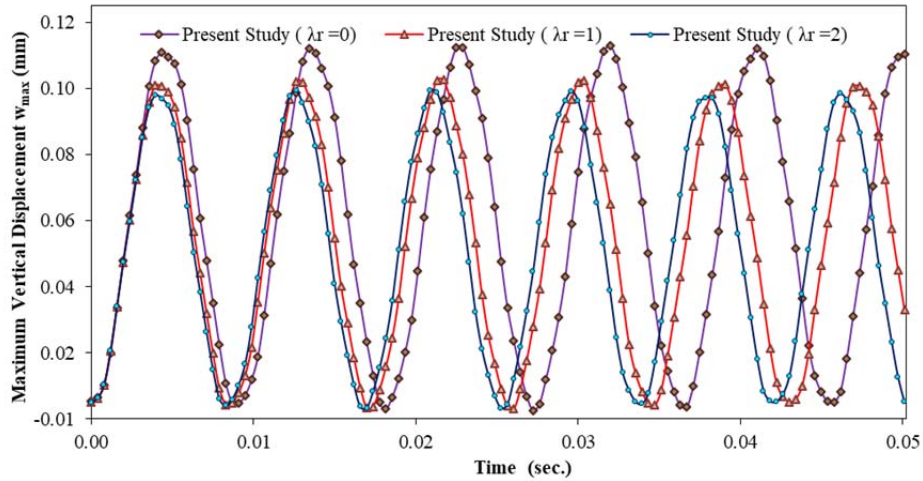


Figure 4.76. Comparison of the vertical displacement ($\lambda_z = 4$ and $\lambda_h = 1$).

Forced vibration of a simply supported circular plate is studied by the presented approach. Results maximum vertical displacement are presented in Figures (4.77 – 4.79).

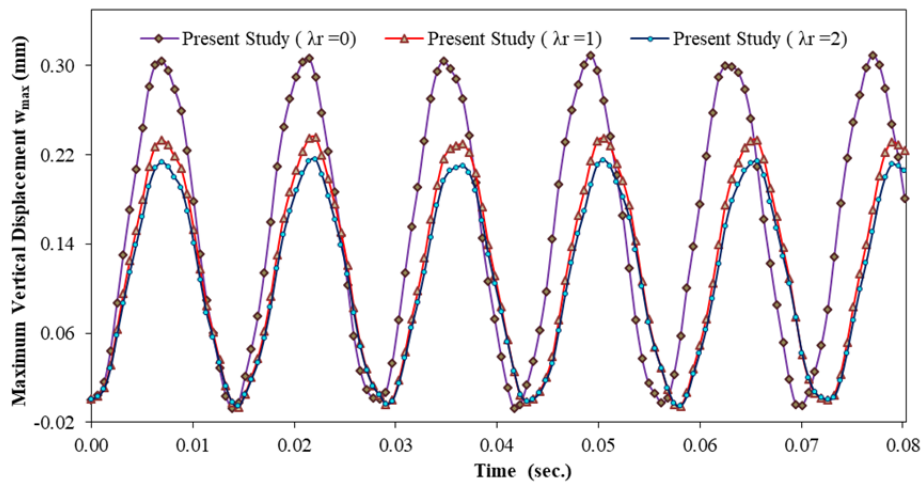


Figure 4.77. Comparison of the vertical displacement ($\lambda_z = 0$ and $\lambda_h = 0.25$).

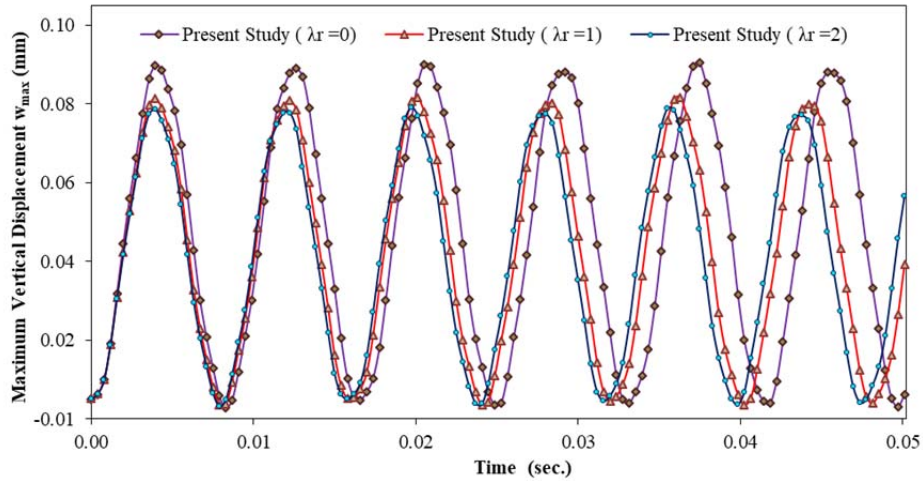


Figure 4.78. Comparison of the vertical displacement ($\lambda_z = 2$ and $\lambda_h = 0.25$).

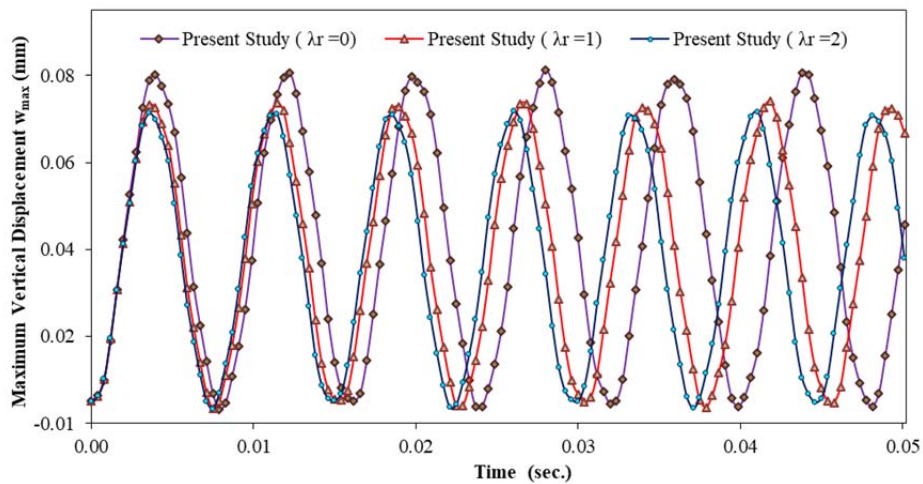


Figure 4.79. Comparison of the vertical displacement ($\lambda_z = 4$ and $\lambda_h = 0.25$).

The results reveal that when the plate is radially FG ($\lambda_z = 0$), λ_r has a significant influence on the forced vibration results. Increasing λ_r decreases the amplitude of the vibration but increases the period of the vibration.

But when the plate is 2D-FG is considered, the λ_r has an insignificant effect on the transient response of the considered structures. It can be concluded

that an increase in the radial exponent of volume fractions leads to a decrease in the period and vibration amplitude of forced vibration results.

Furthermore, a comprehensive parametric study is carried out to investigate the influences of the volume fraction exponents of the thickness direction, λ_z , on the forced vibration response of the 2D-FG thick circular plates. Material properties, dynamic loads, and geometric properties of the plate are the same as the previous cases. Results are obtained for several boundary conditions.

First, the plate is assumed to be clamped. Results are depicted in Figures (4.80 - 4.82) for various λ_z values to compare the time history of maximum vertical displacements. For a clamped circular plate the boundary conditions are given by Eqs. (3.68 – 3.69).

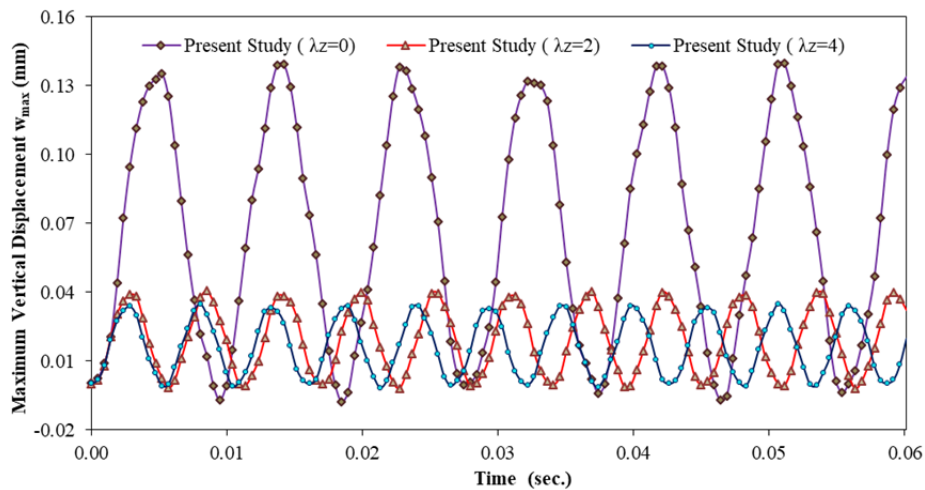


Figure 4.80. Comparison of the vertical displacement ($\lambda_r = 0$ and $\lambda_h = 0.25$).

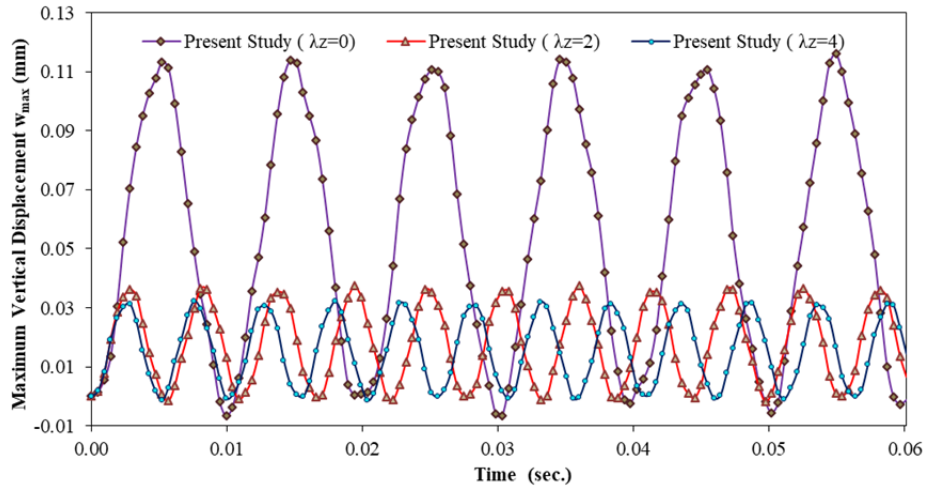


Figure 4.81. Comparison of the vertical displacement ($\lambda_r = 1$ and $\lambda_h = 0.25$).

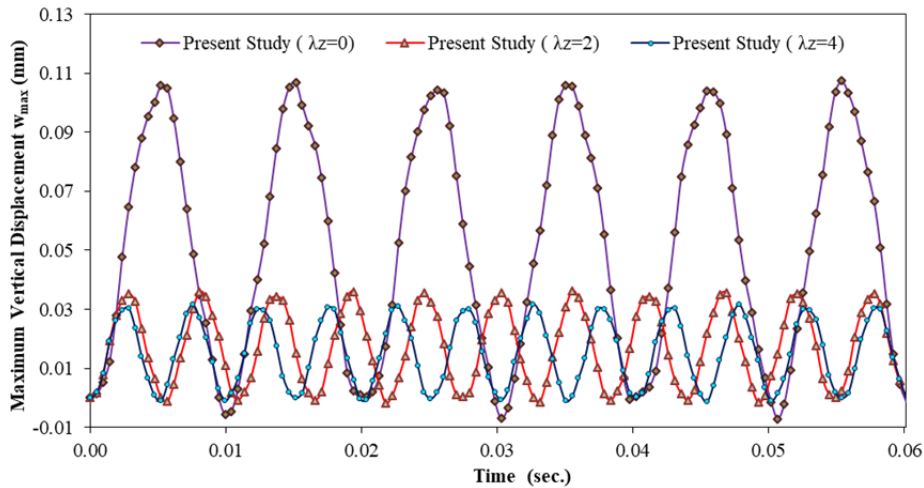


Figure 4.82. Comparison of the vertical displacement ($\lambda_r = 2$ and $\lambda_h = 0.25$).

Next, forced vibration of a simply supported circular plate is studied by the proposed scheme. The time history for maximum vertical displacements is showed in Figures (4.83 – 4.85). For a simply supported circular plate the boundary conditions are given by Eqs. (3.70 – 3.71).

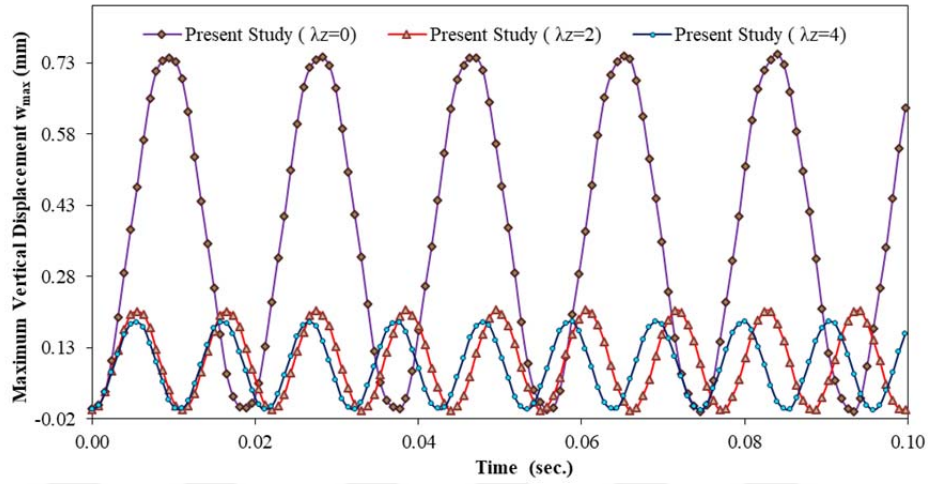


Figure 4.83. Comparison of the vertical displacement ($\lambda_r = 0$ and $\lambda_h = -0.25$).

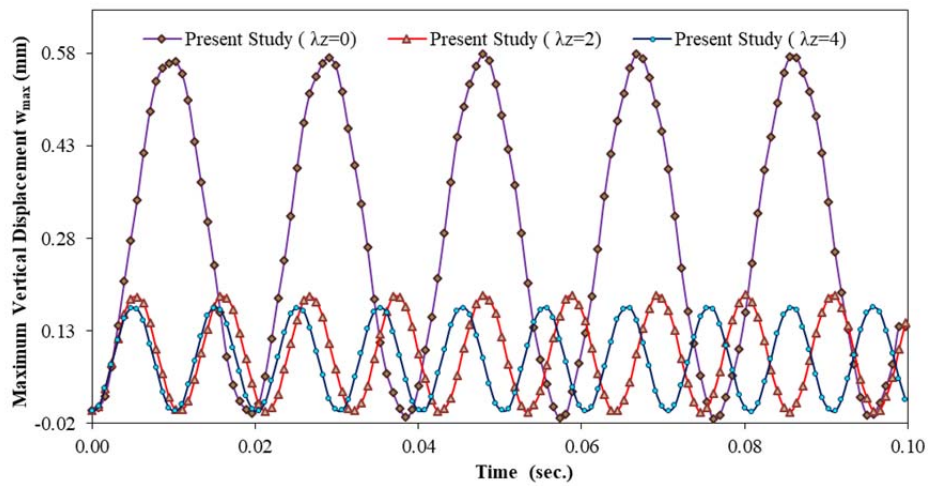


Figure 4.84. Comparison of the vertical displacement ($\lambda_r = 1$ and $\lambda_h = -0.25$).

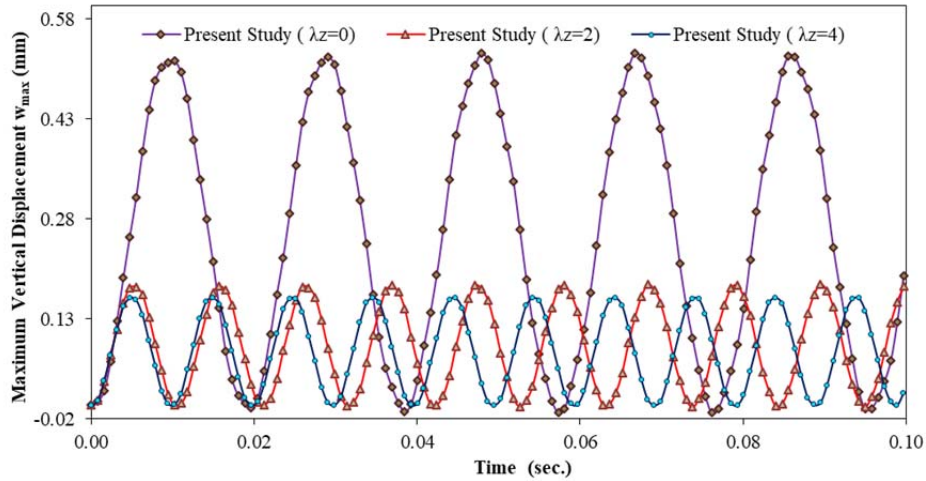


Figure 4.85. Comparison of the vertical displacement ($\lambda_r = 2$ and $\lambda_h = -0.25$).

Finally, undamped transient response of a roller supported 2D FG circular plate is presented. Results of the maximum vertical displacement are demonstrated in Figures (4.86 – 4.88).

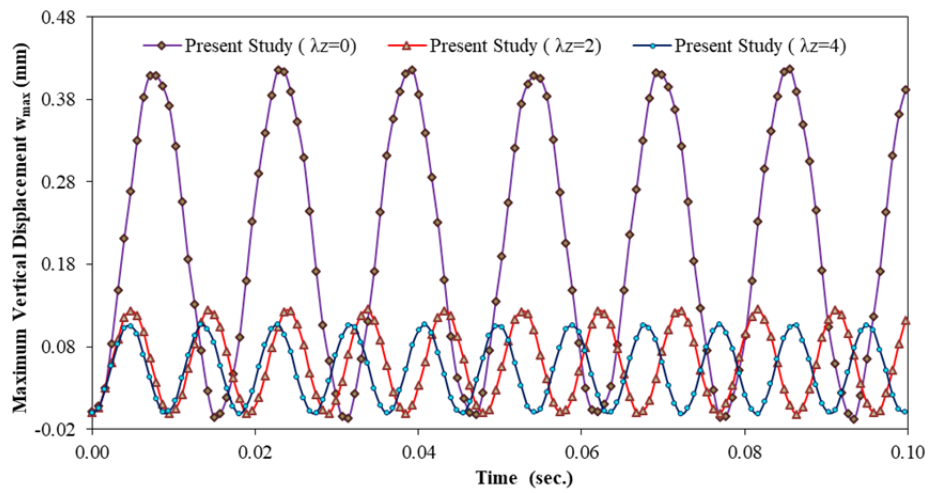


Figure 4.86. Comparison of the vertical displacement ($\lambda_r = 0$ and $\lambda_h = 1$).

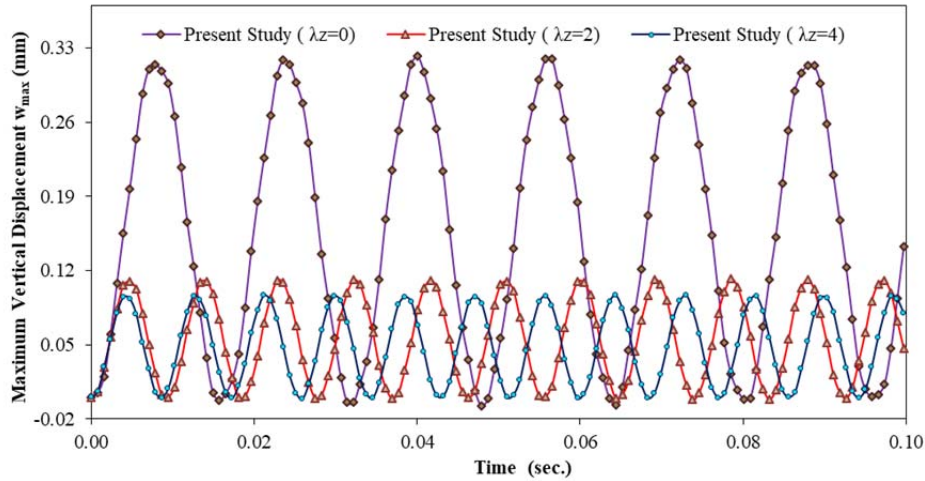


Figure 4.87. Comparison of the vertical displacement ($\lambda_r = 1$ and $\lambda_h = 1$).

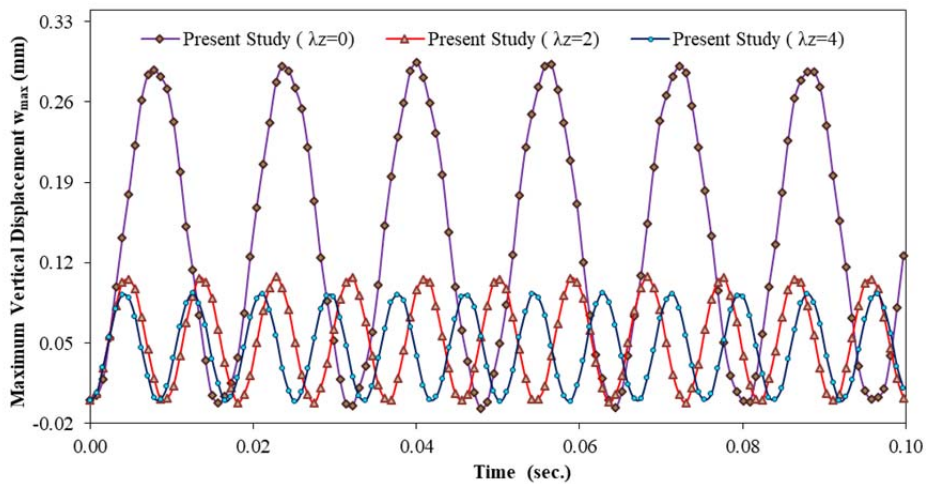


Figure 4.88. Comparison of the vertical displacement ($\lambda_r = 2$ and $\lambda_h = 1$).

It can be clearly seen in Figures (4.80- 4.88) that volume fraction exponent, λ_z , of the thickness direction has a remarkable effect on the forced vibration response of the 2D-FG circular plates of variable thickness. It is observed that with increasing λ_z values periods and amplitudes of displacement reduce. It is

worthwhile noting that the effect of λ_z on the transient response of the 2D-FG plate is more noticeable than the influence of λ_r and λ_h .

4.6.2. Damped Forced Vibration

In this section, the Kelvin damping model is employed in order to investigate the viscoelastic response of the 2D-FG circular plates of variable thickness for various types of impulsive dynamic loads and different boundary conditions. The elastic viscoelastic analogy (see Boley and Weiner (2012)) is used to treat the internal viscoelastic damping case. Viscoelastic material properties are obtained by Eq. (3.141) and substituted to governing equations of considered problem. In order to present the evaluation of the damping effect, many cases with different damping coefficients are calculated.

As a first case, a 2D-FGM circular plate with the clamped edge is considered. The plate is subjected to a right triangle impulsive load as seen in Figure (4.88). The plate has radius of $r_o = 5$ m. The shear correction factor k_s is taken to be $\pi^2/12$. The thickness of the plate is considered to be ($h_i = 2$ m) in inner radii *and* ($h_o = 1$ m) at outer radius. Properties of materials are graded based on Eq. (3.7). The radial coordinate dependent function of the thickness is given by Eq. (3.9). For a clamped circular plate the boundary conditions are given by Eqs. (3.68 – 3.69). Laplace transforms of a right triangle impulsive load is available in closed-form. The volume fraction exponents are assumed to be ($\lambda_r = 2$ and $\lambda_z = 2$). For Laplace transform of the load see Appendix A.

Damped forced vibration results are calculated with the CFM in the Laplace domain. Obtained results are retransferred to the time domain with an efficient numerical inverse Laplace transform method. Obtained results are compared in Figures (4.90 – 4.92). It can be clearly seen from the figures that increasing the damping ratio causes a decrease in the amplitude of dynamic behavior.

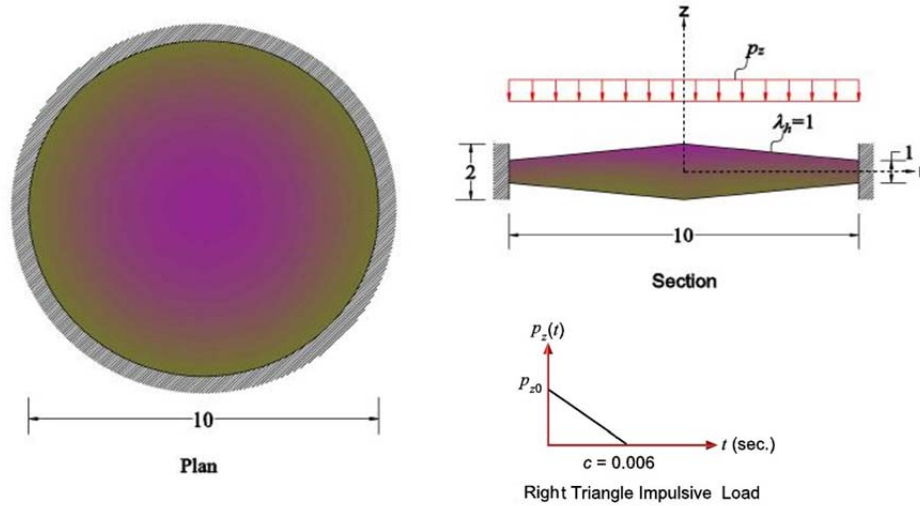


Figure 4.89. Geometry of the clamped circular plate and dynamic load.

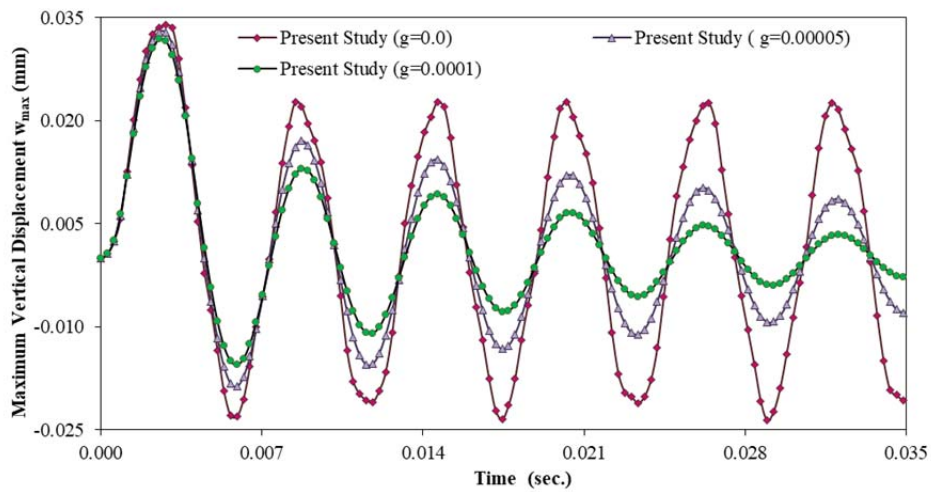


Figure 4.90. Comparison of the viscoelastic vertical displacement of clamped plate.

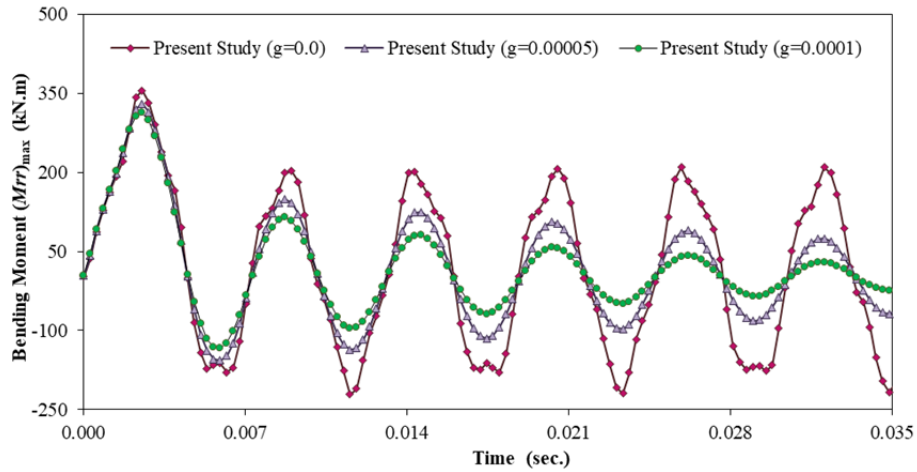


Figure 4.91. Comparison of the viscoelastic bending moments of clamped plate.

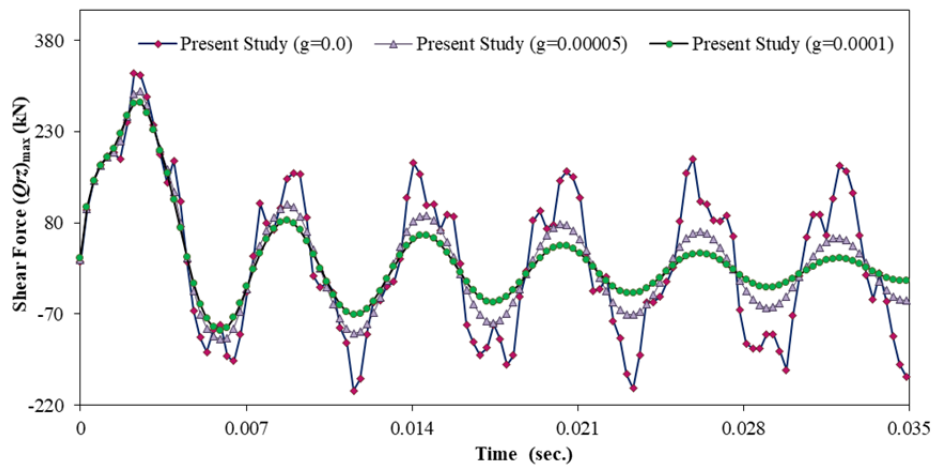


Figure 4.92. Comparison of the viscoelastic shear forces of clamped plate.

Next, the plate is considered to be simply supported. The plate is subjected to a triangular impulsive load as seen in Figure (4.92). Laplace transforms of the triangular impulsive load is available in closed-form. The volume fraction exponents are assumed to be ($\lambda_r = 1$ and $\lambda_z = 4$). Obtained results are compared in Figures (4.94 – 4.95). For Laplace transform of the load see Appendix A.

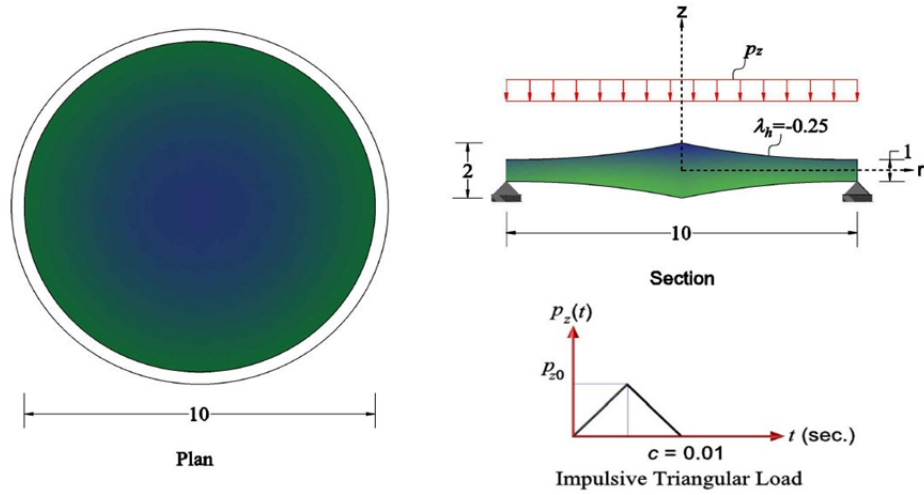


Figure 4.93. Geometry of the simply supported circular plate and dynamic load.

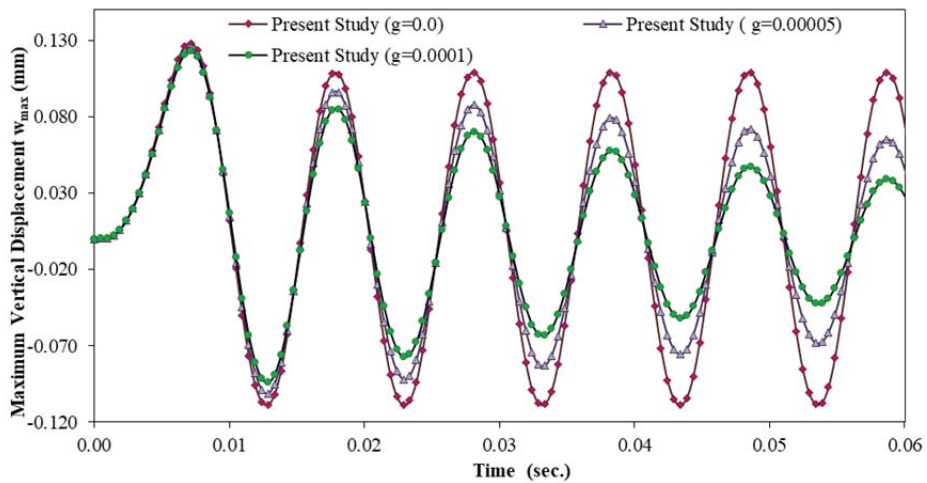


Figure 4.94. Comparison of the viscoelastic displacement of simply supported plate.

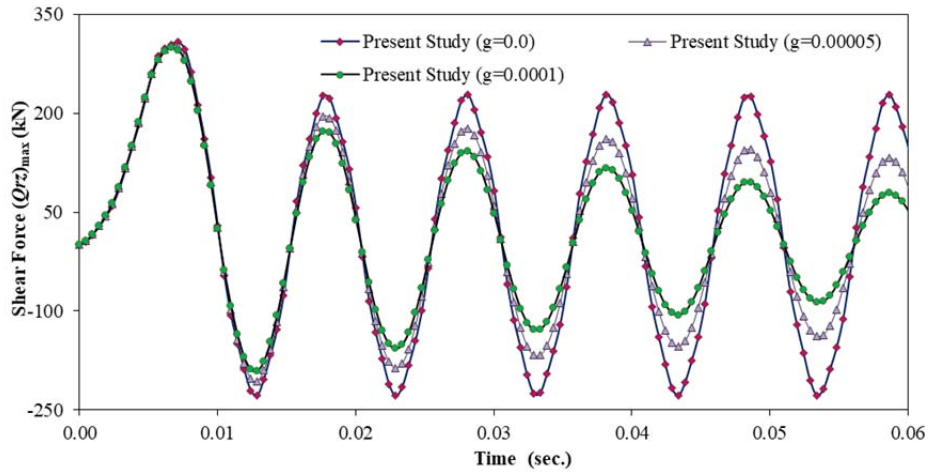


Figure 4.95. Comparison of the viscoelastic shear forces of simply supported plate.

Finally, the plate is considered to be roller supported. The plate is subjected to the impulsive sine load as seen in Figure (4.96). For Laplace transform of the load see Appendix A.

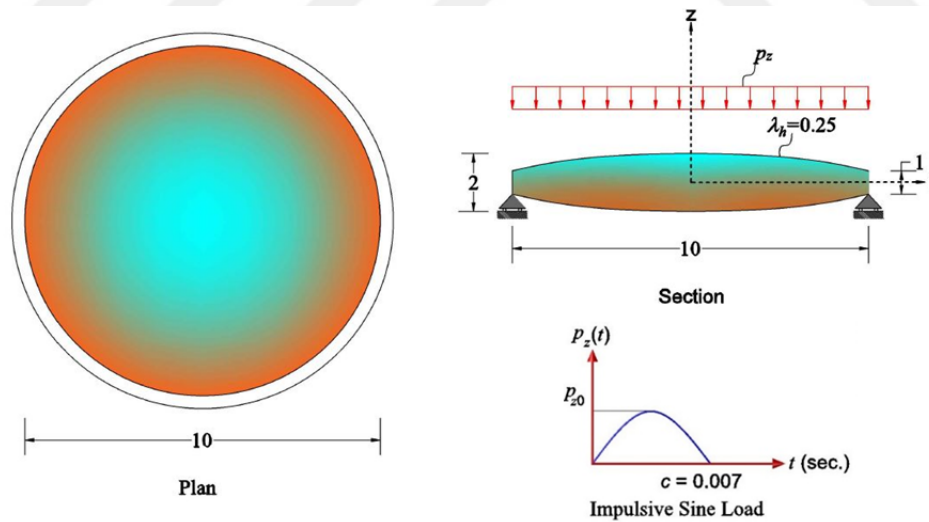


Figure 4. 96. Geometry of the roller supported circular plate and dynamic load.

Laplace transforms of the impulsive sine load is available in closed-form. The volume fraction exponents are assumed to be ($\lambda_r = 2$ and $\lambda_z = 4$). Obtained results are compared in Figures (4.97 – 4.98).

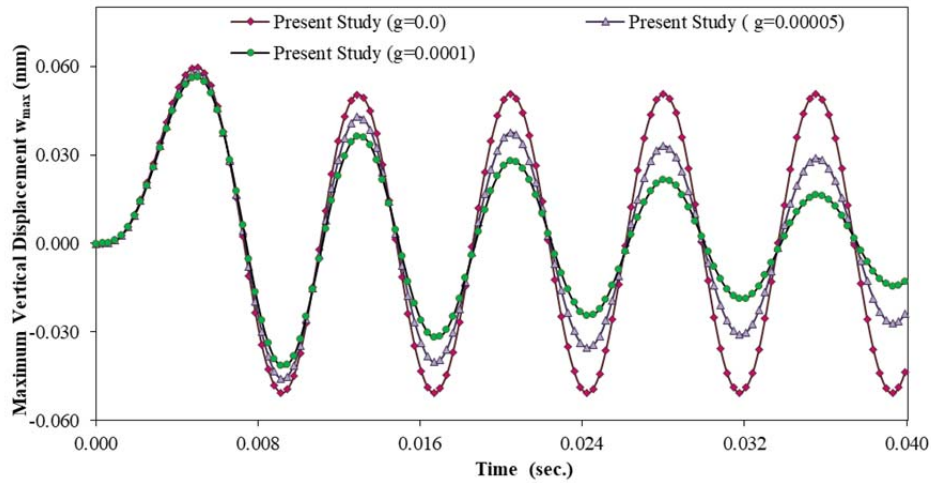


Figure 4.97. Comparison of the viscoelastic displacement of roller supported plate.

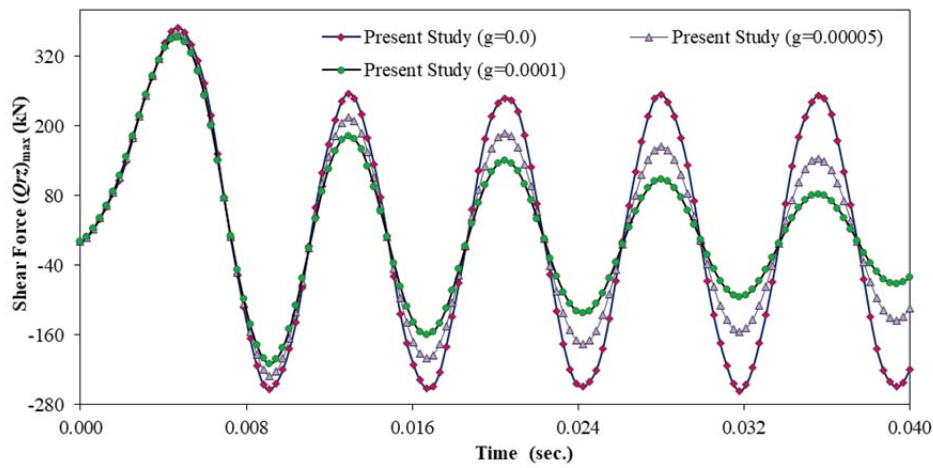


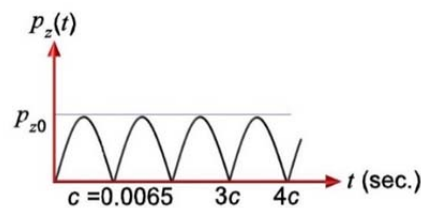
Figure 4.98. Comparison of the viscoelastic shear forces of roller supported plate.

As stated before, the damped dynamic behavior of the 2D - FG circular plates is examined for miscellaneous damping ratios. Several kinds of impulsive loads are applied to the circular plates of variable thickness. In all loadings and boundary conditions, it can be seen that the damping ratio of the structure has a significant influence on their dynamic behavior. By increasing the damping ratio dynamic response of the rod will reach faster to the static state.

4.6.3. Beat phenomenon

In this section, several wave load functions are applied to different types of 2D-FG circular plates. The beating occurs in the considered structures when the frequency of the wave load is close to (but not exactly equal to) the natural frequency of the structure.

First, the beating phenomenon is investigated for a clamped 2D-FG circular plate of variable thickness. The considered plate is subjected to the rectified sine wave function load (Figure (4.99).) The Laplace transform of this load is available in closed-form. The radial coordinate dependent function of the thickness is given by Eq. (3.9). For a clamped circular plate the boundary conditions are given by Eqs. (3.68 – 3.69). For Laplace transform of the load see Appendix A.



Rectified Sine Wave Function Load

Figure 4.99. Dynamic load function

Material properties of the plate are assumed to vary in a power law form. Volume fraction exponents of the material variation are ($\lambda_r = 2$ and $\lambda_z = 2$).

Maximum deflection results are obtained and compared for several values of λ_h . Graphical comparison of the result is depicted in Figure (4.100).

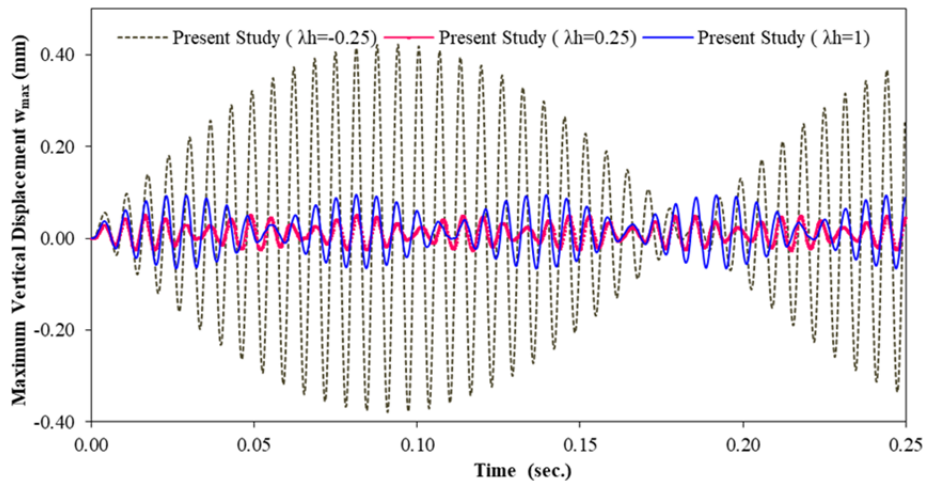


Figure 4.100. Comparison of displacement of clamped circular plate.

In this sample, the frequency of the load (e.g. 153.856 Hz) is close to the vibration characteristics of the considered plate (e.g. 159.3229 Hz for $\lambda_h = -0.25$; 184.1330 Hz for $\lambda_h = 0.25$; 172.06629 Hz for $\lambda_h = 1$). The magnitude of displacements depends on the period of the dynamic load and the vibration characteristics of the plate. As these quantities approach each other, the amplitudes of displacement become larger.

Next, the beating phenomena are examined for a simply-supported 2D-FG circular plate of variable thickness. The considered plate is subjected to the square wave function load (Figure (4.101)). For a simply supported circular plate the boundary conditions are given by Eqs. (3.70 – 3.71). Volume fraction exponent of the material variation in the radial direction is considered to be ($\lambda_r = 2$). The geometric constant is taken as $\lambda_h = -0.25$. Maximum deflection results are obtained and compared for several values of λ_z . Graphical comparison of the result is presented in Figure (4.102). For Laplace transform of the load see Appendix A.

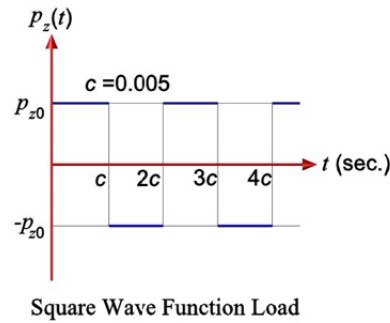


Figure 4.101. Square wave dynamic load function

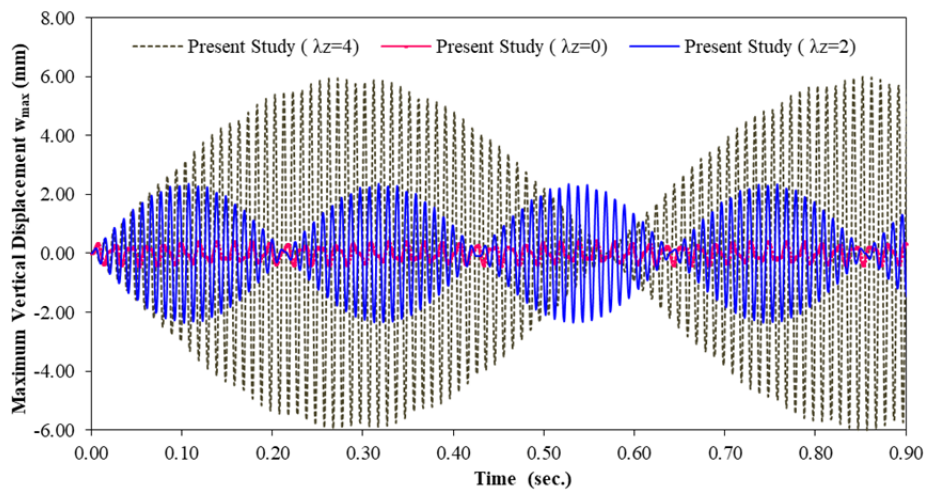


Figure 4.102. Comparison of displacement of simply supported plate.

In this case, the frequency of the load (e.g. 100 Hz) is close to the vibration characteristics of the considered plate (e.g. 101.7568 Hz for $\lambda_z=4$; 52.5028 Hz for $\lambda_z=0$; 95.3231 Hz for $\lambda_z=2$). The magnitude of displacements depends on the period of the dynamic load and the vibration characteristics of the plate. As these quantities approach to each other, the amplitudes of displacement become larger.

5. CONCLUSIONS

In this thesis, the axisymmetric bending, free vibration, damped and undamped forced vibration responses of two-directional functionally graded thick circular and annular plates with variable thickness have been investigated. Infusion of the CFM into the present class of problems is presented.

For the analysis of the bending response of the considered structures, governing equations are obtained by the principle of minimum total potential energy based on the FSDT. By using the suggested method, 2D-FG plates under arbitrary radial and transverse axisymmetric loads and boundary conditions can be analyzed. The present research has been verified for several examples of annular and solid circular plates. Comparison of the results reveals that the present results are in an excellent agreement with those available in the literature. Displacements, rotations, internal shear forces and bending moments are presented for several exponents of volume fractions, thickness variation constants, and boundary conditions. Results demonstrate that material gradient indexes and geometric constants have important impacts on the response of the class of problems on hand. It can be found out from the results that desired design requirements can be derived by selecting optimized volume fraction exponents and thickness variation functions.

Furthermore, the effects of thickness variation functions and volume fraction exponents on the axisymmetric response of 2D-FG solid circular plates have been studied. The deflection of the plate decreases as λ_r and λ_z increase. This response of the plate is related to the resulting increase in Young's modulus. But increasing the geometric constant λ_h , gives rise to the increase of the deflection. It has been seen that λ_z has a more significant effect on the axisymmetric bending response of the considered problems.

In the case of the dynamic analysis of the considered structures, time-dependent governing equations are transformed to the Laplace space. The set of obtained equations are solved numerically by the CFM for a set of Laplace parameters. Modified Durbin's inverse Laplace transform method is employed to retransform the solution results to the time-space. The validity, superiority, and accuracy of the suggested approach are demonstrated through several examples by comparing the results with available literature and those of ANSYS. Good agreement is found. The damped forced vibration of the considered structures is investigated by means of Kelvin damping model. As expected, the damping ratio of the structure has a significant influence on their dynamic behavior. The dynamic behavior of the plate turns to static after a while. Increasing the damping ratio causes a decrease in the amplitude of dynamic behavior. It can be concluded that in the case of periodic loading when the frequencies of the applied load and the considered structure are close to each other the beating occurs. The novelty of the proposed method is that it gives the natural frequencies of 2D-FG circular and annular plates without performing mode shape study. The suggested scheme is simple. High accuracy can be obtained even with fewer number of Laplace parameters and coarse time step sizes. Therefore, it needs less computational time. The suggested model is easily applicable to the dynamic analysis of the considered plates and it works effectively. Also, viscoelastic constants can be easily incorporated in the governing equations. It should be pointed out again that the suggested method is suitable for arbitrary functions of 2D-FGMs.

Influences of various thickness profiles and the power law indices and different boundary conditions on free and forced vibration response of the 2D-FG circular and annular plates have been investigated. It has been revealed that increasing the value of λ_r decreases natural frequencies of the structure for the considered FGM model. When the plate is FG only through the thickness direction ($\lambda_r = 0$), It has been concluded that an increase in the value of λ_z leads to an

increase in the natural frequencies of the structure. It has been shown that the circular and annular plate with convex thickness profile ($\lambda_h = 0.25$) has the highest natural frequencies while the plate with concave thickness profile ($\lambda_h = -0.25$) has the lowest natural frequencies among compared cases.

It has been seen that the thickness variation profile has a highly significant influence on the undamped forced vibration of the considered structures. The results reveal that the λ_r has an insignificant effect on the transient response of the considered structures. It has been shown that volume fraction exponent, λ_z , of the thickness direction has a remarkable effect on the forced vibration response of the 2D-FG circular and annular plates of variable thickness. It has been observed that with increasing λ_z values periods and amplitudes of displacement reduce. It is worthwhile noting that the effect of λ_z on the transient response of the 2D-FG plate is more noticeable than the influence of λ_r and λ_h .



REFERENCES

- Aghdam, M. M., Shahmansouri, N. & Mohammadi, M. 2012. Extended Kantorovich method for static analysis of moderately thick functionally graded sector plates. *Mathematics and Computers in Simulation*, 86, 118-130.
- Ahlawat, N. & Lal, R. 2016. Buckling and Vibrations of Multi-directional Functionally Graded Circular Plate Resting on Elastic Foundation. *Procedia Engineering*, 144, 85-93.
- Alipour, M. & Shariyat, M. 2011. A power series solution for free vibration of variable thickness Mindlin circular plates with two-directional material heterogeneity and elastic foundations. *Journal of Solid Mechanics*, 3, 183-197.
- Alipour, M., Shariyat, M. & Shaban, M. 2010. A semi-analytical solution for free vibration of variable thickness two-directional-functionally graded plates on elastic foundations. *International Journal of Mechanics and Materials in Design*, 6, 293-304.
- Alipour, M. M. 2016. A novel economical analytical method for bending and stress analysis of functionally graded sandwich circular plates with general elastic edge conditions, subjected to various loads. *Composites Part B-Engineering*, 95, 48-63.
- Allahverdizadeh, A., Naei, M. & Bahrami, M. N. 2008. Nonlinear free and forced vibration analysis of thin circular functionally graded plates. *Journal of sound and vibration*, 310, 966-984.
- ANSYS, 2013. *Inc Release 15.0*, Canonsburg, PA.
- Aslan, T. A., Noori, A. R. & Temel, B. 2018. Dynamic response of viscoelastic tapered cycloidal rods. *Mechanics Research Communications*, 92, 8-14.

- Bayat, M., Sahari, B. B., Saleem, M., Ali, A. & Wong, S. V. 2009. Bending analysis of a functionally graded rotating disk based on the first order shear deformation theory. *Applied Mathematical Modelling*, 33, 4215-4230.
- Boley, B. A. & Weiner, J. H. 2012. *Theory of thermal stresses*, Courier Corporation.
- Brigham, E. O. 1974. The Fast Fourier Transform(Book). *Englewood Cliffs, N. J., Prentice-Hall, Inc., 1974. 264 p.*
- Chapra, S. C. & Canale, R. P. 2010. *Numerical methods for engineers*, Boston: McGraw-Hill Higher Education.
- Çalim, F. F. 2009. Free and forced vibrations of non-uniform composite beams. *Composite Structures*, 88, 413-423.
- Çalim, F. F. 2012. Forced vibration of curved beams on two-parameter elastic foundation. *Applied Mathematical Modelling*, 36, 964-973.
- Dong, C. 2008. Three-dimensional free vibration analysis of functionally graded annular plates using the Chebyshev–Ritz method. *Materials & Design*, 29, 1518-1525.
- Durbin, F. 1974. Numerical inversion of Laplace transforms: an efficient improvement to Dubner and Abate's method. *The Computer Journal*, 17, 371-376.
- Ebrahimi, F. & Rastgoo, A. 2008. An analytical study on the free vibration of smart circular thin FGM plate based on classical plate theory. *Thin-Walled Structures*, 46, 1402-1408.
- Ebrahimi, F. & Rastgoo, A. 2008. Free vibration analysis of smart annular FGM plates integrated with piezoelectric layers. *Smart Materials and Structures*, 17, 015044.
- Ebrahimi, F., Rastgoo, A. & Kargarnovin, M. 2008. Analytical investigation on axisymmetric free vibrations of moderately thick circular functionally graded plate integrated with piezoelectric layers. *Journal of mechanical science and technology*, 22, 1058-1072.

- Efraim, E. & Eisenberger, M. 2007. Exact vibration analysis of variable thickness thick annular isotropic and FGM plates. *Journal of Sound and Vibration*, 299, 720-738.
- Eratli, N., Argeso, H., Çalim, F. F., Temel, B. & Omurtag, M. H. 2014. Dynamic analysis of linear viscoelastic cylindrical and conical helicoidal rods using the mixed FEM. *Journal of Sound and Vibration*, 333, 3671-3690.
- Fereidoon, A., Mohyeddin, A., Sheikhi, M. & Rahmani, H. 2012. Bending analysis of functionally graded annular sector plates by extended Kantorovich method. *Composites Part B-Engineering*, 43, 2172-2179.
- Gupta, U., Lal, R. & Sharma, S. 2007. Vibration of non-homogeneous circular Mindlin plates with variable thickness. *Journal of Sound and Vibration*, 302, 1-17.
- Hosseini-Hashemi, S., Derakhshani, M. & Fadaee, M. 2013. An accurate mathematical study on the free vibration of stepped thickness circular/annular Mindlin functionally graded plates. *Applied Mathematical Modelling*, 37, 4147-4164.
- Hosseini-Hashemi, S., Fadaee, M. & Es' Haghi, M. 2010. A novel approach for in-plane/out-of-plane frequency analysis of functionally graded circular/annular plates. *International Journal of Mechanical Sciences*, 52, 1025-1035.
- Irie, T., Yamada, G. & Takagi, K. 1982. Natural frequencies of thick annular plates. *Journal of Applied Mechanics*, 49, 633-638.
- Jodaeei, A., Jalal, M. & Yas, M. 2012. Free vibration analysis of functionally graded annular plates by state-space based differential quadrature method and comparative modeling by ANN. *Composites Part B: Engineering*, 43, 340-353.
- Kermani, I. D., Ghayour, M. & Mirdamadi, H. R. 2012. Free vibration analysis of multi-directional functionally graded circular and annular plates. *Journal of Mechanical science and Technology*, 26, 3399-3410.

- Kumar, Y. & Lal, R. 2013. Prediction of frequencies of free axisymmetric vibration of two-directional functionally graded annular plates on Winkler foundation. *European Journal of Mechanics-A/Solids*, 42, 219-228.
- Lal, R. & Ahlawat, N. 2015. Axisymmetric vibrations and buckling analysis of functionally graded circular plates via differential transform method. *European Journal of Mechanics-A/Solids*, 52, 85-94.
- Lal, R. & Ahlawat, N. 2017. Buckling and vibrations of two-directional FGM Mindlin circular plates under hydrostatic peripheral loading. *Mechanics of Advanced Materials and Structures*, 1-16.
- Li, X. Y., Ding, H. J. & Chen, W. Q. 2008a. Axisymmetric elasticity solutions for a uniformly loaded annular plate of transversely isotropic functionally graded materials. *Acta Mechanica*, 196, 139-159.
- Li, X. Y., Ding, H. J. & Chen, W. Q. 2008b. Elasticity solutions for a transversely isotropic functionally graded circular plate subject to an axisymmetric transverse load $q_r(k)$. *International Journal of Solids and Structures*, 45, 191-210.
- Liew, K. M., Wang, C. M., Xiang, Y. & Kitipornchai, S. 1998. Chapter Three - Formulation in Polar Coordinates. In: Liew, K. M., Wang, C. M., Xiang, Y. & Kitipornchai, S. (eds.) *Vibration of Mindlin Plates*. Oxford: Elsevier Science Ltd.
- Liu, C.-F. & Lee, Y.-T. 2000. Finite element analysis of three-dimensional vibrations of thick circular and annular plates. *Journal of Sound and Vibration*, 233, 63-80.
- Ma, L. & Wang, T. 2004. Relationships between axisymmetric bending and buckling solutions of FGM circular plates based on third-order plate theory and classical plate theory. *International Journal of Solids and Structures*, 41, 85-101.

- Malekzadeh, P., Haghghi, M. G. & Atashi, M. 2011. Free vibration analysis of elastically supported functionally graded annular plates subjected to thermal environment. *Meccanica*, 46, 893-913.
- Malekzadeh, P., Shahpari, S. & Ziaee, H. 2010. Three-dimensional free vibration of thick functionally graded annular plates in thermal environment. *Journal of Sound and Vibration*, 329, 425-442.
- Mengi, Y., 1993. Numerical methods in engineering. *Lecture notes*, Çukurova University, Adana.
- Mirtalaie, S. H. & Hajabasi, M. A. 2011. Free vibration analysis of functionally graded thin annular sector plates using the differential quadrature method. *Proceedings of the Institution of Mechanical Engineers, Part C: Journal of Mechanical Engineering Science*, 225, 568-583.
- Mousavi, S. M. & Tahani, M. 2012. Analytical solution for bending of moderately thick radially functionally graded sector plates with general boundary conditions using multi-term extended Kantorovich method. *Composites Part B-Engineering*, 43, 1405-1416.
- Nie, G. J. & Zhong, Z. 2007a. Axisymmetric bending of two-directional functionally graded circular and annular plates. *Acta Mechanica Sinica*, 20, 289-295.
- Nie, G. J. & Zhong, Z. 2007b. Semi-analytical solution for three-dimensional vibration of functionally graded circular plates. *Computer Methods in Applied Mechanics and Engineering*, 196, 4901-4910.
- Nie, G. J. & Zhong, Z. 2008. Vibration analysis of functionally graded annular sectorial plates with simply supported radial edges. *Composite Structures*, 84, 167-176.
- Nie, G. & Zhong, Z. 2010. Dynamic analysis of multi-directional functionally graded annular plates. *Applied Mathematical Modelling*, 34, 608-616.

- Noori, A. R., Aslan, T. A. & Temel, B. 2018a. Damped transient response of in-plane and out-of-plane loaded stepped curved rods. *Journal of the Brazilian Society of Mechanical Sciences and Engineering*, 40, 28.
- Noori, A. R., Aslan, T. A. & Temel, B. 2018b. An efficient approach for in-plane free and forced vibrations of axially functionally graded parabolic arches with nonuniform cross section. *Composite Structures*, 200, 701-710.
- Rad, A. B. 2012a. Semi-Analytical Solution for Functionally Graded Solid Circular and Annular Plates Resting on Elastic Foundations Subjected to Axisymmetric Transverse Loading. *Advances in Applied Mathematics and Mechanics*, 4, 205-222.
- Rad, A. B. 2012b. Static analysis of two directional functionally graded circular plate under combined axisymmetric boundary conditions. *International Journal Of Engineering & Applied Sciences*, 4, 13.
- Rad, A. B. & Alibeigloo, A. 2013. Semi-Analytical Solution for the Static Analysis of 2D Functionally Graded Solid and Annular Circular Plates Resting on Elastic Foundation. *Mechanics of Advanced Materials and Structures*, 20, 515-528.
- Rad, A. B., Alibeigloo, A. & Malihi, S.S. 2010. Static analysis of functionally graded annular plate resting on elastic foundation subject to an axisymmetric transverse load based on the three dimensional theory of elasticity. *Journal Of Solid Mechanics*, 2, 15.
- Reddy, J. N. 1984. *Energy principles and variational methods in applied mechanics*, John Wiley & Sons Texas.
- Reddy, J. N., Wang, C. M. & Kitipornchai, S. 1999. Axisymmetric bending of functionally graded circular and annular plates. *European Journal of Mechanics - A/Solids*, 18, 185-199.
- Sahraee, S. 2009. Bending analysis of functionally graded sectorial plates using Levinson plate theory. *Composite Structures*, 88, 548-557.

- Sahraee, S. & Saidi, A. R. 2009. Axisymmetric bending analysis of thick functionally graded circular plates using fourth-order shear deformation theory. *European Journal of Mechanics a-Solids*, 28, 974-984.
- Saidi, A. R., Rasouli, A. & Sahraee, S. 2009. Axisymmetric bending and buckling analysis of thick functionally graded circular plates using unconstrained third-order shear deformation plate theory. *Composite Structures*, 89, 110-119.
- Sayar, K. 1970. *Dönel kabuk sistemlerin diferansiyel geçiş matrisiyle çözümü*, Istanbul Technical University, Istanbul. (In Turkish)
- Shamekhi, A. 2013. On the use of meshless method for free vibration analysis of circular FGM plate having variable thickness under axisymmetric condition. *International Journal of Research and Reviews in Applied Sciences*, 14, 257-268.
- Shariyat, M. & Alipour, M. 2010. A differential transform approach for modal analysis of variable thickness two-directional FGM circular plates on elastic foundations. *Iranian Journal of Mechanical Engineering*, 11, 15 - 38.
- Shariyat, M. & Alipour, M. 2011. Differential transform vibration and modal stress analyses of circular plates made of two-directional functionally graded materials resting on elastic foundations. *Archive of Applied Mechanics*, 81, 1289-1306.
- Sharma, S., Lal, R. & Singh, N. 2017. Effect of non-homogeneity on asymmetric vibrations of non-uniform circular plates. *Journal of Vibration and Control*, 23, 1635-1644.
- Shi, P. & Dong, C. Y. 2012. Vibration analysis of functionally graded annular plates with mixed boundary conditions in thermal environment. *Journal of Sound and Vibration*, 331, 3649-3662.
- Spiegel, M. R. 1965. *Laplace transforms*, McGraw-Hill New York.

- Su, Z., Jin, G., Shi, S., Ye, T. & Jia, X. 2014. A unified solution for vibration analysis of functionally graded cylindrical, conical shells and annular plates with general boundary conditions. *International Journal of Mechanical Sciences*, 80, 62-80.
- Tajeddini, V., Ohadi, A. & Sadighi, M. 2011. Three-dimensional free vibration of variable thickness thick circular and annular isotropic and functionally graded plates on Pasternak foundation. *International Journal of Mechanical Sciences*, 53, 300-308.
- Temel, B. 2004. Transient analysis of viscoelastic helical rods subject to time-dependent loads. *International journal of solids and structures*, 41, 1605-1624.
- Temel, B., Çalim, F. F. & Tütüncü, N. 2004. Quasi-static and dynamic response of viscoelastic helical rods. *Journal of sound and vibration*, 271, 921-935.
- Temel, B. & Noori, A. R. 2019. Transient analysis of laminated composite parabolic arches of uniform thickness. *Mechanics Based Design of Structures and Machines*, 1-9.
- Temel, B. & Şahan, M. F. 2013. Transient analysis of orthotropic, viscoelastic thick plates in the Laplace domain. *European Journal of Mechanics-A/Solids*, 37, 96-105.
- Temel, B., Yıldırım, S. & Tutuncu, N. 2014. Elastic and viscoelastic response of heterogeneous annular structures under Arbitrary Transient Pressure. *International Journal of Mechanical Sciences*, 89, 78-83.
- Tornabene, F. 2009. Free vibration analysis of functionally graded conical, cylindrical shell and annular plate structures with a four-parameter power-law distribution. *Computer Methods in Applied Mechanics and Engineering*, 198, 2911-2935.
- Tutuncu, N. & Temel, B. 2009. A novel approach to stress analysis of pressurized FGM cylinders, disks and spheres. *Composite Structures*, 91, 385-390.

- Vivio, F. & Vullo, V. 2010. Closed form solutions of axisymmetric bending of circular plates having non-linear variable thickness. *International Journal of Mechanical Sciences*, 52, 1234-1252.
- Wang, C. M., Reddy, J. N. & Lee, K. H. 2000. *Shear deformable beams and plates relationships with classical solutions*, ELSEVIER New York.
- Wang, Q., Shi, D., Liang, Q. & Shi, X. 2016a. A unified solution for vibration analysis of functionally graded circular, annular and sector plates with general boundary conditions. *Composites Part B: Engineering*, 88, 264-294.
- Wang, Y., Ding, H. J. & Xu, R. Q. 2016b. Three-dimensional analytical solutions for the axisymmetric bending of functionally graded annular plates. *Applied Mathematical Modelling*, 40, 5393-5420.
- Wang, Y., Xu, R.-Q. & Ding, H.-J. 2009. Free axisymmetric vibration of FGM circular plates. *Applied Mathematics and Mechanics*, 30, 1077-1082.
- Wang, Y., Xu, R. Q. & Ding, H. J. 2011. Axisymmetric bending of functionally graded circular magneto-electro-elastic plates. *European Journal of Mechanics a-Solids*, 30, 999-1011.
- Washizu, K. 1975. *Variational methods in elasticity and plasticity*, Pergamon Press New York.
- Wirowski, A. Free vibrations of thin annular plates made from functionally graded material. PAMM: Proceedings in Applied Mathematics and Mechanics, 2009. Wiley Online Library, 261-262.
- Wu, T. Y., Wang, Y. Y. & Liu, G. R. 2002. Free vibration analysis of circular plates using generalized differential quadrature rule. *Computer Methods in Applied Mechanics and Engineering*, 191, 5365-5380.
- Yas, M. & Tahouneh, V. 2012. 3-D free vibration analysis of thick functionally graded annular plates on Pasternak elastic foundation via differential quadrature method (DQM). *Acta Mechanica*, 223, 43-62.

- Yıldırım, S. & Tutuncu, N. 2018a. Axisymmetric plane vibration analysis of polar-anisotropic disks. *Composite Structures*, 194, 509-515.
- Yıldırım, S. & Tutuncu, N. 2018b. Radial vibration analysis of heterogeneous and non-uniform disks via complementary functions method. *The Journal of Strain Analysis for Engineering Design*, 53, 332-337.
- Yıldırım, S. & Tutuncu, N. 2019. Effect of Magneto-Thermal Loads on the Rotational Instability of Heterogeneous Rotors. *AIAA Journal*, <https://doi.org/10.2514/1.J058124>.
- Zafarmand, H. & Kadkhodayan, M. 2015. Three dimensional elasticity solution for static and dynamic analysis of multi-directional functionally graded thick sector plates with general boundary conditions. *Composites Part B-Engineering*, 69, 592-602.
- Žur, K. K. 2018. Quasi-Green's function approach to free vibration analysis of elastically supported functionally graded circular plates. *Composite Structures*, 183, 600-610.

CURRICULUM VITAE

Ahmad Reshad NOORI was born in Wardak/Afghanistan in 1987. He completed his primary school and high school education in Kabul/Afghanistan and then he enrolled in the Civil Engineering Department of Çukurova University in 2007. He started the double major program in the Environmental Engineering Department of Çukurova University in 2008. He graduated as a civil engineer and environmental engineer from the university in 2011. The same year, he started his Master of Science degree in the Department of Civil Engineering of Çukurova University. He completed the degree of Master of Science in 2013. In 2014, he started his Ph.D. degree in the same department. He also graduated from the Department of Business Administration of Anadolu University in 2019.



APPENDICES



Appendix A

Laplace transform of dynamic loads

Type No	Load Function $P(t)$	Laplace Transform $\bar{P}(s)$
1	<p>Step Load</p>	$\frac{P_{z0}}{s}$
2	<p>Half Rectified Sine Wave Function Load</p>	$P_{z0} \frac{\pi c}{(c^2 s^2 + \pi^2)(1 - e^{-cs})}$
3	<p>Right Triangle Impulsive Load</p>	$P_{z0} \left[\frac{1}{s} - \frac{1 - e^{-cs}}{cs^2} \right]$
4	<p>Impulsive Triangular Load</p>	$P_{z0} \left[\frac{1 - e^{-\frac{cs}{2}}}{s} \right]^2 \frac{2}{c}$
5	<p>Impulsive Sine Load</p>	$P_{z0} \frac{\pi c(1 + e^{-cs})}{(c^2 s^2 + \pi^2)}$
6	<p>Rectified Sine Wave Function Load</p>	$P_{z0} \frac{\pi c}{(\pi^2 s^2 + \pi^2)} \frac{e^{cs} + 1}{e^{cs} - 1}$
7	<p>Square Wave Function Load</p>	$P_{z0} \frac{1}{s} \frac{e^{cs} - 1}{e^{cs} + 1}$